Investigating the contribution of the rs13376333 genetic variant to lone atrial fibrillation in human induced pluripotent stem cell-derived atrial cardiomyocytes

by

Ekaterina Stogova

Bachelor of Science, Simon Fraser University, 2020

Thesis Submitted in Partial Fulfillment of the
Requirements for the Degree of
Master of Science

in the
Department of Biomedical Physiology and Kinesiology
Faculty of Science

SIMON FRASER UNIVERSITY
Summer 2023

Declaration of Committee

Name:	**Ekaterina Stogova**
Degree:	**Master of Science**
Title:	**Investigating the contribution of the rs13376333 genetic variant to lone atrial fibrillation in human induced pluripotent stem cell-derived atrial cardiomyocytes**
Committee:	**Chair: David C. Clarke** Associate Professor, Biomedical Physiology and Kinesiology
	Glen F. Tibbits Supervisor Professor, Biomedical Physiology and Kinesiology
	Peter Ruben Committee Member Professor, Biomedical Physiology and Kinesiology
	Zachary Laksman Committee Member Clinical Assistant Professor, Medicine University of British Columbia
	Leif Hove-Madsen Committee Member Tenured Scientist, Experimental Pathology Institute of Biomedical Research of Barcelona
	Thomas Claydon Examiner Associate Professor, Biomedical Physiology and Kinesiology

Abstract

Atrial fibrillation (AF), the most common arrhythmia globally, is characterized by irregular and rapid electrical activity in the atria. AF is linked to increased morbidity, mortality, and decreased quality of life. Although multiple modifiable risk factors have been associated with a higher incidence of AF, there is a strong genetic component in the development of lone AF. The effect of the intronic rs13376333 variant located within the *KCNN3* gene encoding for the small-conductance Ca^{2+}-activated K^+ channel 3 (SK3) was investigated with multielectrode array and optical mapping. Gene-edited human-induced pluripotent stem cell-derived atrial cardiomyocytes (hiPSC-aCMs) harboring the rs13376333 variant exhibited a prolonged action potential duration and a diminished response to apamin, an SK channel blocker, compared to the isogenic wild-type hiPSC-aCMs measured with optical mapping. The results of this project suggest that SK channels could be a potential and more specific novel therapeutic target for the treatment of AF.

Keywords: hiPSCs; cardiomyocytes; molecular cardiology; multielectrode array; optical mapping

To my parents, who have provided unconditional love and support throughout all my endeavors.

Acknowledgements

Firstly, I would like to thank my senior supervisor Dr. Glen Tibbits for the opportunity to be a part of his lab and his continuous support and guidance throughout my graduate studies. My passion for cardiac physiology started after I had taken BPK 412 taught by Dr. Tibbits in my last semester as an undergraduate student. His passion and interest in cardiac research have left a lasting impression on me and eventually led me to being a graduates student in his lab. Dr. Tibbits provided immense support and mentorship, especially during some of the toughest moments, both personal and professional.

I would like to extend my gratitude to my committee supervisors Dr. Leif Hove-Madsen, Dr. Zachary Laksman, and Dr. Peter Ruben. Dr. Hove-Madsen has helped with troubleshooting and optimizing optical mapping experiments, which were crucial to my project. His experience and knowledge in cardiac physiology and data analysis was invaluable. Dr. Laksman has provided the guidance on the clinical relevance and translation of my studies and shared his experience using human-induced pluripotent stem cell-derived cardiomyocytes as an arrhythmia model. Dr. Ruben has provided a great input on the experimental design offering his expertise in electrophysiology and ion channels.

This thesis would not have been possible without the support of my dearest friends. To Alia Arslanova, thank you for always being there for me and pushing me beyond my limits. Our friendship has allowed me to grow as a person, a friend, and a researcher. Alia has done a tremendous amount of work optimizing cell culture and differentiation protocols and adapting new instruments which are crucial for all ongoing projects in our lab. To Tiffany Barszczewski, I am so grateful to have gained you as a friend and for your kindness and empathy. Thank you for helping me out in the beginning of my project and for teaching me about gene editing. To Mariam Butt, thank you for bringing so much happiness and light to everyone around you. I am so grateful to call you my friend. To Alia, Tiffany, and Mariam, thank you for doing my daily media changes when I could not and for all the brunch places we have tried together.

I would like to give a special thanks to all members of the Tibbits Lab and the Molecular Cardiac Physiology Group who were part of this journey. It has been a

pleasure getting to know you all and learning about your research. I will forever be grateful for all the experience, knowledge, and friendships I have gained throughout the past three years.

Lastly, I would like to thank the staff at the Department of Biomedical Physiology and Kinesiology for their administrative assistance.

Table of Contents

List of Tables

List of Figures

List of Acronyms

AF	Atrial fibrillation
AHA	American Heart Association
AP	Action potential
APD	Action potential duration
AVN	Atrioventricular node
cAF	Chronic atrial fibrillation
CaM	Calmodulin
CaMBD	Calmodulin-binding domain
CICR	Calcium-induced calcium release
CK2	Casein kinase 2
CM	Cardiomyocyte
CRISPR	Clustered regularly interspaced short palindromic repeats
CV	Conduction velocity
DAD	Delayed afterdepolarization
EAD	Early afterdepolarization
ECG	Electrocardiogram
EJC	Exon-junction complex
ERP	Effective refractory period
FACS	Fluorescence-activated cell sorting
FPD	Field potential duration
GFP	Green fluorescent protein
GWAS	Genome-wide association study
HDR	Homology-directed repair
hiPSC	Human induced pluripotent stem cell
hiPSC-aCM	Human induced pluripotent stem cell-derived atrial cardiomyocyte
hiPSC-vCM	Human induced pluripotent stem cell-derived ventricular cardiomyocyte
LAA	Left atrial appendage
LTCC	L-type calcium channel
MEA	Multielectrode array

mRNA	Messenger ribonucleic acid
NCX	Sodium calcium exchanger
NHEJ	Non-homologous end joining
NMD	Nonsense-mediated decay
OM	Optical mapping
OR	Odds ratio
PCR	Polymerase chain reaction
PP2A	Protein phosphatase 2A
PTC	Premature termination codon
PV	Pulmonary vein
RA	Retinoic acid
RAA	Right atrial appendage
RyR	Ryanodine receptor
SAN	Sinoatrial node
sgRNA	Single guide ribonucleic acid
SK	Small-conductance calcium-activated potassium channel
SNP	Single nucleotide polymorphism
SOICR	Store-overload-induced calcium release
SR	Sarcoplasmic reticulum
ssODN	Single-stranded oligodeoxynucleotide
ZLS	Zimmermann-Laband Syndrome

Chapter 1.

General Introduction

1.1. Atrial Fibrillation Overview

Atrial fibrillation (AF), the most common arrhythmia globally, is characterized by irregular and rapid electrical activity in the cardiac atria. AF is linked to increased morbidity and mortality and is associated with decreased quality of life. According to the Global Burden of Disease Study from 2010[1], AF has begun to emerge as a global epidemic with estimated annual new cases at nearly 5 million highlighting an increasing burden of AF worldwide. Recognizing an increased incidence of AF and its burden on the individual, healthcare system, and economy contributes to a growing number of studies looking to identify personalized and specific treatments for AF. Among the associated risk factors for developing AF are age, male sex, hypertension, diabetes, obesity, myocardial infarction, and heart failure which puts certain populations at a much higher risk.[2] Clinical presentation of AF can be asymptomatic or present with palpitations, dyspnea, fatigue, dizziness, and/or angina. AF can be further subdivided into three types: paroxysmal, persistent, and permanent. In paroxysmal AF, the episodes last less than 7 days and typically resolve spontaneously. In contrast, persistent and permanent AF are defined as episodes of AF of the duration longer than 12 months, with permanent AF being resistant to treatments and failure to be terminated. Electrocardiogram (ECG) findings show poorly defined or absent P waves replaced by irregular F (atrial flutter) waves, and elevated heart rate at typically > 100 beats per minute (bpm) (Figure 1.1).

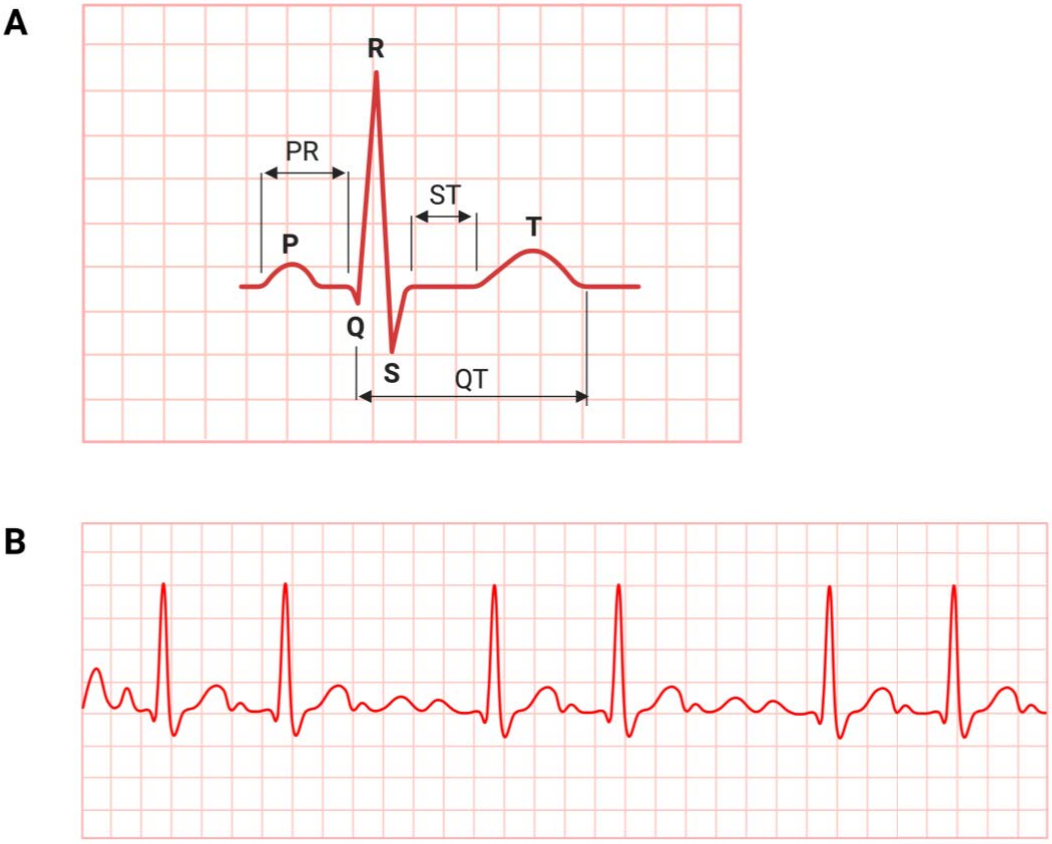

Figure 1.1 Normal ECG and typical ECG findings in atrial fibrillation.
(A) Representative normal ECG trace with labeled P and T waves, QRS complex, and PR and QT intervals. (B) ECG showing typical atrial fibrillation findings such as absent P waves replaced by irregular atrial flutter F waves and irregular heart rate represented by variable R-R intervals. Created with BioRender.com.

However, AF may also occur without any overt underlying structural or electrophysiological pathologies or in fact be the precedent for these changes. Therefore, the progressive nature of AF from paroxysmal to persistent or permanent may be explained by electrophysiological and structural remodelling of the atria occurring as a result of the arrhythmic behavior in the atria. Despite the high prevalence of AF in older populations (9.33-fold higher risk for participants aged 80-89 compared to 50-59)[1], lone AF is documented in patients under 60. Based on the Framingham Heart Study, lone AF constitutes 1.7% of all cases when defined as AF without evident comorbidities without consideration for the age.[3] In other cases, lone AF is defined as any AF in patients ≤ 60 years without evident cardiac pathologies or known risk factors

and comorbidities and comprises from 1.6% to 30% of AF cases.[4,5] This syndrome demonstrates a strong genetic component in the development of atrial fibrillation. Lone AF has been viewed as focal AF in which ectopic discharge, typically originating from the pulmonary veins (PVs), serves as a single site from which the arrhythmia arises and ultimately represents the trigger.[4] It is important to distinguish early-onset lone AF from idiopathic AF, which is AF of an unknown etiology and in the absence of clinical risk factors in adults > 60 years old.

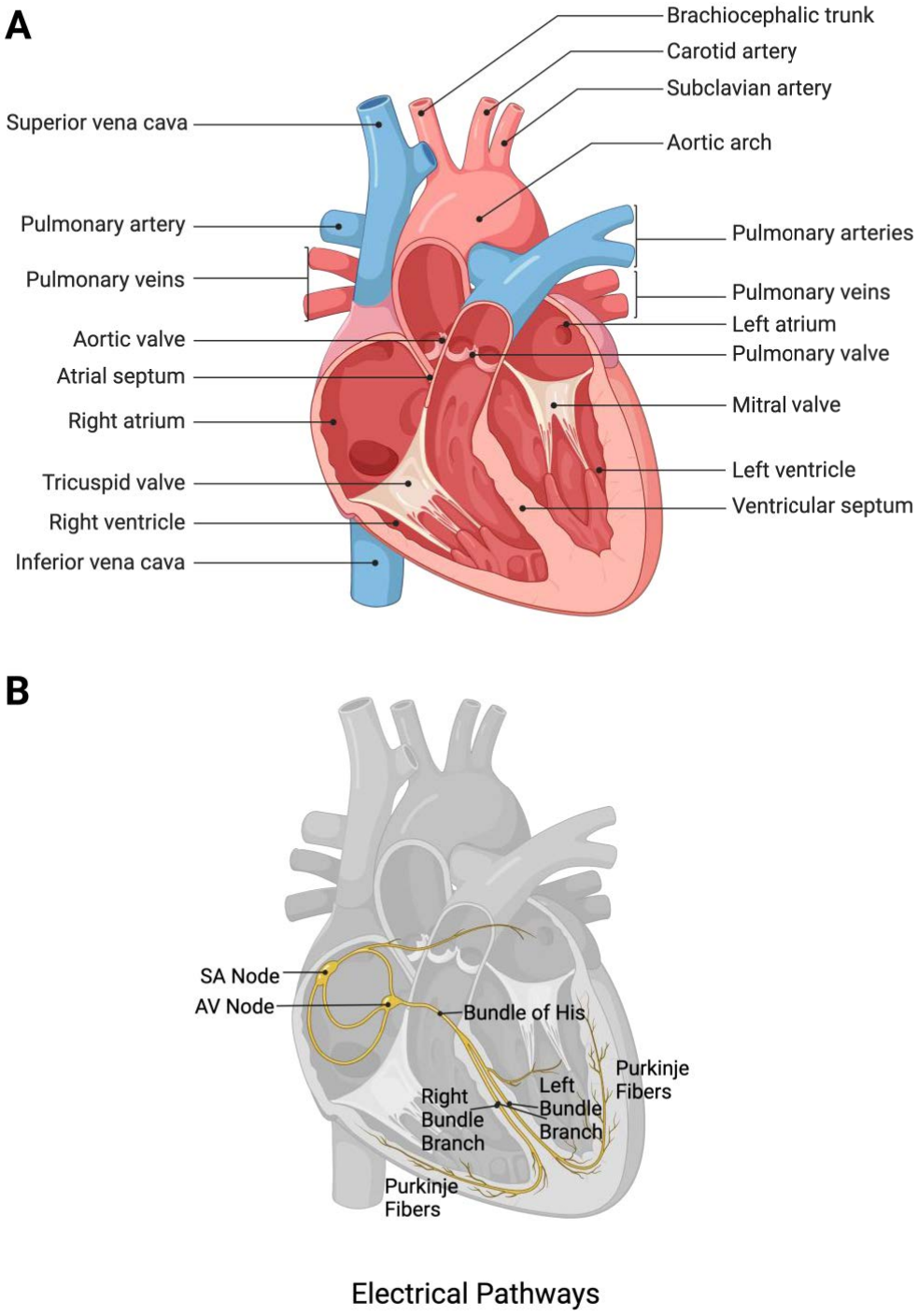

Figure 1.2 Heart anatomy and electrical pathways of the heart.
(A) Shows normal heart anatomy including the atria where atrial fibrillation originates; distal structures such as ventricles can also be affected by atrial fibrillation. (B) Shows electrical pathways of the heart including the sinoatrial (SA) node, atrioventricular (AV) node, bundle of His, bundle branches, and Purkinje fibers. Created with BioRender.com.

1.2. Risk Factors

Amongst the unmodifiable risk factors for AF are genetics, age, sex, and racial differences. AF has a strong genetic component demonstrated by identified rare familial forms of AF on various genetic loci. A study examining the heritability of AF in Icelanders showed familial aggregation of the disease with first-degree relatives having a four-fold increased risk of developing AF before the age of 60 than the general population when family history of lone AF is present.[6] To further identify the familial basis of AF, classic Mendelian genetics and candidate gene approaches have been used, which led to the discovery of a number of variants in genes encoding ion channels and structural proteins important in maintaining healthy cardiac physiology. One of the most prominent risk factors for increased prevalence and incidence of AF is advancing age which appears to be the greatest risk factor for AF when compared to other risk factors.[7] The epidemiology of AF differs between men and women: the Framingham Heart Study showed that AF incidence in women is 1.6 cases per 1000 person-years compared to 3.8 cases per 1000 person-years in men accounting for a 1.5-fold higher risk of AF in men when adjusted for age and predisposing conditions.[7] However, women tend to be more symptomatic from AF with longer paroxysmal episodes as reported in the Analysis of Canadian Registry of Atrial Fibrillation (CARAF) study.[8] Women who are suffering from AF have a four-fold increased risk of stroke compared to men, as well as greater mortality rate, both cardiovascular and all-cause.[9] The prevalence of AF in Hispanics, Asians, and blacks older than 65 years old was reported to be 46% to 65% lower compared to non-Hispanic whites in the Multi-Ethnic Study of Atherosclerosis (MESA).[10] Marcus et al. used genetic analysis to determine whether the degree of European ancestry in African Americans correlates with an increased risk of AF and reported that for every 10% increase in European ancestry there was a 10% increased risk of incident AF.[11] This suggests that there is likely an undiscovered genetic predisposition to AF in those of European descent.

There are many modifiable risk factors for AF that have been reported including but not limited to hypertension and other cardiovascular diseases, diabetes mellitus, smoking, and obesity. In the Framingham Heart Study cohort, hypertension was found to be an independent risk factor for AF with an increased risk of 1.5 in men and 1.4 in women.[12] Hypertension predisposes individuals to many cardiovascular complications

such as coronary heart disease and heart failure[13], both of which can contribute to the development of AF, and leads to structural remodelling and profibrotic changes within the left atrium and left ventricle.[14]

1.3. Genetics of Atrial Fibrillation

Along with evidence that parental AF increases the risk of AF development in offspring, which demonstrates familial clustering of the disease, multiple genetic loci have also been linked to a higher susceptibility to AF in genome-wide association studies (GWAS).[15] One of the early familial aggregation studies in an Icelandic population showed that first-degree relatives of patients with AF <60 years to have a higher than four-fold risk of having AF at age <60 than general population confirming significant familial clustering of the disease.[6] However, it is important to consider the genetic heterogeneity of AF when attempting to establish an association with new variants as multiple genetic loci (e.g., *KCNQ1, NPPA, TBX5, MYL4)* have been linked to the disease and may be co-present with new variants of interest.[15]

1.3.1. Genome-wide Association Studies (GWAS)

GWAS is a phenotype-first approach and commonly involves comparing two large groups of individuals, one healthy control group and one case group. Genotyping arrays are used to determine the status of many genetic variants or single nucleotide polymorphisms (SNPs) throughout the genome and ultimately link a region or locus to the disease of interest. The odds ratio (OR) is a measure of association between an exposure and an outcome and is used to report effect size in a GWAS. With advances in genetics and decreasing cost of genotyping arrays, GWAS have become more common, and lone AF has been linked to variants found in or near genes coding for several ion channels, including K^+ and Na^+ channels, and other proteins including transcription factors. Interestingly, many of the identified SNPs are located in non-coding regions of the genome and are likely involved in modifying the transcription of a nearby gene via affecting the activity of the transcriptional regulatory element (e.g., enhancer or repressor). In a study by Ellinor et al.[16], a locus identified on chromosome 1q21 exceeded genome-wide significance and was linked to AF. However, there is a lack of studies investigating the possible mechanism and pathophysiology of this variant. Of six

SNPs significantly associated with AF on chromosome 1q21, the most significant one was rs13376333 (C>T; OR=1.56).[16] This non-coding variant is located within the *KCNN3* gene, which encodes for the small conductance Ca^{2+}-activated K^+ channel 3 (SK3), in the intron between first and second exon of the gene. A meta-analysis has confirmed that the rs13376333 variant is associated with increased risk of lone AF[17], and the association has also been demonstrated to be significant in a Chinese Han population.[18] Although the variant has been linked to AF in multiple genomic studies, it is important to conduct functional studies to investigate a possible mechanism of SK channels being involved in arrhythmogenesis and development of AF.

1.3.2. Zimmermann-Laband Syndrome 3 (ZLS3)

One known genotype-phenotype relationship is between gain-of-function de novo missense *KCNN3* variants and Zimmermann-Laband syndrome 3 (ZLS3) which is inherited in an autosomal dominant pattern. De novo variants are variants that appear for the first time in an individual and have not appeared in previous generations, and missense variants are genetic alterations resulting in an altered codon which encodes for a different amino acid due to a single base pair substitution. Zimmermann-Laband syndrome 3 is a rare congenital disorder characterized by intellectual and developmental disabilities along with gingival fibromatosis, hypoplastic or aplastic fingernails and toenails, and coarse facial features. The de novo heterozygous mutations Lys269Gly, Gly350Asp, and Ser436Cys were identified by Bauer and colleagues in three unrelated patients with ZLS3.[19] All three identified de novo mutations appeared at highly conserved residues, and functional analysis revealed a gain-of-function effect through a four-fold increase in apparent Ca^{2+} sensitivity of pathophysiological ion channels compared to wild-type ion channels in intact cells. More novel de novo mutations were identified later by Gripp and colleagues: Val555Phe, Val539del, and Ala287Ser.[20] Schwarz et al. further reported a de novo *KCNN3* variant Ala536Thr in monozygotic twins which is located within the part of the *KCNN3* gene coding for the S6 channel forming segment.[21]

1.3.3. Intron Function and Pathogenic Intronic Variants – Possible Mechanisms

An intron is a nucleotide sequence residing within a gene which does not code for amino acids and therefore does not remain in the final mRNA transcript. Precursor messenger RNA (pre-mRNA) contains both exons and introns, the latter of which are excised by the spliceosomes to form a coding sequence consisting of only exons that can be further translated into a functional protein.[22] A number of intronic functions have been identified: (1) transcription initiation/termination and genome organization by genomic introns, (2) transcription regulation and alternative splicing by spliced introns, (3) expression of non-coding RNAs by excised introns, and (4) nonsense-mediated decay (NMD) and nuclear export by exon-junction complex- (EJC-) harboring transcript.[23]

EJCs form on pre-mRNAs and are found at the junction of two exons joined together during RNA splicing. Nonsense-mediated decay acts as a quality control process whereby a premature stop codon, or premature termination codon (PTC), that would lead to a truncated protein triggers mRNA degradation. PTCs act to halt translation to prevent expression of an incorrectly translated gene. Exon-junction complexes consist of four core proteins and get deposited upstream of spliced exon-exon junctions to orient the nonsense-mediated decay machinery once the mRNA is exported to the cytoplasm for translation-dependent inspection by nonsense-mediated decay factors.[24] When a premature termination codon is present, translation is stopped upstream of the exon-junction complex which is retained, and nonsense-mediated decay is induced. When the mRNA with stop codons is placed into site A of the ribosome, protein synthesis is terminated.

A different combination of exons can be selected through the splicing of certain introns resulting in alternative splicing variants. Proper alternative splicing is highly dependent on the correct recognition of exons. Although introns historically have been considered as non-functional sequences, there are a lot of conserved elements within introns including splice site sequences, binding sites for regulatory proteins and sequences of non-coding RNA transcripts which, when altered, can result in disruption of final protein translation and expression.[25]

One of the mechanisms of an intronic variant causing disease is by introducing pseudo-exons. Pseudo-exon inclusion is triggered by intronic mutations that activate a non-canonical splice site. With point mutations being more common than small intronic deletions, pseudo-exon inclusion can introduce a novel donor or acceptor splice site or create or disrupt an existing splicing enhancer or silencer elements.[26] Another pathophysiological mechanism acts by disrupting transcription regulatory motifs as identified in multiple cases of genetic diseases such as demyelinating peripheral neuropathy[27] and Bethlem myopathy[28].

1.4. Atrial Fibrillation Arrhythmogenesis

AF can be maintained by focal ectopic activity and re-entry, and the mechanism sustaining AF usually involves a substrate and a trigger. Initially, AF presents as paroxysmal with shorter episodes resolving spontaneously without pharmacological interventions. In these cases, focal ectopic activity predominantly originates in the region around the pulmonary veins.[29] As the disease progresses, other functional and structural substrates can result in persistent and permanent AF and the progression of the disease.[29]

1.4.1. Focal Ectopic Activity

Focal ectopic activity can be generated by enhanced automaticity, early afterdepolarizations (EADs) or delayed afterdepolarizations (DADs). PVs have been identified as the main site of enhanced automaticity and increased triggered activity contributing to initiation and maintenance of paroxysmal AF.[30] Other sources of focal ectopic activity implicated in maintenance of AF include the vena cavae, the coronary sinus, and the inter-atrial septum.[31] PVs have distinctive action potential (AP) properties which predispose them to arrhythmogenesis such as a less negative resting membrane potential, a lower amplitude of the AP, and a shorter action potential duration (APD).[31,32] Automaticity is the basis of cardiac pacemaker function, and although various areas of the heart can show automaticity, rhythmicity is normally controlled by the sinoatrial node (SAN) in part because of its higher intrinsic frequency. When the depolarization rate is increased, abnormal rapid firing may occur in the areas of the heart outside the SAN.[32] Generation of AF-inducing ectopic foci in the case of enhanced automaticity may also

occur due to changes in currents that maintain normal atrial resting potential such as decreased inward rectifier K^+ current, $I_{K1,}$ and pacemaker cardiomyocyte-specific "funny" I_f currents.[29] However, large I_{K1} currents overdrive I_f current in normal atrial cardiomyocytes and no manifest automaticity occurs.

EADs involve abnormal secondary depolarizations during the repolarization phase of an occurring AP. The main mechanism behind EADs is prolongation of AP duration which typically allows L-type Ca^{2+} channels (LTCCs) to recover from inactivation, reactivate, and result in a depolarizing inward current of Ca^{2+} ions. On the contrary, DADs are spontaneous depolarizations occurring after completion of cellular repolarization and are predominantly caused by abnormalities in Ca^{2+} handling and depolarizations resulting from Na^+/ Ca^{2+} exchanger, NCX1, extruding one Ca^{2+} using the energy from the influx of 3 Na^+.[33] When DADs become large enough to reach threshold potential for activation of Na^+ channels and therefore initiate depolarization, AP firing occurs in the form of either a single ectopic beat or sustained tachycardia. In healthy atrial cardiomyocytes, ryanodine receptors (RyR2) located in the sarcoplasmic reticulum (SR) membrane open through Ca^{2+}-induced Ca^{2+}-release (CICR) mechanism during systole when Ca^{2+} enters the cell via voltage-gated LTCCs. The opening of RyR2 channels then allows for Ca^{2+} release from the SR further increasing cytosolic Ca^{2+} concentration during cardiac contraction. RyR2 are normally closed during diastole but may open and lead to SR Ca^{2+} leak if they are defective or when the SR stores are Ca^{2+} overloaded. The concept of SR Ca^{2+} leak due to overloaded SR stores is known as store-overload-induced Ca^{2+} release (SOICR). NCX1 is activated in response to SR Ca^{2+} leak during diastole causing a net depolarizing inward current underlying DADs. SR Ca^{2+} overload is seen in congestive HF resulting in DADs and incidence of AF.[34] Furthermore, DAD-promoted AF can be a result of RyR2 variants associated with catecholaminergic polymorphic ventricular tachycardia and other ion channels.[35]

1.4.2. Atrial Fibrillation and Re-Entry

Re-entry is another arrhythmogenic mechanism by which AF can be promoted. Re-entry requires a trigger, which is typically a premature ectopic beat, and a vulnerable substrate, which can be created by altered structural or electrical properties of the atria. AF can be the result of either a single localized re-entry circuit or multiple functional re-entry circuits located spatially and temporally different. Under normal conditions, a

premature ectopic beat travels through the cardiac tissue, and its conduction time is shorter than the refractory period such that the impulse cannot re-enter. However, an ectopic beat can encounter refractory tissue (e.g., fibrosis) when propagating in one direction while able to conduct in the direction of a faster-recovering tissue creating a unidirectional block. Conduction time, determined by the circuit path length and conduction velocity, must be greater than the longest refractory period in the circuit for re-entry to be maintained. Re-entry can be further subdivided into anatomical and functional type re-entry. Anatomical re-entry typically occurs due to a unidirectional block or slow conduction, which are the conditions often encountered in the atria of patients with AF, making the wavelength shorter than the length of the circuit.[31] Alternatively, functional re-entry occurs without underlying substrates and anatomical obstacles and is the result of a dysfunctional or structurally altered ion channels which disrupts electrical conduction in the heart.

1.4.3. Arrhythmogenesis Hypotheses and Models

The “leading circle model” was first proposed in 1977 and states that there are centripetal waves moving toward the centre of the circuit maintaining it in a refractory state.[36] The circular movement in one direction is initiated by a unidirectional block in tissue, and the impulse is able to spread inward and outward to sustain the circuit and to activate adjacent myocardium. This model illustrates functional re-entry as the refractory area forms a functional barrier.

Another model is the spiral wave model, wherein re-entry is promoted by reduced refractory period through accelerating and stabilizing spiral-wave rotors.[36] Rotors represent a special type of functional re-entry in which the wavefront is spiral, and the wavefront and wavetail meet at a focal point called a phase singularity.[37] A rotor, however, is not fixed in space like a re-entrant circuit in the leading circle model, which contributes to arrhythmogenesis. This is another type of functional re-entry as the tissue core is unexcitable due to high wavefront curvature and slow conduction velocity at the phase singularity creating a functional block.[37]

The “multiple wavelet hypothesis” was initially described in 1959 by Moe et al.[38] and is currently the most accepted hypothesis underlying AF arrhythmogenesis. This theory assumes that if some number of re-entrant wavefronts existed in an appropriate

atrial substrate, these wavefronts could continuously re-excite the atria and result in fibrillatory conduction.[38] Therefore, these multiple waves are randomly occurring throughout the atria causing wavebreaks and giving rise to new wavelets. This theory complements the leading circle model because both wavelength and atrial size determine the number of re-entrant circuits that can be sustained.

1.5. Current Treatments

Despite advances in healthcare as well as biomedical and pharmaceutical research, treatment options are limited by one-fits-all approach and the lack of efficacy resulting in a variety of serious side effects including life-threatening ventricular arrhythmias. According to the Clinical Practice Guideline for the Management of Patients with Atrial Fibrillation (2019) developed and published by the American Heart Association (AHA), current pharmaceutical treatments typically include anticoagulation medications such as warfarin or more recently non-vitamin K Novel Oral Anti-Coagulants (NOACs) to reduce the risk of stroke. In addition to prevention of thromboembolic event, antiarrhythmic drug therapy is necessary to restore and maintain sinus rhythm.[39]

Rate control, which is the first-line treatment option, primarily focuses on limiting the rate of atrioventricular conduction and keeping the ventricular beating rate below 100 bpm by administering β-blockers, calcium channel blockers, and/or digitalis, a potent Na^+/K^+ ATPase inhibitor.[40] The rhythm control therapy which aims to restore sinus rhythm can be achieved via either electrical or pharmacological cardioversion, and catheter- and surgery-based invasive procedures.[40] The current stage of AF and other factors such as patient's age, symptoms, and comorbidities should be considered when deciding to introduce rhythm control therapy in addition to rate control. Patients who have persistent symptoms despite adequate rate control therapy, younger patients (<50 years), and patients with lone AF are particularly suitable for rhythm control strategy.[41,42]

In cases where AF cannot be corrected with first-line less invasive treatment, catheter ablation (radiofrequency ablation or cryoablation) may be recommended to reduce the burden of AF. The procedure normally involves advancing catheters through the femoral vein to the heart and using radiofrequency heating energy to create lesions and disrupt abnormal electrical signals. Catheter ablation of AF is centred on electrical isolation of arrhythmogenic sites typically within PVs which are the most common

anatomical sources of ectopic atrial beats that can trigger episodes of paroxysmal AF.[30] Although catheter ablation procedure has become safer and more optimized over the past decade, its efficacy differs on patient-by-patient basis and varies greatly on the type and presentation of AF at the moment of consideration of catheter ablation. The general guideline is to reserve more invasive procedures for patients with symptomatic AF with the goal of improving quality of life.[43] A more recent study by Andrade et al. for the Early Aggressive Invasive Intervention for Atrial Fibrillation (EARLY-AF) study showed that catheter cryoballoon ablation had a significantly lower rate of AF recurrence when used as initial treatment of symptomatic paroxysmal AF compared to antiarrhythmic drug therapy at one year of follow-up.[44] These findings were further confirmed over three years of follow-up with catheter cryoballoon ablation being associated with a lower incidence of AF or atrial tachyarrhythmia when compared to initial use of antiarrhythmic drugs alone.[45]

However, there are a few disadvantages of each treatment option. For instance, antiarrhythmic medications might not be as effective in reducing the symptoms due to the lack of target specificity, or there might be a need for a repeat procedure of catheter ablation for the long-term management of AF and improving quality of life. For catheter-based and surgical procedures there remain risks associated with any surgical intervention: hemorrhage, infection, deep vein thrombosis, pulmonary embolism, and death. Risks specific to catheter ablation of AF include cardiac tamponade, pulmonary vein stenosis, injury to phrenic nerve, mitral valve, and/or esophagus, as well as vascular access complications and stroke.[40]

1.6. Atrial Action Potential and Ion Channels

Action potentials are changes in the membrane potential of excitable cells such as neurons, cardiac, and skeletal muscle cells. Cardiac APs, both atrial and ventricular, consist of five distinct phases: rapid upstroke, or depolarization (phase 0); early rapid repolarization (phase 1); plateau phase (phase 2); repolarization (phase 3); and return to resting membrane potential (phase 4).

Phase 0 is driven by an influx of Na^+ through Nav1.5 channels encoded by *SCN5A*. Nav1.5 channels conduct the main depolarizing current, I_{Na}, in the atria and ventricles. Nav1.5 channels are voltage-dependent and activate quickly at membrane

potentials around -55 mV and this current is reflected in the rapid upstroke phase of the action potential.[46]

Fast inactivation of Nav1.5 channels and activation of the transient outward K^+ current (I_{to}) are responsible for the initial or early repolarization phase. I_{to} current can be further subdivided into $I_{to,\,fast}$ and $I_{to,\,slow}$ based on their inactivation kinetics, however both activate at membrane potentials above -30 mV.[47] The fast component of transient outward current is conducted through Kv4.2 and Kv4.3 channels encoded by the *KCND2* and *KCND3* genes, respectively, with the additional accessory subunit KChIP2 (*KCNIP2*) required for a fully functional $I_{to,\,fast}$. Kv1.4 (*KCNA4*) is responsible for the slow component of the transient outward current. An additional ultra-rapid current I_{Kur} produced by Kv1.5 channels is seen specifically in the atria.[48–50] This current also contributes to phases 2 and 3 of the atrial action potential due to its slow and partial inactivation.[51]

Compared to phase 2 of the action potential in ventricular cardiomyocytes, the plateau phase in atrial cardiomyocytes is shorter but both are maintained primarily by the LTCC current.[52] Cardiac L-type Ca^{2+} channels (Cav1.2) are primary voltage-gated Ca^{2+} channels in the heart conducting inward Ca^{2+} current and are encoded by the *CACNA1C* gene. Additionally, atrial cardiomyocytes express another type of Ca^{2+} channel α -subunit, Cav1.3 (*CACNA1D*), which is significantly more abundant in the atria and Purkinje fibers than in the ventricles.[53] Cav1.2 LTCC α-subunits remain the primary expressed subunits in both atria and ventricles, with atrial cardiomyocytes expressing Cav1.3 at significantly lower levels compared to Cav1.2.[53] Cav1.3 channels have been shown to be expressed in the SA and AV nodes and demonstrated to have an important role in the SA and AV node automaticity and firing frequency.[54–59] A combination of inward Ca^{2+} current through these channels along with a reduction in inward rectifying I_{K1} current is necessary to maintain the plateau phase. Additionally, Cav1.2 channels use extracellular calcium to increase cytosolic Ca^{2+} and are critical in excitation-contraction (EC) coupling since their activation by depolarization triggers CICR from the SR.[60,61]

During phase 3 of the atrial AP, there is an increase in outward K^+ currents such as I_{Kr}, I_{Ks} and I_{K1} and concurrent decrease in inward Ca^{2+} current due to inactivation of LTCCs. I_{Kr} and I_{Ks} are rapid and slow components of delayed rectifier outward K^+ current, respectively, and are conducted by two distinct ion channels. I_{Kr} is conducted by the

hERG channel (Kv11.1) which is a gene product of the *KCNH2* gene and exists in several splice variants. The slow K^+ outward current I_{Ks} is conducted via Kv7.1 channels (*KCNQ1*). The I_{K1}, inward rectifier current, is conducted via Kir2.1 (*KCNJ2*), Kir2.2 (*KCNJ12*), Kir2.3 (*KCNJ4*) and Kir2.4 (*KCNJ14*). Additionally, $I_{K,ACh}$ current is present during the repolarization phase of the atrial AP. These are acetylcholine-gated K^+ channels consisting of two Kir3.1 (*GIRK1*) and two Kir3.4 (*GIRK4*) subunits with increased expression in the sinoatrial (SA) node, atrioventricular (AV) node, and atria compared to the ventricles.[53,62–64] Lastly, Kv1.5 (*KCNA5*) channels are responsible for the ultrarapid delayed rectifier current I_{Kur} which contributes to repolarization in the atria and is significantly large compared to the corresponding current produced by the Kv1.5 channels in the ventricles.[53]

Finally, the resting membrane potential, which ranges between -65 to -80 mV in atrial cardiomyocytes is achieved primarily by the increase in inward rectifying potassium channels and K^+ leak channel currents.

1.7. Small Conductance Ca^{2+}-activated K^+ (SK) Channels

1.7.1. Structure and Function of SK Channels

Small-conductance Ca^{2+}-activated K^+ (SK) channels were first identified in the central nervous system by Kohler et al. and are known to be sensitive to the neurotoxin apamin found in bee venom.[65] The sequences of the identified SK channel paralogs (SK1, SK2, and SK3 encoded by the *KCNN1*, *KCNN2,* and *KCNN3* genes, respectively) are highly conserved with variations being found predominately in their NH2- and COOH-terminal domains. These channels represent a unique family of K^+ channels as they are regulated by microdomain-specific Ca^{2+} concentration ($[Ca^{2+}]_i$) in a voltage-independent manner providing a link between changes in $[Ca^{2+}]_i$ and membrane potential. The three SK channels have very similar sensitivities to Ca^{2+} (EC_{50} values of 0.3-0.5 μM)[65] and share a common calcium-gating mechanism. In the central nervous system, SK channels play various roles in neural signaling and development.[66] Similar in structure to voltage-gated K^+ channels, SK channels consist of six transmembrane segments S1-S6 and a single pore loop with the N- and C-termini oriented towards the cytoplasm. Four subunits are needed to form a central pore to constitute a functional homotetrameric channel, however heteromultimers consisting of SK2 and SK3 subunits

have been reported.[67] The mechanism of SK channel activation by a rise in $[Ca^{2+}]_i$ is not fully understood. Calmodulin (CaM), an intermediate calcium-binding messenger protein, has been found to be associated with SK channels through a CaM-binding domain (CaMBD) in the C-terminus of an SK channel subunit.[68] CaM has two globular domains (in the N- and C-termini), each containing a pair of EF hands, and is able to bind two Ca^{2+} molecules per globular domain. An SK channel is activated when Ca^{2+} binds the EF hands in the N-terminus of CaM, which has a lower binding affinity for Ca^{2+} than the EF hands in the C-terminus. While SK channels are voltage insensitive, they are altered by binding of activated CaM thus allowing membrane potential to respond to changes in the cytosolic calcium signals. Calcium gating is further regulated by serine/threonine-selective proteins casein kinase 2 (CK2) and protein phosphatase 2A (PP2A).[69,70] Allen and colleagues showed a complex arrangement and interaction of SK2 subunits, CaM, CK2, and PP2A.[70] The results of their study suggested there is a single lysine residue in the N-terminal of SK2 that functions as a molecular switch to activate CK2 in a state-dependent manner and phosphorylate CaM when channels are closed decreasing their activity. For PP2A to function within the SK2 channel complex, it is required to directly bind to the C-terminal domain of the SK2 channel.

Furthermore, SK2 channels have been shown to be functionally coupled to an L-type Ca^{2+} channel via the cytoskeletal protein α-actinin 2.[71] A study by Lu et al. demonstrated that α-actinin 2 interacts with CaMBD in the C-terminus of SK2 channels and can co-exist or compete with apo-CaM, or calcium-free calmodulin, at the CaMBD.[72] Another cytoskeletal protein that has been documented to interact with SK channel subunits, specifically with the N-terminal domain, is filamin A.[73] Interestingly, both α-actinin 2 and filamin A increase the surface membrane expression of SK2 channels through recycling pathways as demonstrated in HEK 293 cells.[74]

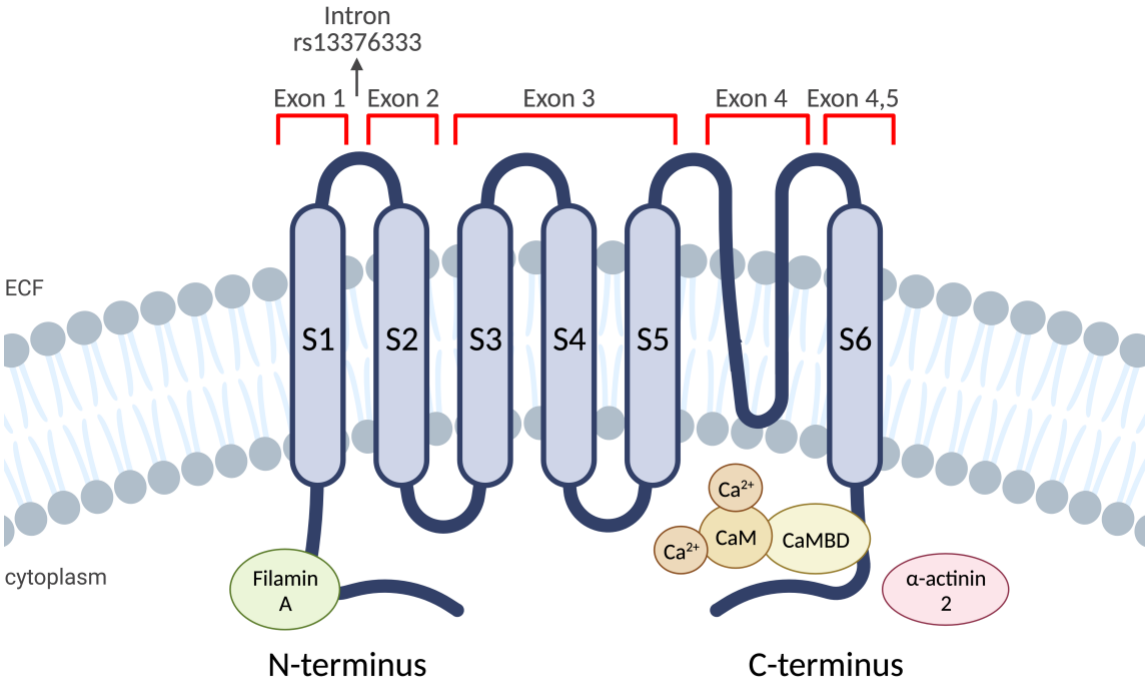

Figure 1.3. SK channel structure and location of the rs13376333 variant.
Each SK channel subunit comprises six transmembrane domains S1-S6 with both N- and C-termini facing the cytoplasm. Calmodulin (CaM) is associated with the C-terminus of an SK channel subunit through calmodulin-binding domain (CaMBD). Cytoskeletal proteins α-actinin 2 and filamin A are shown interacting with C-terminus and N-terminus domains, respectively. Created with BioRender.com.

1.7.2. SK Channel Expression and Function

It has been proposed that SK1-3 channels are involved in the late repolarization phase of the atrial AP and contribute to APD shortening when cytosolic Ca^{2+} rises. In a study conducted by Zhang et al., the SK3 contribution to the repolarization phase of the atrial AP was tested using a genetically engineered mouse model with a tetracycline-based switch (the Tet-Off system) that allowed for the control of SK3 channel expression by administering dietary tetracycline to block transcription of the downstream *KCNN3* locus.[75] In the Tet-Off system, the gene harboring inserted tetracycline-controlled transactivator protein (tTA) and the tetracycline operator (*tetO*) is expressed normally unless tetracycline, or its analogue doxycycline (DOX), is administered. In this model, homozygous $SK3^{T/T}$ mice showed a 50-fold increase in the SK3 mRNA expression in both atrial and ventricular tissues compared to wild-type animals.[75,76] APD was shortened in $SK3^{T/T}$ mice compared to wild-type animals, specifically through decreased

repolarization at 90%, APD_{90}, and prolonged in $SK3^{T/T}$ mice with administration of DOX.[75] Additionally, atrial fibrillation was successfully induced using programmed stimulation in $SK3^{T/T}$ animals but not in wild-type mice.[75] Interestingly, SK2 current appeared to be decreased with the knock-out of SK3 channels which suggests that the two paralogs may form heteromultimers in vivo, and both may contribute to the late phase of the atrial AP repolarization.[75] These results are in agreement with the study done by Tuteja et al. where they demonstrated that SK2 and SK3 paralogs may form heteromultimers and co-localise in clusters in both atrial and ventricular mouse and human cardiomyocytes.[67] However, one of the main disadvantages of using a small mammalian model, such as mice, is that their cardiac electrophysiology differs significantly from large mammalian species, as a consequence, in part, because the heart rates are almost an order of magnitude higher. Therefore, it is important to create a human physiological model to verify the existing evidence pertaining to the effect of SK3 channels on atrial APD and therefore AF in humans.

The pattern of SK channel expression throughout the heart remains controversial. In mouse models, SK2 channel presence in atrial and ventricular cardiomyocytes was documented by the Chiamvimonvat group.[77] They later reported mRNA expression profiles of SK channels in isolated mouse atrial and ventricular cardiomyocytes.[78] The results showed *KCNN1* and *KCNN2* paralogs being predominantly expressed in the atrial tissue, whereas *KCNN3* was reported to be expressed at a low level in both atrial and ventricular cardiomyocytes.[78] Immunocytochemistry labeling with anti-SK2 and anti-SK3 antibodies further confirmed SK2 and SK3 channels residing in the intracellular non-junctional sarcoplasmic reticulum in mouse atrial cardiomyocytes.[79] Another study reported SK1-SK3 paralogs expressed at both mRNA and protein levels in dog right atrial appendage (RAA) and pulmonary vein cardiomyocytes.[80] The results reported no significant difference in the levels of SK1 and SK3, whereas SK2 mRNA transcript was significantly elevated in PV samples compared to RAA.[80]

Cardiac mRNA expression profiling of the SK channels has also been done in porcine models. A study looking at the effect of SK channel inhibition in vernakalant-resistant porcine model of AF reported the presence of *KCNN1* transcript in diminutive amounts in all chambers of both healthy control and pigs with sustained AF.[81] The *KCNN2* transcript was found in both atria and ventricles with a higher level in the left

atrium compared to the left ventricle and the right atrium versus the right ventricle.[81] *KCNN3* transcript was also expressed in both atria and ventricles without being affected by tachypacing and the presence of AF in any of the chambers.[81]

In native human cardiomyocytes obtained from right atrial tissue, SK2 and SK3 expression levels were reported to be significantly higher compared to SK1.[82] In the same study, Skibsbye et al. further hypothesised that the structural and electrical remodelling of the atria associated with long-term AF resulted in decreased expression of these channels as seen in patients with chronic AF (cAF).[82] It is possible that SK3 expression may be initially upregulated at the early paroxysmal AF stages contributing to electrophysiological and structural remodelling of the atrial tissue. This would promote AF and ultimately result in a downregulation of these channels in cAF (i.e., *AF begets AF*). In agreement with the proposed hypothesis, RAA and left atrial appendage (LAA) cardiomyocytes obtained from cAF patients had been reported to show significantly decreased mRNA and protein levels of SK1 and SK2 channels with no significant difference in SK3 mRNA and protein expression compared to sinus rhythm controls.[83] A later study by Shamsaldeen et al. using immunocytochemistry showed significant overlap of SK2 and SK3 subunits, both being expressed at approximately the same level across the human atrial cardiomyocytes suggesting the presence of SK2-3 heteromeric channels.[84] Heijman et al. found a significantly increased apamin-sensitive current, I_{SK}, and a stronger apamin effect on the prolongation of AP in cAF versus control cardiomyocytes. However, this increase in I_{SK} was not attributed to increases in mRNA or protein levels of SK channel subunits. An increase in I_{SK} was attributed to reduced CaM-Threonine 80 phosphorylation due to increased PP2A levels in the SK channel complex.[85] No chamber-selective mRNA expression of *KCNN2* and *KCNN3* has also been reported, whereas the *KCNN1* transcript was found to be significantly decreased in control left ventricle compared to control RAA and left atrium.[86] When comparing AF and sinus rhythm tissue samples, *KCNN1* and *KCNN3* transcripts did not show a significant difference, while *KCNN2* was downregulated.[86] Of interest are the results of a study done by Bentzen et al. showing that the rs13376333 variant, which has been linked to an increased risk of AF[16], is associated with increased mRNA expression of *KCNN3* in human atrial tissue based on expression quantitative trait loci (eQTL) analysis.[87]

1.8. hiPSC-Derived Atrial Cardiomyocytes Model

A variety of animal models have been implemented to study inherited cardiac arrhythmias including murine, canine, and porcine models. One of the advantages of implementing an intact animal model is having the interaction between organ systems allowing one to study drug responses and effects on multiple metabolic processes. It is particularly important to have access to organ systems to study hepatotoxicity of the drugs and their ability to cross the blood-brain barrier. However, animal models cannot fully recapitulate human physiology and have a number of limitations including a different ion channel expression profile and therefore different cardiac physiology including a much higher heart rate than in humans.

Human-induced pluripotent stem cells (hiPSCs) are commonly obtained from human fibroblasts or peripheral blood mononucleated cells (PBMCs) for further reprogramming and differentiation allowing to obtain patient- and disease-specific phenotype cell lines. hiPSC-derived cardiomyocytes (hiPSC-CMs) have been increasingly popular in studying and modeling heart diseases and arrhythmias. Aside from providing a significant advantage in being widely commercially available, hiPSC-CMs have a more physiologically relevant ion channel expression profile and heart rate. hiPSC-CMs model is the closest model to native cardiomyocytes and cardiac tissue which are limited and difficult to obtain due to ethics and eligible patients undergoing heart surgeries.

1.9. Objectives and Hypothesis

I hypothesize that the rs13376333 variant is a loss-of-function variant of the *KCNN3* gene that will result in irregular beating, mimicking the AF phenotype, with a prolonged APD in genome edited hiPSC-aCMs when compared to their isogenic control.

In order to test this hypothesis, there are three objectives: (1) To genome edit hiPSCs using CRISPR-Cas9 technology to produce a new cell line carrying the rs13376333 variant within the *KCNN3* gene and its isogenic control; (2) To determine the effect of the rs13376333 variant on field potential duration, beat rate, spike amplitude, and conduction velocity with and without drug treatments (e.g., SK channel blocker/positive modulator) using a multielectrode array (MEA) instrument; (3) To

determine the effect of the rs13376333 variant on action potential duration and morphology using confocal (μ) optical mapping (OM) assay, including changes in electrophysiology of the cells in response to electrical stimulation.

Chapter 2.

Materials and Methods

2.1. hiPSC Cell Culture

2.1.1. Coating Plates

Non-tissue culture treated 6-well plates (Corning) were coated with Geltrex matrix (Gibco) diluted in DMEM/F12 medium (Gibco) to a final concentration of 1 mg/mL. Following coating, Geltrex was left to set for 1 hour prior to adding 1 mL/well of DMEM/F12 and storing in an incubator at 37ºC and 5% CO_2 for up to two weeks before use.

2.1.2. hiPSC Thawing

Wild-type and genome-edited hiPSC lines were stored as 1 mL aliquots in cryovials in liquid nitrogen. To thaw frozen hiPSCs, a cryovial was removed from the liquid nitrogen tank and placed in a warm bead bath to gently thaw the cells until small ice crystals were visible. The contents of the cryovial were then transferred to a 50 mL Falcon tube (Corning) and 10 mL of mTeSR Plus (STEMCELL Technologies) was gently added while slowly rotating the tube to avoid excessive osmotic stress. The cell suspension was centrifuged for 4-5 minutes at 1200 rpm at room temperature, and the supernatant was aspirated following centrifugation. The cell pellet was resuspended in 2 mL of mTeSR Plus supplemented with Rho-associated kinase (ROCK) inhibitor Y-27632 (Tocris Bioscience). Resuspended cells were then added to one well of a Geltrex coated 6-well plate for further maintenance and passaging.

2.1.3. hiPSC Maintenance and Passaging

Low passage wild-type hiPSCs were acquired from the Knollmann Lab where they were obtained from a healthy male donor (C2 control) in his late 20s (Caucasian, non-Hispanic). Cells were maintained in 6-well plates in mTeSR Plus medium which was changed daily. Upon reaching mature morphology and confluency of about 60-70% as seen in the microscope, cells were passaged using ReLeSR selection and passaging

reagent (STEMCELL Technologies). ReLeSR was added at 1 mL/well, aspirated, and hiPSCs were allowed to incubate for 4-6 minutes at 37ºC and 5% CO_2. mTeSR Plus (1-2 mL/well) was added to stop the dissociation reaction and the cells were then manually detached by tapping the plate and collecting them with a 5 mL serological pipette. Lifted hiPSCs were further transferred to a 50 mL Falcon tube and triturated by gently pipetting up and down. Clumps of a few hiPSC colonies were seeded at a split ratio of 1:10-1:20 in a 6-well plate containing 2 mL of mTeSR Plus supplemented with 1 µM of the ROCK inhibitor Y-27632.

2.2. Genome Editing Using CRISPR-Cas9

A low passage hiPSC line was used to introduce the variant of interest (rs13376333, C>T) using CRISPR-Cas9 technology. Benchling software was used to design a CRISPR-Cas9 construct including sequencing primers, single-stranded oligodeoxynucleotides (ssODNs) and single-guide RNAs (sgRNAs) specific to the *KCNN3* gene and region of interest. The protocol kindly provided by the Lynn lab at BC Children's Hospital Research Institute was adapted to introduce the variants in our hiPSC line.

2.2.1. hiPSC DNA Sequencing

Prior to initiating the genome editing protocol and introducing the variant, a specific region of interest containing location of the rs13376333 variant was sequenced to ensure the wild-type genotype of our cell line. Following hiPSC dissociation as described above (Method 2.1.3), DNeasy Blood & Tissue Kit (Qiagen) was used to extract DNA from a cell pellet. The following polymerase chain reaction (PCR) contained 10 µM forward (FWD) and reverse (REV) sequencing primers, DNA template obtained using the DNeasy Kit, Taq 2X Master Mix (New England BioLabs), SYBR Safe DNA Gel Stain (Invitrogen), and double-distilled H_2O (ddH_2O). The PCR reaction contained steps for initial denaturation, denaturation, primer-specific annealing, extending and final extension. The correct PCR product was confirmed with gel electrophoresis, purified using QIAquick PCR Purification Kit (Qiagen) and sent for DNA sequencing.

2.2.2. Designing rs13376333 CRISPR-Cas9 Construct

To design the construct, the human DNA sequence of the *KCNN3* gene and the location of the rs13376333 variant was looked up on Benchling. Then a protospacer adjacent motif (PAM) sequence (5'-NGG-3'), recognized by the Cas9 protein, was found along with the cut site, which should optimally be about 3-4 nucleotides upstream of the PAM site. To improve efficiency of the homology-directed repair (HDR) instead of non-homologous end joining (NHEJ), a silent mutation was introduced into the PAM site (AGG → AGA; Arginine) to prevent Cas9 from re-cutting the region after the point mutation had been inserted. sgRNA pairs were run through the Benchling algorithm and the most optimal ones were picked based on their on- and off-target effects, length (25 base pairs, bp), GC content, and melting temperatures (Tm). The ssODN was designed around the cut site as indicated in Figure 2.1 with one PAM-proximal 91 bp arm and one PAM-distal 36 bp arm. The sequences for the primers, ssODN, and sgRNAs CRISPR-Cas9 design for the rs13376333 variant insertion can be found in Table 2.1.

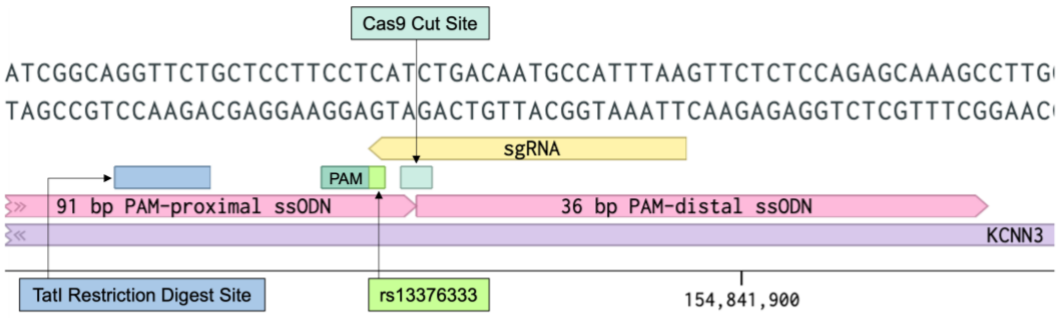

Figure 2.1 CRISPR-Cas9 construct design within intronic region between exon 1 and 2 of the *KCNN3* gene.

A zoomed in portion of the intronic region between exon 1 and exon 2 of the *KCNN3* gene showing the location of the rs13376333 variant and CRISPR-Cas9 construct design. Two arms of the ssODN, proximal and distal to PAM, are labeled in pink; PAM is labeled in dark green along with sgRNA in yellow and TatI restriction digest site in blue. Visualized using Benchling.

Table 2.1. rs13376333 CRISPR-Cas9 Design

FWD Sequencing Primer	5' CCTGTTATTCCATCACAGAGCCC 3'
REV Sequencing Primer	5' AAGGTTCTGGTTTGGAGCACTCCC 3'
ssODN (+)	/5Phos/GGGGCTGTGCAGGGCTGGGGAGAGCGGGCTGAGTGTGT GCAGATGGCCTATTGGGAGGTCATGGGATCGGCA**AGTACT**GCTC CTTTCTTATCTGACAATGCCATTTAAGTTCTCTCCAGAGCAAAGC
sgRNA FWD	/5Phos/CACCGTTAAATGGCATTGTCAGATG
sgRNA REV	/5Phos/AAACCATCTGACAATGCCATTTAAC

Note: FWD = forward; REV = reverse; underlined is restriction digest site (GGTTCT → AGTACT). Silent PAM mutation (C→T). rs13376333 variant (C→T)

2.2.3. Designing *KCNN3* Knock-out CRISPR-Cas9 Construct

The CRISPR-Cas9 construct for the knock-out of the SK3 channel was designed based on modifying exon 6 of the *KCNN3* gene to have a premature stop codon. Similar to designing a genome editing construct for the insertion of the rs13376333 variant, a PAM sequence was found along with the cut site located 3 nucleotides upstream of it. A silent mutation was introduced into the PAM site (GTC→ GTT; Valine) to improve efficiency of the HDR and prevent Cas9 from re-cutting the region following the insertion of the point mutation. sgRNA pairs were run through the Benchling algorithm and the most optimal ones were picked based on their on- and off-target effects, length, GC content, and Tm. The ssODN was designed around the cut site as indicated in Figure 2.2 with PAM-proximal and PAM-distal arms. The sequences for the primers, ssODN, and sgRNAs CRISPR-Cas9 design for the SK3 channel knock-out can be found in Table 2.2.

The point mutation for the knock-out construct replaced the third nucleotide of Tryptophan (TGG → TGA) to introduce an early stop codon in the exon 6 of the *KCNN3* gene and activate the NMD pathway.

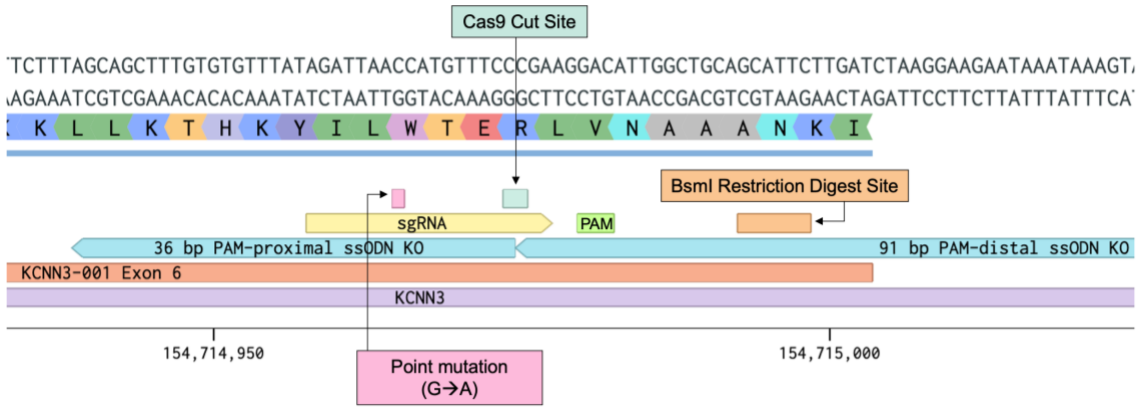

Figure 2.2 CRISPR-Cas9 construct design to produce a point mutation within exon 6 of the *KCNN3* gene.

A zoomed in portion of exon 6 of the *KCNN3* gene showing the CRISPR-Cas9 construct design for SK3 knock-out. Two arms of the ssODN, proximal and distal to PAM, are labeled in blue; PAM is labeled in bright green along with sgRNA in yellow and BsmI restriction digest site in orange. Visualized using Benchling.

Table 2.2. SK3 Channel Knock-Out CRISPR-Cas9 Design

FWD Sequencing Primer	5' CCCAGTCTGGTCATCTGATG 3'
REV Sequencing Primer	5' GTGCCCGGCCTTAATCATCTT 3'
ssODN (+)	/5Phos/CCACAAAAATGAACCTAAGAAAATGAACCTGATAGCAGCCT ACTTTATTTATTCTTCCTTAGATCAA**GAATGCT**GCAGCCAATGTTCT TCGGGAAACATGATTAATCTATAAACACACAAAGCTGCT
sgRNA FWD	/5Phos/CACCGAGATTAACCATGTTTCCCGA
sgRNA REV	/5Phos/AAACTCGGGAAACATGGTTAATCTC

Note: FWD = forward; REV = reverse; underlined is restriction digest site (GAATGCT). Silent PAM mutation (C→T). rs13376333 variant (G→A)

2.2.4. sgRNA Preparation

sgRNAs were annealed into a duplex containing forward and reverse sgRNAs by setting up a PCR reaction and cycling at 95ºC for 5 minutes followed by a ramp down to 25ºC at a rate of 5ºC/min. The duplex was then cloned into the pCCC vector using Golden-Gate cloning.

2.2.5. hiPSC Transfection

hiPSCs were transfected in a 6-well plate using Lipofectamine 3000 (Invitrogen) reagents combined with 5000 ng pCCC-KCNN3 and 10 pmol ssODN according to the outlined protocol. Positive control condition contained 5000 ng of pmax Cloning Vector and control plasmid containing GFP (Lonza). Transfected cells were sorted using a fluorescence-activated cell sorting (FACS) instrument (BD FACS Aria II) and seeded into a new 6-well plate containing 2 mL mTeSR Plus, 1x CloneR (STEMCELL Technologies), and 100 µM penicillin-streptomycin antibiotic (Gibco). Following cell sorting, the cells were allowed to reach confluency and colonies were manually picked into 96-well plates (clonal isolation). The cells were observed and wells containing viable colonies noted and passaged into two 96-well plates for DNA sequencing and further expansion. DNA was extracted using QuickExtract DNA Extraction Solution (Lucigen) and amplified with a PCR reaction before sending the lysate for sequencing. Wild-type and positive homozygous and heterozygous clones were expanded and frozen for future experiments.

2.3. hiPSC Differentiation

To seed hiPSCs for differentiation, cells were dissociated from a 6-well plate according to the passage methods described above (Method 2.1.3). Resuspended hiPSCs were manually broken down into single cells or colonies of few cells by gently pipetting up and down prior to seeding for differentiation. Cells were seeded at seeding density of 200,000 cells/mL/well of a 6-well plate and maintained with daily changes of mTeSR Plus medium until 80% confluency was reached. Differentiation was then initiated (day 0) using a GSK3 inhibitor and Wnt signaling pathway activator CHIR99021 (Tocris Bioscience) at 12 μM in Roswell Park Memorial Institute (RPMI)-1640 basal medium with L-glutamine (Gibco) supplemented with B27 minus insulin (Gibco). The medium was replaced 24 hours later (day 1) with RPMI-1640 and B27 minus insulin. On day 3, half medium change (conditioning) was performed with RPMI-1640 and B27 minus insulin supplemented with 5 μM Wnt inhibitor IWP-4 (Tocris Bioscience). hiPSCs were differentiated into atrial cardiomyocytes (aCM) according to our lab's optimized version of existing differentiation protocols.[88,89] To produce hiPSC-aCMs, a protocol using retinoic acid (RA) at early stages of differentiation was implemented since it has shown to promote mostly atrial and some nodal cell programming.[89] To facilitate differentiation into aCMs, 0.75 μM RA (dose timing and concentration were optimized by former lab members Sarabjit Sangha and Marvin Gunawan) was added days 4-6 of differentiation with RPMI-1640 and B27 minus insulin medium changes at day 5 and 6.[89] On day 7, the medium was changed to maintenance medium RPMI-1640 supplemented with B27 with insulin. Thereafter, the maintenance medium was changed every 3 days. To purify hiPSC-derived aCMs from fibroblasts, a metabolic selection protocol with RPMI-1640 containing L-glutamine and no D-glucose (Gibco) supplemented with 5 mM sodium L-lactate (Sigma) and B27 with insulin was induced on day 10.

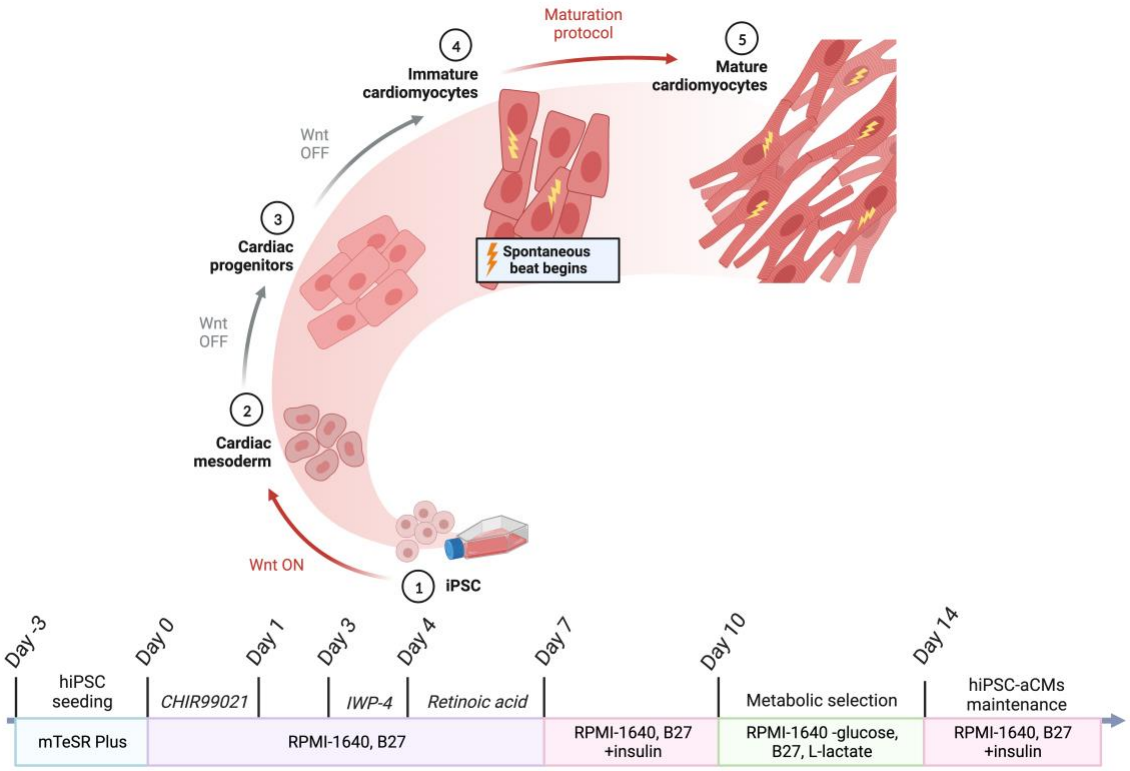

Figure 2.3 Differentiation of hiPSCs into hiPSC-derived atrial cardiomyocytes. hiPSCs were seeded at a specific cell density and allowed to reach about 80% confluency before initiating differentiation. Differentiation was started with the activation of the Wnt pathway with the small molecule CHIR99021 which is later deactivated with another small molecule IWP-4. Retinoic acid was used to activate cellular pathways leading to atrial-like hiPSC-derived CMs. To decrease the presence of cell types other than hiPSC-aCMs, chemical metabolic selection was implemented by utilizing the ability of hiPSC-aCMs to use L-lactate as energy source. The cells were further maintained in RPMI-1640 medium supplemented with B27 and insulin. Created with BioRender.com.

2.4. Multielectrode Array

A Maestro Pro (Axion BioSystems) multielectrode array (MEA) instrument was used to assess any changes in field potential duration (FPD), beat period, spike amplitude (SA), and conduction velocity (CV) of wild-type isogenic control hiPSC-aCMs and heterozygous rs13376333$^{+/-}$ hiPSC-aCMs.

2.4.1. MEA Plate Coating

Fibronectin (STEMCELL Technologies) was used to coat 24-well CytoView MEA plates (Axion BioSystems). Fibronectin that was diluted to a final concentration of 50 µg/mL was kept on ice while coating MEA plates to prevent the matrix from solidifying.

Sterile ddH_2O was added to the outside rim of the plate which was then placed in a 37ºC and 5% CO_2 incubator for 1-2 hours. Following incubation time, the plate was used immediately for hiPSC-aCMs replating.

2.4.2. Cell Replating on MEA Plates

Following metabolic selection, the hiPSC-aCMs were dissociated from 6-well plates for replating onto 24-well CytoView MEA plates. First, the cells were incubated in TrypLE Express Enzyme (Gibco) for 8-12 minutes and RPMI-1640 supplemented with B27 and insulin was added to stop the reaction. The cells were manually dissociated from the wells using a 5 mL serological pipette and transferred into a 50 mL Falcon tube. The cells were then centrifuged for 4-5 minutes at 1200 rpm at room temperature. The supernatant was aspirated, and the cell pellet resuspended in RPMI-1640 with B27 containing insulin and supplemented with Y-27623 and triturated by manually pipetting up and down with a 5 mL serological pipette to achieve single-cell clumps. The cells were seeded at 50,000 cells/mL per each well of the 24-well CytoView plate. The medium was changed the next day and thereafter replaced every 3 days.

2.4.3. Drug Treatment Preparation and Dilution

All drugs were dissolved in DMSO, with the exception of apamin which was dissolved in ddH_2O and diluted to stock concentrations for storage in small aliquots stored at -20ºC. Stock concentrations varied based on desired working concentrations to avoid exceeding a final concentration of 0.1% DMSO in prepared solutions.

2.4.4. MEA Recordings

Replated hiPSC-aCMs were allowed to adhere and stabilize following replating for 7 days prior to obtaining data. Recordings were made prior to (pre-treatment) and following application of drug treatments (post-treatment) including spontaneous and electrically paced conditions for 60 seconds per recording. AxIS Navigator Software (Axion BioSystems) was used to analyze hiPSC-aCMs behaviour in real time, manipulate electrical stimulation, and to collect data for FPD and contractility configurations. The following parameters were set and maintained for electrical stimulation at 1 Hz, 2 Hz, and 3 Hz: stimulus duration = 400 µs; voltage = 800 mV; max

current = 40 µA. The following treatments were tested using the MEA assay: DMSO control (0.1%), apamin (100 nM), CyPPA (1 µM), and ivabradine (2 µM). The concentration of DMSO did not exceed 0.1%.

2.5. Optical Mapping

Two setups of optical mapping (OM) were utilized to analyze Ca^{2+} transients (CaTs) and AP morphology in hiPSC-aCMs: high-speed (1000 fps) optical mapping (HS-OM) and confocal optical mapping (µOM). Data collection was performed on hiPSC-aCMs from at least three independent differentiation batches.

2.5.1. Coating Dishes and Coverslips

Geltrex was used as the matrix of choice for both 35 mm polymer µ-dishes (Ibidi) and custom-ordered 25 mm polymer coverslips (Ibidi) and the coating was done with Geltrex diluted in DMEM/F12 medium as described above for monolayer adherence. Coated dishes and coverslips were left to set for 1 hour prior to replating.

2.5.2. Cell Replating on Dishes and Coverslips

Metabolically selected hiPSC-derived aCMs were dissociated from a 6 well plate for replating onto polymer dishes and coverslips. The cells were incubated with TrypLE Express Enzyme for 8-12 minutes, and the dissociation reaction was stopped with RPMI-1640 medium supplemented with B27 and insulin. The cells were manually dissociated from the wells using a 5 mL serological pipette and transferred into a 50 mL Falcon tube. Following centrifugation for 4-5 minutes at 1200 rpm at room temperature, the supernatant was aspirated, and the cell pellet was resuspended in RPMI-1640 with B27 containing insulin and supplemented with Y-27623. Cell suspension was triturated by manually pipetting up and down with a 5mL serological pipette to achieve single-cell clumps. The cells were seeded at 300,000 cells/mL per each dish and coverslip. The medium was changed the next day and thereafter replaced every 3 days.

2.5.3. Imaging Solution Preparation

Ca^{2+} Tyrode's solution was made in-house and stored at -20ºC in 50 mL aliquots. The following ion concentrations were used (in mM): 117 NaCl, 5.7 KCl, 4.4 $NaHCO_3$, 1.5 NaH_2PO_4-H_2O, 1.7 $MgCl_2$, 10 Na-HEPES ($C_8H_{18}N_2O_4S$), 5 glucose, 5 creatine, 5 Na-Pyruvic acid, 1.8 $CaCl_2$. The media was replaced with Ca^{2+} Tyrode's solution prior to imaging and allowed to equilibrate for 20 min in a 37ºC and 5% CO_2 incubator. Ca^{2+} Tyrode's solution containing MOPS was used for µOM to control for 5% CO_2 concentration due to limitations of the setup.

2.5.4. High-Speed Optical Mapping

High-speed OM utilized a SciMedia rig with a frame rate of 1000 fps with a CMOS camera. The setup included environmental chamber to control for 37ºC temperature and 5% CO_2 gas concentration. Isogenic control and heterozygous variant hiPSC-aCMs replated on 35 mm polymer dishes were imaged using Calbryte 520 (AAT Bioquest) calcium indicator and physiological probe (Ex: 493 nm, Em: 515 nm). Parameters such as Ca^{2+} transients (CaTs) along with activation maps and space maps of the atrial potential conduction, and conduction velocity vectors were measured for spontaneous beating and electrical stimulation conditions of 1 Hz, 2 Hz, and 3 Hz. Each recording had a duration of 10 s.

2.5.5. Confocal Optical Mapping

Confocal OM, or µOM, setup was based on a Leica SP8 confocal microscope and was used to record CaT, Ca^{2+} sparks and voltage at a lower temporal resolution (100 fps or 10 ms). Prior to imaging, coverslips containing replated wild-type and heterozygous variant hiPSC-aCMs following metabolic selection were loaded with two fluorescent probes: Calbryte 630 (Ex: 607 nm, Em: 624 nm) (AAT Bioquest), a Ca^{2+} probe, and FluoVolt (Invitrogen), a membrane potential (Vm) probe (Ex: 491 nm, Em: 516 nm; FITC spectrum). The parameters were recorded at spontaneous beating rate and electrically stimulated 1 Hz, 2 Hz, and 3 Hz. Sample coverslips were contained within a temperature-controlled environmental chamber (LCI, Seoul, Korea) maintained at 37ºC and 5% CO_2 was controlled with in-house made MOPS Tyrode's solution. Recordings were made before adding any drug treatments (pre-treatment) from multiple

regions of interests (ROIs) in the following order: spontaneous beating; electrical stimulation at 1 Hz, 2 Hz, and 3 Hz. Treatments were further added at specified concentrations and allowed to equilibrate for 5-10 minutes before proceeding with recordings. Ivabradine was the first treatment added following by a media change containing apamin. Post-treatments recordings were made accordingly at spontaneous beating rate and electrically stimulated 1 Hz, 2 Hz, and 3 Hz.

Table 2.2 Confocal OM Leica SP8 settings.

Leica SP8 Settings			
Logical size of the image	256 (X-direction) x 128 (Y-direction) pixels	**Refractive index**	1.451
Pixel size	0.181 µm	**Zoom**	4
Field of view	X: 46.13 µm; Y: 22.98 µm	**Pinhole**	102.8
Scan mode	xyt	**Pinhole airy**	1 AU
Scan direction and speed	Bidirectional; 8,000 Hz	**Laser WLL**	70%
Objective/immersion	63x/1.30 GLYC 37ºC	**Laser: Calbryte 630 (HyD4)**	Ex=607nm/Em=615-740nm; Gain=50.6; Gating=0.3ns-6ns
NA	1.3	**Laser: FluoVolt (HyD2)**	Ex=488nm/Em=500-567nm; Gain=50.6; Gating=0.3ns-6ns

2.6. Statistical Analysis

Data were reported as mean ± SEM unless noted otherwise. All data were analyzed using Microsoft Excel, R, and GraphPad Prism using a two-way ANOVA test unless specified otherwise. Normality of the data was analyzed visually and using Shapiro Wilk test in R, and an F-Test was applied to test for equal variance assumption for parametric tests. The µOM data for AP were averaged from 10 consecutive cycles and normalized to convert fluorescence intensity to the scale of 0 to 1. Duration measurement for waveform and duration analysis starts at 50% of upstroke and ends with the indicated percentage of repolarization. Where applicable, p-value was reported for two-way ANOVA tests. Significance levels for all statistical analysis were set at *p<0.5, **p<0.01, ***p<0.001, ****p<0.0001.

Chapter 3.

Results

3.1. Genome Editing Using CRISPR-Cas9 Technology

3.1.1. Fluorescence-Activated Cell Sorter (FACS) Analysis

FACS was used to select for and separate hiPSCs expressing GFP from hiPSC colonies that did not successfully undergo Lipofectamine 3000 transfection with the designed ssODN which includes the desired nucleotide base changes such as point mutations, silent PAM mutations, and restriction digest site. Both negative and positive controls were included to confirm the absence of contamination with other DNA and to ensure plasmid insertion, expression, and adequate GFP expression in our cell line. The hiPSC population transfected with the rs13376333$^{+/-}$ construct contained 0.1% GFP-positive cells (Figure 3.1) which were successfully seeded into a new 6-well plate for further manual colony picking and DNA sequencing to confirm correct insertion of the variant. hiPSCs transfected with the CRISPR-Cas9 construct designed to produce a functional knock-out of the SK3 channel had a similar efficiency of 0.1% GFP-positive events of the total population (Figure 3.2) which were seeded into a 6-well plate for manual colony picking and DNA sequencing.

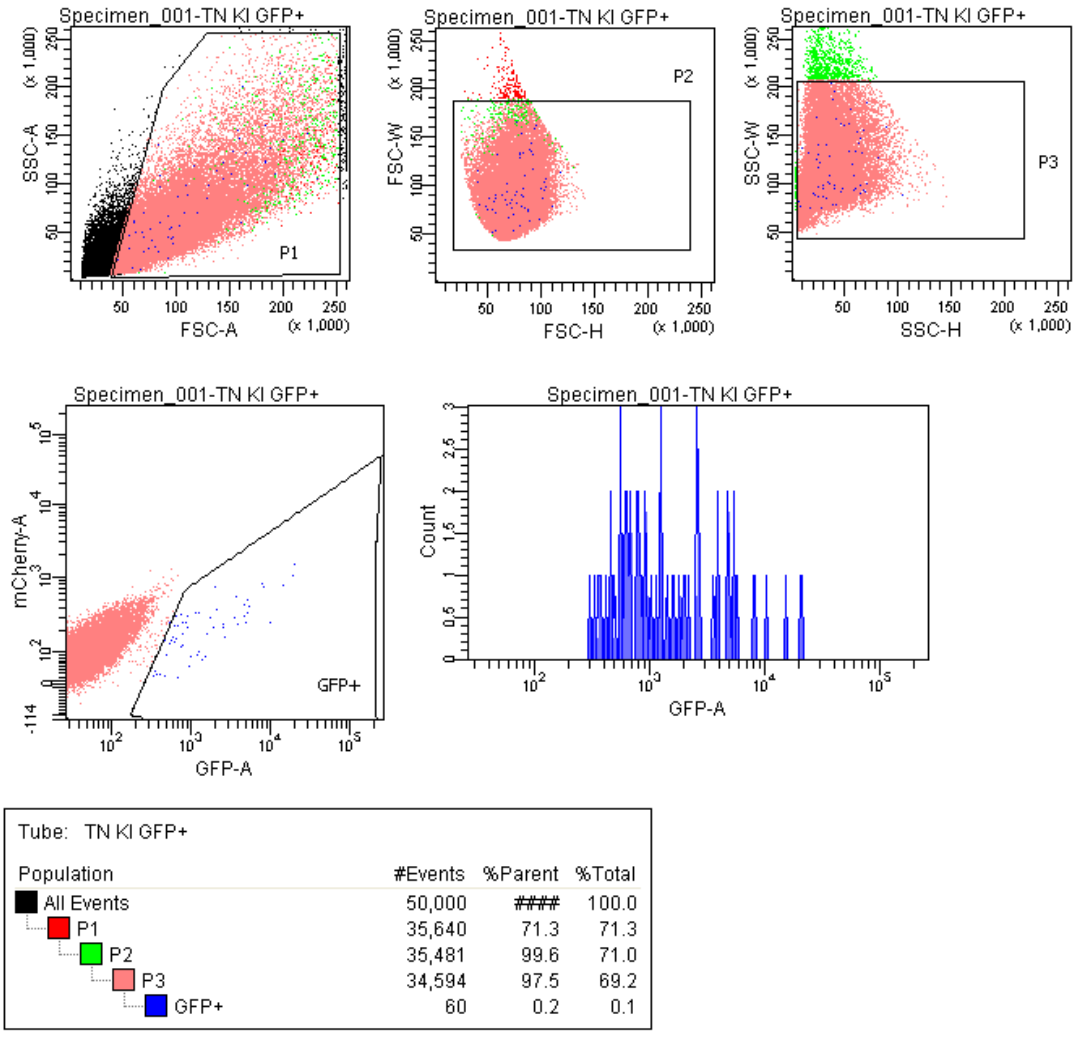

Tube: TN KI GFP+

Population	#Events	%Parent	%Total
All Events	50,000	####	100.0
P1	35,640	71.3	71.3
P2	35,481	99.6	71.0
P3	34,594	97.5	69.2
GFP+	60	0.2	0.1

Figure 3.1. FACS of rs13376333$^{+/-}$ hiPSCs 72 hours post-transfection with Lipofectamine 3000.

Fluorescence-activated cell sorting (FACS) of hiPSCs transfected with a CRISPR-Cas9 construct containing the ssODN carrying the rs13376333 C→T variant; GFP positive events constitute 0.1% of total events.

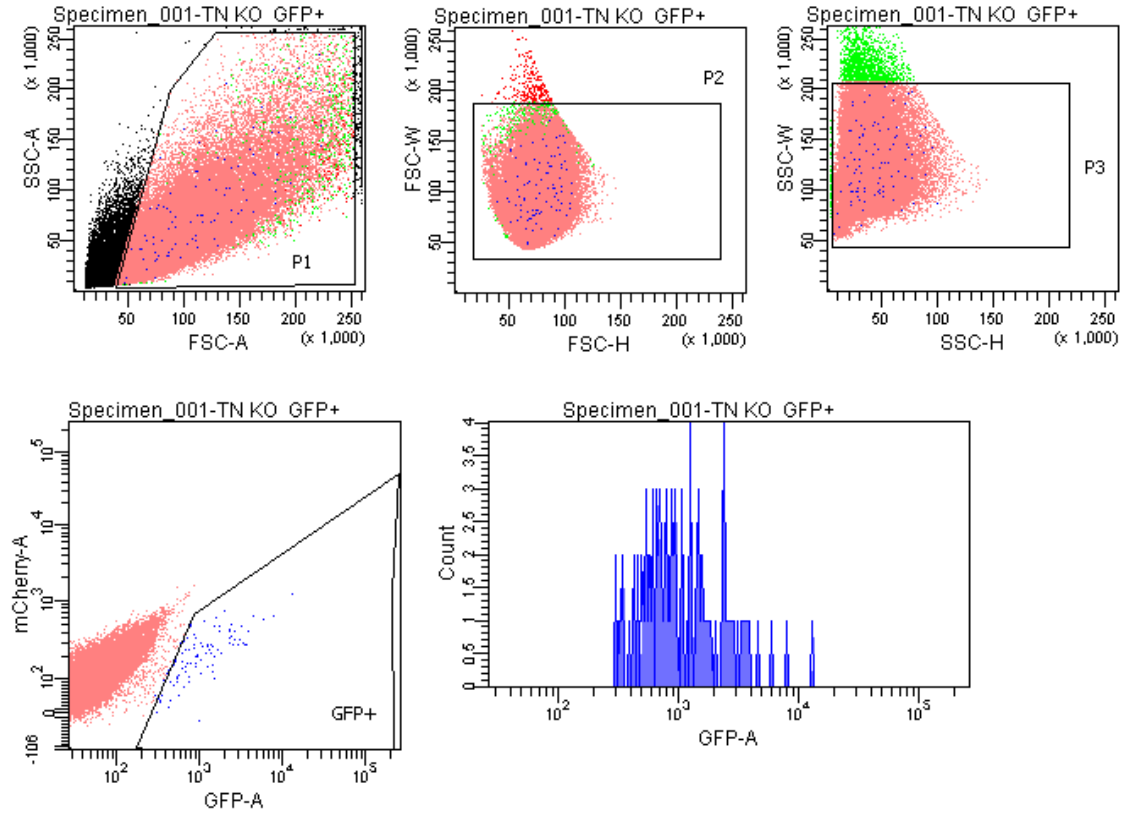

Tube: TN KO GFP+

Population	#Events	%Parent	%Total
All Events	73,920	####	100.0
P1	54,292	73.4	73.4
P2	54,044	99.5	73.1
P3	52,598	97.3	71.2
GFP+	95	0.2	0.1

Figure 3.2. FACS of SK3 knock-out hiPSCs 72 hours post-transfection with Lipofectamine 3000.

Fluorescence-activated cell sorting (FACS) of hiPSCs transfected with a CRISPR-Cas9 construct containing ssODN carrying the premature stop codon for the SK3 knock-out; GFP positive events constitute 0.1% of total events.

3.1.2. Sanger Sequencing of GFP-Positive Clones to Confirm the Genotype of the Transfected hiPSC Cell Line

Following FACS, hiPSCs transfected with the rs13376333 variant and the knock-out constructs were allowed to sufficiently grow for manual colony picking and expansion of the individual clones. Sanger sequencing was used to identify isogenic control clones and clones which were either homo- or heterozygous for the insertion of the respective construct. All of the 21 hiPSC colonies picked for potential insertion of the knock-out

construct showed wild-type genotype and NHEJ. Therefore, there was no successful insertion of the SK3 knock-out construct. There were 19 hiPSC colonies that survived through expansion and passaging which were picked from the 6-well plate containing potentially positive clones for the rs13376333 variant insertion. Two of these colonies showed successful heterozygous insertion of the intronic rs13376333 variant as well as silent PAM mutation and TatI restriction digest site (Figure 3.3). One of the two clones (B11) showed better survival and growth in culture, as well as more efficient and successful differentiation into hiPSC-aCMs as demonstrated by a uniform 2D spontaneously beating monolayer and was picked for all further experiments.

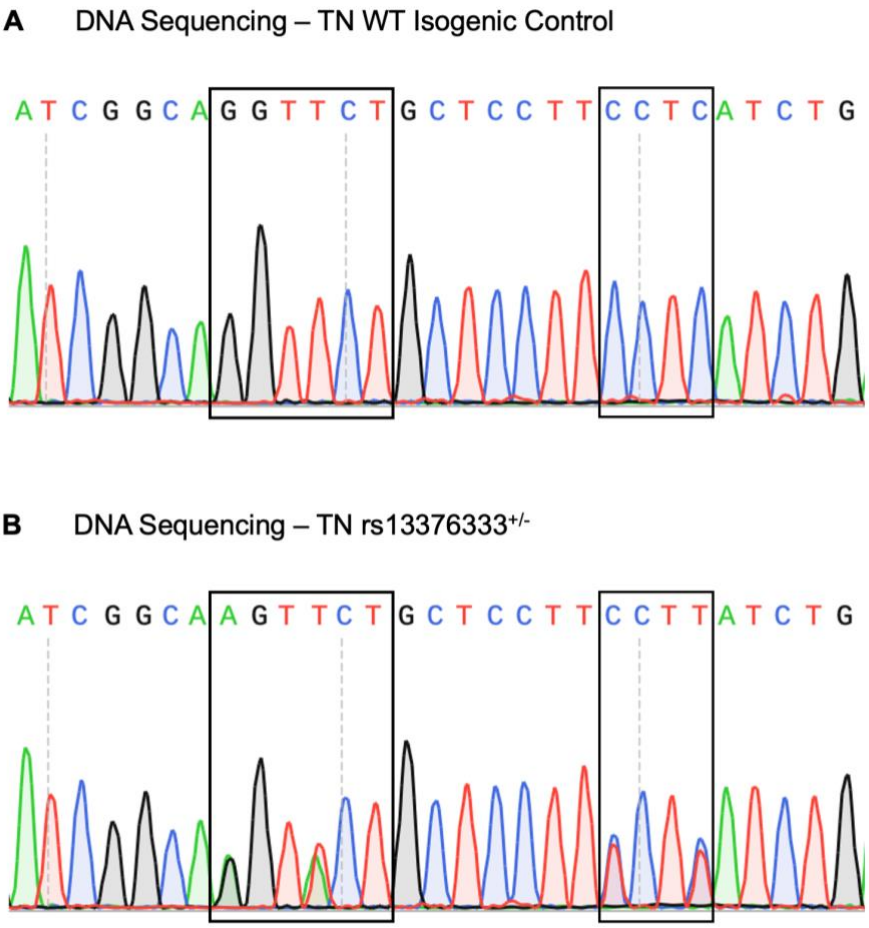

Figure 3.3. DNA sequencing results of the intronic region between exon 1 and 2 of the *KCNN3* gene.

(A) Sanger sequencing results confirming the wild-type genotype in an isogenic control clone; (B) Sanger sequencing results from the rs13376333 variant B11 clone showing successful heterozygous insertion of the ssODN containing the variant (C→T), silent PAM mutation (C→T), and TatI restriction digest site (GGTTCT → AGTTCT). Sequences visualized using SnapGene Viewer.

3.2. MEA

To compare and analyze the differences between beat period, FPD, and other parameters in wild-type (WT) and rs13376333$^{+/-}$ hiPSC-aCMs, one-minute recordings were made using the MEA instrument including both no electrical stimulation and electrical stimulation (1 Hz, 2 Hz, 3 Hz) conditions with and without addition of drug treatments. In this MEA assay, FPD reflects the time (ms) from the depolarization spike to the peak of the T-wave, whereas beat period (ms) is measured as the time between successive depolarizations. Spike amplitude (mV) is the peak-to-peak (positive plus negative) amplitude of the depolarization spike. Conduction velocity (CV; mm/ms) is measured as the speed of depolarization propagation across the culture. Data from the Axion MEA recordings were extracted using Axion Metric Plotting Tool software, and the GraphPad Prism software was used to produce the boxplots for the beat period mean, FPD mean, spike amplitude velocity mean, and CV mean in WT and heterozygous variant hiPSC-aCMs.

3.2.1. Intrinsic Beating Rate is Increased in rs13376333$^{+/-}$ hiPSC-aCMs

A high intrinsic beating rate (>60 bpm) affected the ability of hiPSC-aCMs to fully entrain to lower frequencies of electrical field stimulation frequencies below the intrinsic beating rate. None of the wells containing WT hiPSC-aCMs were observed to entrain to 1 Hz; 18/18 wells entrained to 2 Hz and 3 Hz electrical field stimulation. Within rs13376333$^{+/-}$ hiPSC-aCMs wells, none entrained to 1 Hz, 3/24 wells entrained to 2 Hz and 20/24 wells entrained to 3 Hz electrical field stimulation. For this reason, data points collected with electrical stimulation at 1 Hz in both wild-type and rs13376333 hiPSC-aCMs were excluded from analysis.

The average pre-treatment beating rate of WT hiPSC-aCMs was 113 ± 1 bpm which was significantly slower ($p<0.001$) than the average pre-treatment beating rate of rs13376333$^{+/-}$ hiPSC-aCMs of 150 ± 7 bpm. Additionally, both FPD (wt: 134 ± 3 ms; rs: 94 ± 3 ms; $p<0.001$) and beat period (wt: 534 ± 3 ms; rs: 416 ± 15 ms; $p<0.001$) were significantly reduced in the variant-carrying hiPSC-aCMs compared to the control reflecting the observed higher beating rate of the hiPSC-aCMs with the rs13376333 variant. Prior to addition of any drug treatments, FPD was also significantly reduced in rs13376333+/- hiPSC-aCMs compared to WT hiPSC-aCMs when electrically stimulated

at 3 Hz (wt: 128 ± 2 ms; rs: 96 ± 3 ms; p<0.001). There was no significant difference between spike amplitude of WT and rs13376333$^{+/-}$ hiPSC-aCMs without electrical stimulation and when paced at 2 Hz and 3 Hz. No difference was observed between CV of WT and rs13376333+/- hiPSC-aCMs except when paced at 3 Hz (wt: 0.29 ± 0.01 mm/ms; rs: 0.33 ± 0.01 mm/ms; p<0.05).

Most drug solutions were made using DMSO as a solvent, therefore the effect of the maximum DMSO concentration (0.1%) was tested. There were no significant differences in FPD, beat period, spike amplitude, and CV without and with electrical field stimulation at 2 Hz, or 3 Hz in WT and rs13376333$^{+/-}$ hiPSC-aCMs with addition of 0.1% DMSO (Figure 3.4).

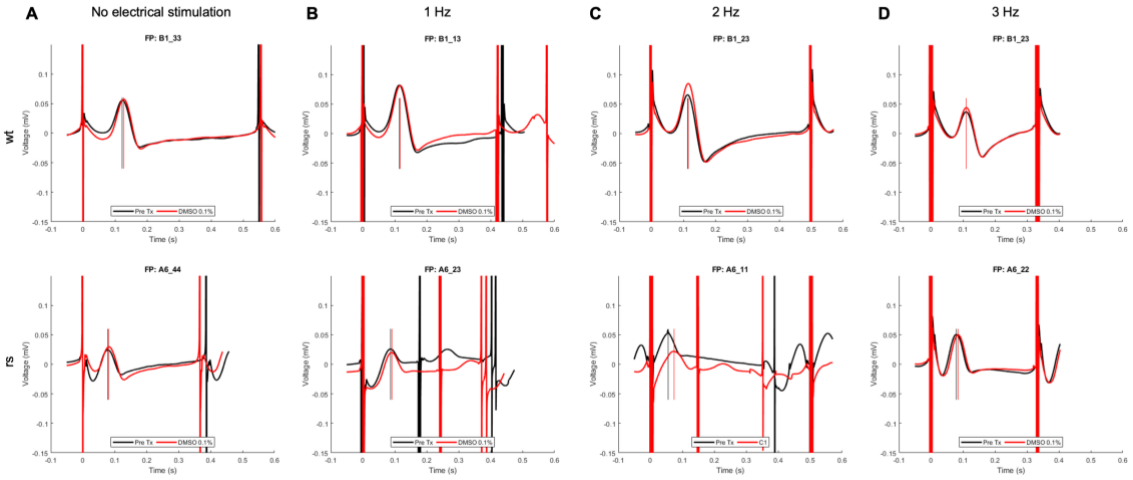

Figure 3.4 Field potential traces of wild-type and rs13376333$^{+/-}$ hiPSC-aCMs before and after treatment with 0.1% DMSO.
Representative field potential (FP) traces obtained with the Axion MEA instrument of wild-type (wt, top panel) and rs13376333$^{+/-}$ (rs, bottom panel) hiPSC-aCMs before and after treatment with 0.1% DMSO. Representative traces of (A) non-electrically stimulated hiPSC-aCMs, (B) paced at 1 Hz, (C) paced at 2 Hz, and (D) paced at 3 Hz. Each beat waveform is an average of 5 beats from the stable region. Black traces represent pre-treatment recordings, while post-treatment recordings are showed in red. Vertical lines indicate FPD measurement.

3.2.2. Apamin Increases FPD in Wild-Type hiPSC-aCMs with No Effect on rs13376333$^{+/-}$ hiPSC-aCMs

Apamin (100 nM) did not produce a significant increase in FPD of WT hiPSC-aCMs without electrical pacing (before: 129 ± 6 ms; after: 152 ± 5 ms) and paced at 2 Hz (before: 132 ± 4 ms; after: 156 ± 3 ms), and 3 Hz (before: 119 ± 5 ms; after: 135 ± 4 ms) (Figure 3.8B). Furthermore, application of 100 nM apamin did not have an effect on beat

period of WT hiPSC-aCMs without electrical stimulation (before: 524 ± 0 ms; after: 538 ± 0 ms) (Figure 3.10B). Spike amplitude was not significantly altered in WT hiPSC-aCMs with addition of 100 nM apamin without pacing (before: 4.9 ± 0.3 ms; after: 5.4 ± 0.4 ms) and when paced at 2 Hz and 3 Hz (Figure 3.11B). There was no effect of 100 nM apamin on conduction velocity in WT hiPSC-aCMs without electrical stimulation, and with pacing at 2 Hz and 3 Hz (Figure 3.13B).

Treatment with 100 nM apamin did not result in any change in FPD, beat period, spike amplitude, and CV in rs13376333$^{+/-}$ hiPSC-aCMs without pacing and paced at 2 Hz and 3 Hz (Figures 3.8B, 3.10B, 3.11B, 3.13B).

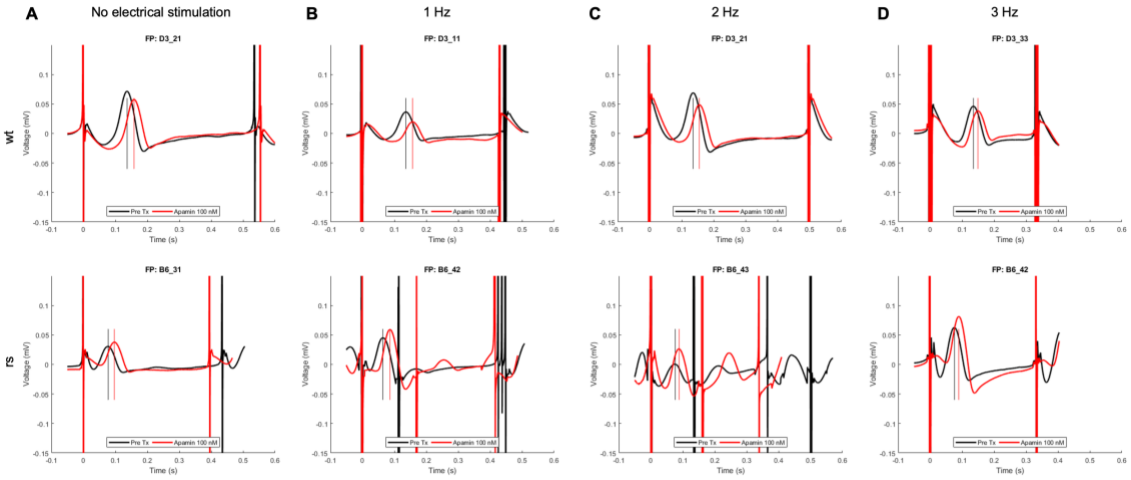

Figure 3.5 Field potential traces of wild-type and rs13376333$^{+/-}$ hiPSC-aCMs before and after treatment with 100 nM apamin.

Representative field potential (FP) traces obtained with the Axion MEA instrument of wild-type (wt, top panel) and rs13376333$^{+/-}$ (rs, bottom panel) hiPSC-aCMs before and after treatment with 100 nM apamin. Representative traces of (A) not electrically stimulated hiPSC-aCMs, (B) paced at 1 Hz, (C) paced at 2 Hz, and (D) paced at 3 Hz. Each beat waveform is an average of 5 beats from the stable region. Black traces represent pre-treatment recordings, while post-treatment recordings are showed in red. Vertical lines indicate FPD measurements.

3.2.3. CyPPA Decreased Conduction Velocity in Wild-Type and rs13376333$^{+/-}$ hiPSC-aCMs

CyPPA is an SK channel positive modulator which binds within the CaM-CaMBD interface and increases channel activation via Ca^{2+} regulation[90]. FPD of WT hiPSC-aCMs was not significantly changed without electrical stimulation and paced at 2 Hz and 3 Hz. In rs13376333+/- hiPSC-aCMs, addition of 1 µM CyPPA did not significantly alter FPD when the cells were not electrically stimulated and when paced at 2 Hz and 3 Hz.

Furthermore, beat period was not significantly increased or decreased in non-stimulated WT hiPSC-aCMs treated with 1 μM CyPPA (before: 535 ± 0 ms; after: 560 ± 0 ms). There was no significant effect of 1 μM CyPPA on beat period of rs13376333$^{+/-}$ hiPSC-aCMs.

In WT hiPSC-aCMs, treatment with 1μM CyPPA resulted in a significant decrease in CV when paced at 3 Hz (before: 0.29 ± 0.01 mm/ms; after: 0.23 ± 0.01 mm/ms; $p<0.001$) but not without pacing and pacing at 2 Hz. Conduction velocity was not significantly changed before and after the addition of 1 μM CyPPA in rs13376333$^{+/-}$ hiPSC-aCMs without electrical and paced at 2 Hz and 3 Hz.

There were no significant changes in spike amplitude with the addition of 1 μM CyPPA in both WT and rs13376333$^{+/-}$ hiPSC-aCMs with either no electrical stimulation or pacing at 2 Hz and 3 Hz (Figure 3.12A).

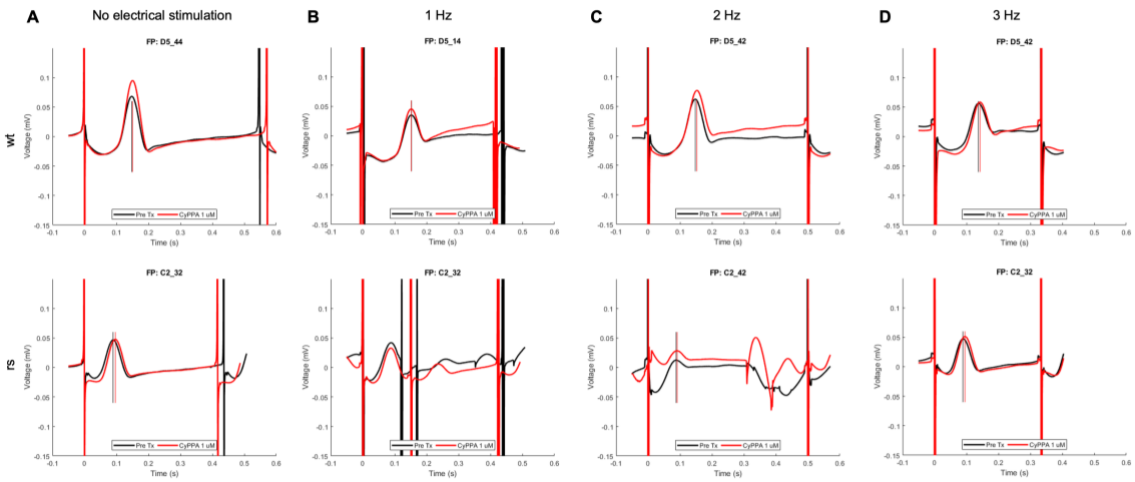

Figure 3.6 Field potential traces of wild-type and rs13376333+/- hiPSC-aCMs before and after treatment with 1 μM CyPPA.
Representative field potential (FP) traces obtained with the Axion MEA instrument of wild-type (wt, top panel) and rs13376333$^{+/-}$ (rs, bottom panel) hiPSC-aCMs before and after treatment with 1 μM CyPPA. Representative traces of (A) not electrically stimulated hiPSC-aCMs, (B) paced at 1 Hz, (C) paced at 2 Hz, and (D) paced at 3 Hz. Each beat waveform is an average of 5 beats from the stable region. Black traces represent pre-treatment recordings, while post-treatment recordings are showed in red. Vertical lines indicate FPD measurements.

3.2.4. Ivabradine Increases FPD and Beat Period and Decreases Spike Amplitude and Conduction Velocity

The effect of 2 μM ivabradine, an *HCN* blocker, on FPD, beat period, spike amplitude, and CV of hiPSC-aCMs was tested using MEA. *HCN4* is the principal cardiac

paralog of the *HCN1-4* ion channels and contributes to generating the pacemaker I_f current in the SAN. Although *HCN4* is expressed primarily in the SAN, it is also expressed in hiPSC-CMs.[91] Ivabradine inhibits all *HCN1-4* isoforms with similar IC_{50} values and decreases heart rate by increasing the diastolic interval without affecting AP duration.[92–94] In mice, ivabradine was documented to have an effect on variability of the heart rate in addition to increased diastolic intervals and therefore reduced heart rate.[95] Ivabradine was used in this study in an attempt to decrease the observed high intrinsic beating rate (>60 bpm) in our hiPSC-aCMs without affecting APD.

Ivabradine significantly prolonged FPD in WT hiPSC-aCMs without electrical stimulation (before: 137 ± 4 ms; after: 183 ± 6 ms; $p<0.01$) and when paced at 2 Hz (before: 146 ± 1 ms; after: 188 ± 5 ms; $p<0.01$) but not at 3 Hz (before: 137 ± 0 ms; after: 169 ± 6 ms) (Figure 3.9A). In rs13376333$^{+/-}$ hiPSC-aCMs, ivabradine increased FPD when the cells were not electrically paced (before: 96 ± 6 ms; after: 131 ± 9 ms; $p<0.01$), and when paced at 2 Hz (before: 99 ± 7 ms; after: 135 ± 11 ms; $p<0.01$) and 3 Hz (before: 94 ± 4 ms; after: 121 ± 5 ms; $p<0.05$) (Figure 3.9A). Ivabradine was the only drug treatment that affected beat period in both WT and variant-carrying hiPSC-aCMs. In WT hiPSC-aCMs, the addition of 2 μM ivabradine resulted in prolonged beat period under conditions of no electrical stimulation (before: 539 ± 0 ms; after: 918 ± 0 ms; $p<0.0001$). Beat period was also increased in rs13376333$^{+/-}$ hiPSC-aCMs after the addition of 2 μM ivabradine when the cells were not electrically stimulated (before: 443 ± 0 ms; after: 731 ± 0 ms; $p<0.0001$).

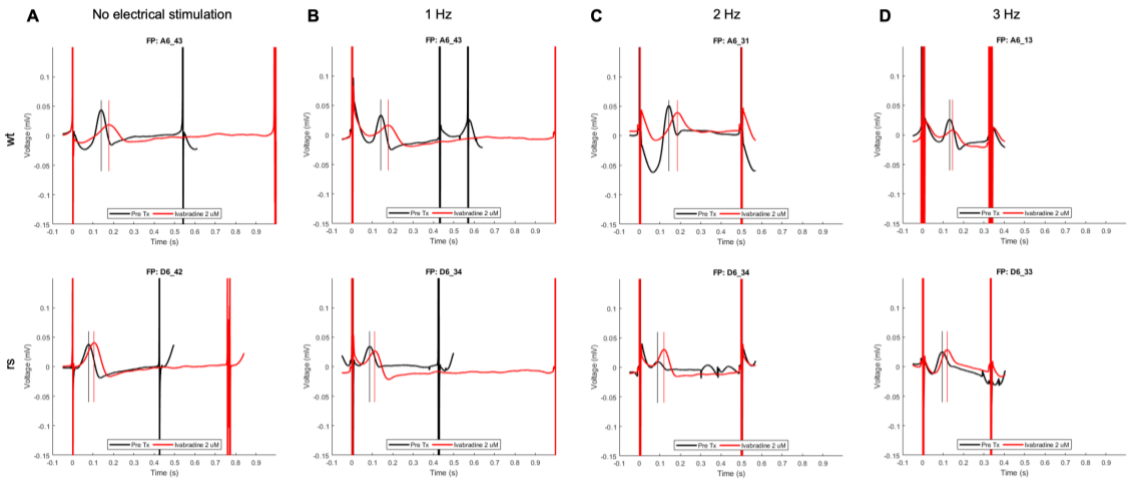

Figure 3.7 Field potential traces of wild-type and rs13376333$^{+/-}$ hiPSC-aCMs before and after treatment with 2 μM ivabradine.

Representative field potential (FP) traces obtained with the Axion MEA instrument of wild-type (wt, top panel) and rs13376333$^{+/-}$ (rs, bottom panel) hiPSC-aCMs before and after treatment with 2 μM ivabradine. Representative traces of (A) not electrically stimulated hiPSC-aCMs, (B) paced at 1 Hz, (C) paced at 2 Hz, and (D) paced at 3 Hz. Each beat waveform is an average of 5 beats from the stable region. Black traces represent pre-treatment recordings, while post-treatment recordings are showed in red. Vertical lines indicate FPD measurements.

Spike amplitude was decreased in WT hiPSC-aCMs electrically stimulated at 3 Hz (before: 5.3 ± 0.2 mV; after: 4.5 ± 0.1 mV; $p<0.001$) but not without stimulation and pacing at 2 Hz after treatment with 2 μM ivabradine (Figure 3.12A). Ivabradine did not result in altering spike amplitude of rs$^{+/-}$ hiPSC-aCMs without pacing and when paced at 2 Hz and 3 Hz (Figure 3.12A).

Furthermore, CV of WT hiPSC-aCMs was not significantly changed under conditions of no electrical stimulation and when the cells were electrically stimulated at 2 Hz and 3 Hz after the addition of 2 μM ivabradine (Figure 3.14A). In rs13376333$^{+/-}$ hiPSC-aCMs, CV was not changed with addition of 2 μM ivabradine without pacing and when paced at 2 Hz and 3 Hz (Figure 3.14A).

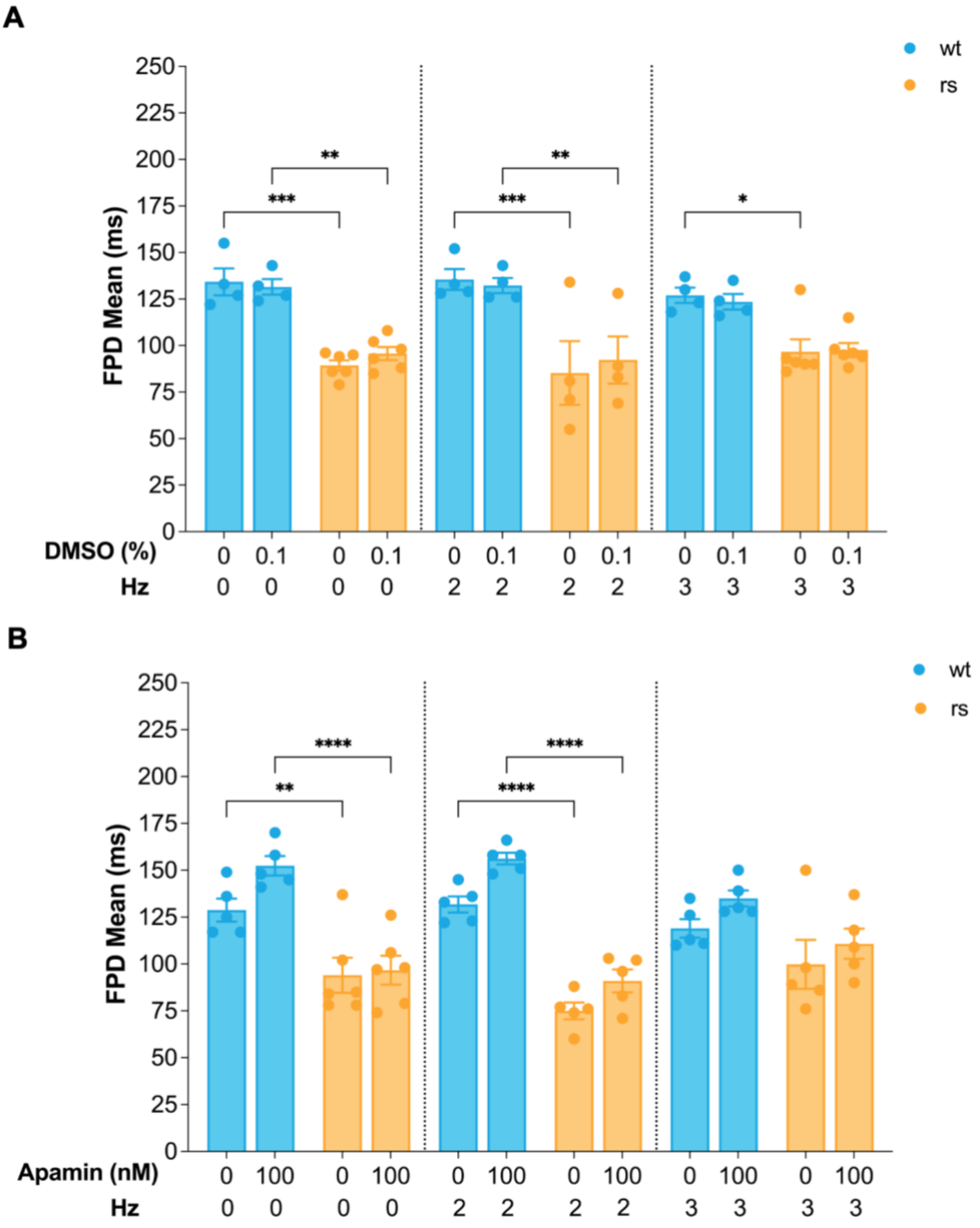

Figure 3.8 Field potential duration in wild-type and rs13376333$^{+/-}$ hiPSC-aCMs treated with control DMSO solution and apamin.

Mean field potential duration (FPD) (ms) comparison between wild-type (wt, blue) and rs13376333$^{+/-}$ (rs, orange) hiPSC-aCMs. Each plot shows data from wt and rs hiPSC-aCMs treated with (A) DMSO 0.1% and (B) 100 nM apamin. Electrical stimulation conditions are indicated in each graph in Hz (0, 2, 3). Error bars reflect standard error of means (SEMs). Samples from at least 3 different differentiation batches of wild-type and rs13376333$^{+/-}$ hiPSC-aCMs were used. Significance level for the two-way ANOVA was determined as following: *p<0.5, **p<0.01, ***p<0.001, ****p<0.0001.

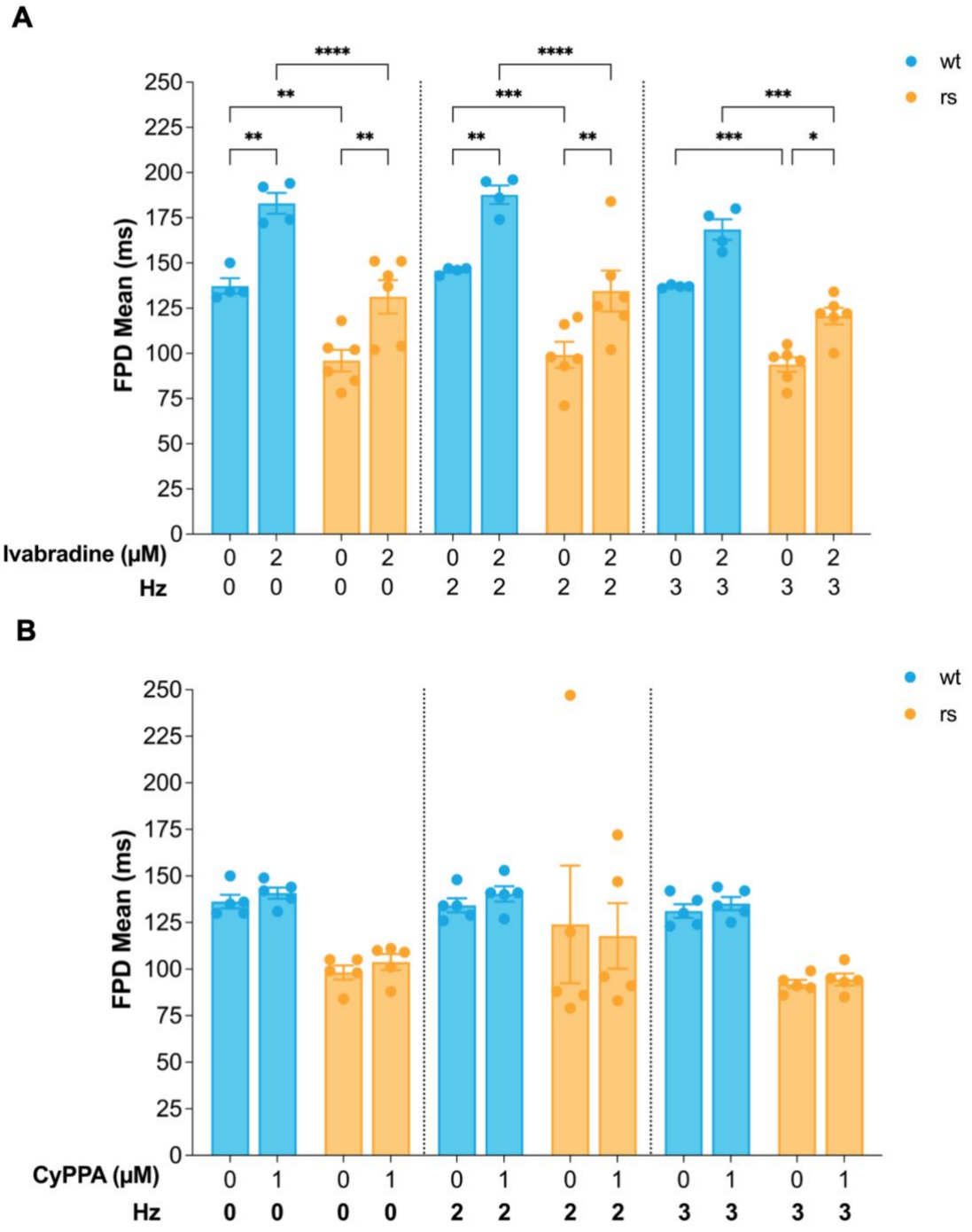

Figure 3.9 Field potential duration in wild-type and rs13376333$^{+/-}$ hiPSC-aCMs treated with ivabradine and CyPPA.

Mean field potential duration (FPD) (ms) comparison between wild-type (wt, blue) and rs13376333$^{+/-}$ (rs, orange) hiPSC-aCMs. Each plot shows data from wt and rs hiPSC-aCMs treated with (A) 2 μM ivabradine and (B) 1 μM CyPPA. Electrical stimulation conditions are indicated in each graph in Hz (0, 2, 3). Error bars reflect standard error of means (SEMs). Samples from at least 3 different differentiation batches of wild-type and rs13376333$^{+/-}$ hiPSC-aCMs were used. Significance level for the two-way ANOVA was determined as following: *p<0.5, **p<0.01, ***p<0.001, ****p<0.0001.

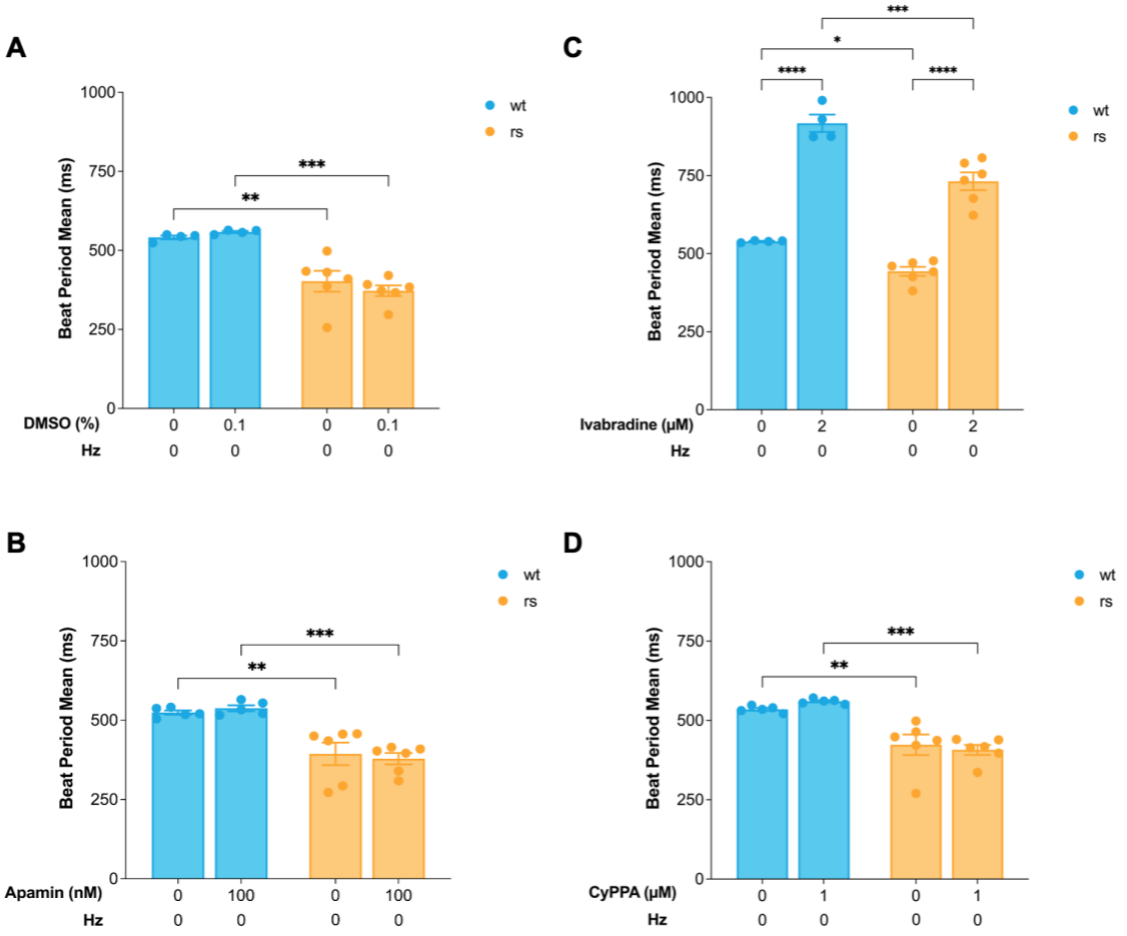

Figure 3.10 Beat period in wild-type and rs13376333$^{+/-}$ hiPSC-aCMs without electrical stimulation.

Mean beat period (s) comparison between non-paced wild-type (wt, blue) and rs13376333$^{+/-}$ (rs, orange) hiPSC-aCMs before and after administering drug treatments. Each plot shows data from wt and rs hiPSC-aCMs treated with (A) DMSO 0.1% (control), (B) 100 nM apamin, (C) 2 μM ivabradine, and (D) 1 μM CyPPA. Error bars reflect standard error of means (SEMs). Samples from at least 3 different differentiation batches of wild-type and rs13376333$^{+/-}$ hiPSC-aCMs were used. Significance level for the two-way ANOVA was determined as following: *p<0.5, **p<0.01, ***p<0.001, ****p<0.0001.

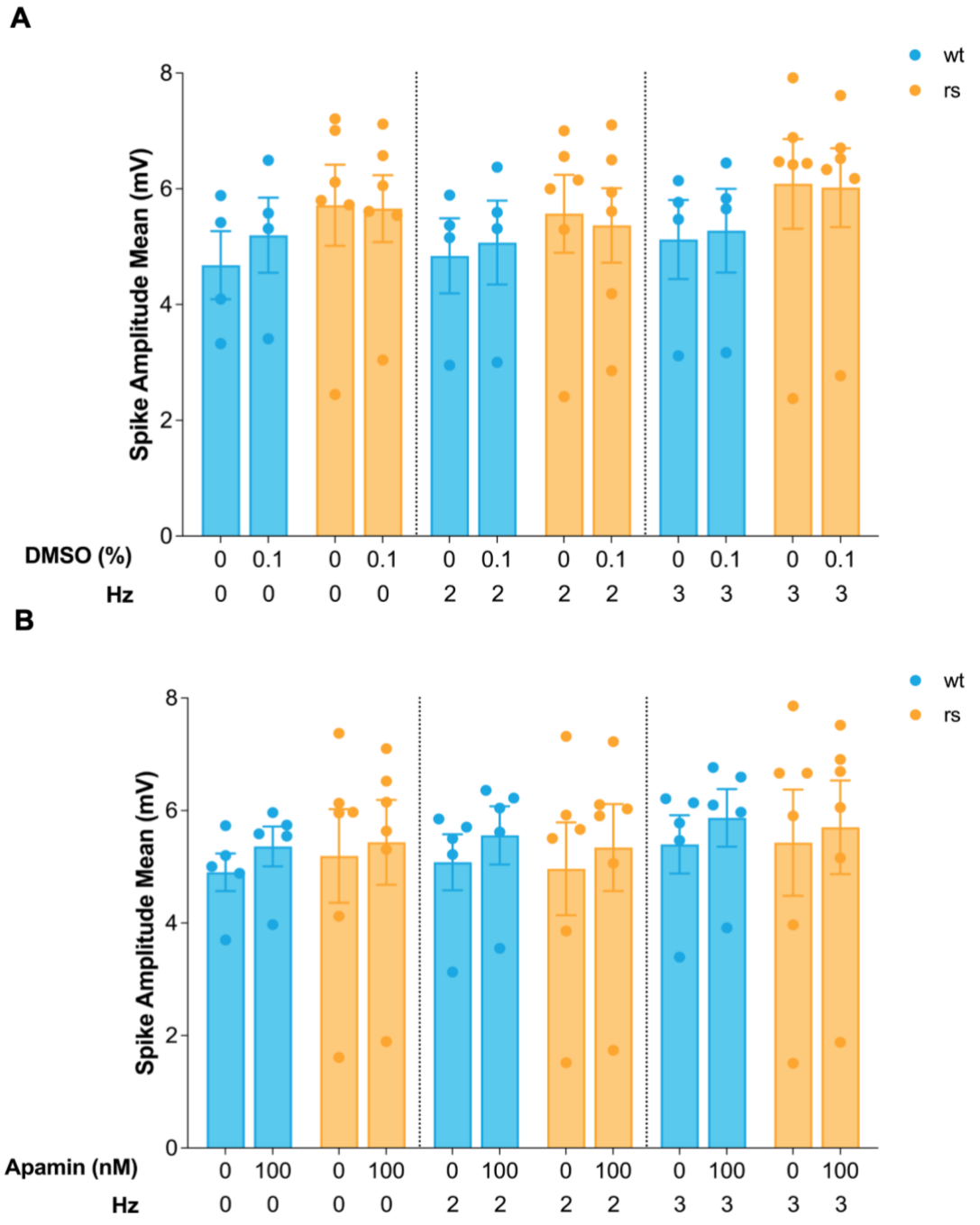

Figure 3.11 Spike amplitude in wild-type and rs13376333$^{+/-}$ hiPSC-aCMs treated with control DMSO solution and apamin.

Mean spike amplitude (mV) comparison between wild-type (wt, blue) and rs13376333$^{+/-}$ (rs, orange) hiPSC-aCMs. Each plot shows data from hiPSC-aCMs treated with (A) DMSO 0.1% and (B) 100 nM apamin. Electrical stimulation conditions are indicated in each graph in Hz (0, 2, 3). Error bars reflect standard error of means (SEMs). Samples from at least 3 different differentiation batches of wild-type and rs13376333$^{+/-}$ hiPSC-aCMs were used. Significance level for the two-way ANOVA was determined as following: *p<0.5, **p<0.01, ***p<0.001, ****p<0.0001.

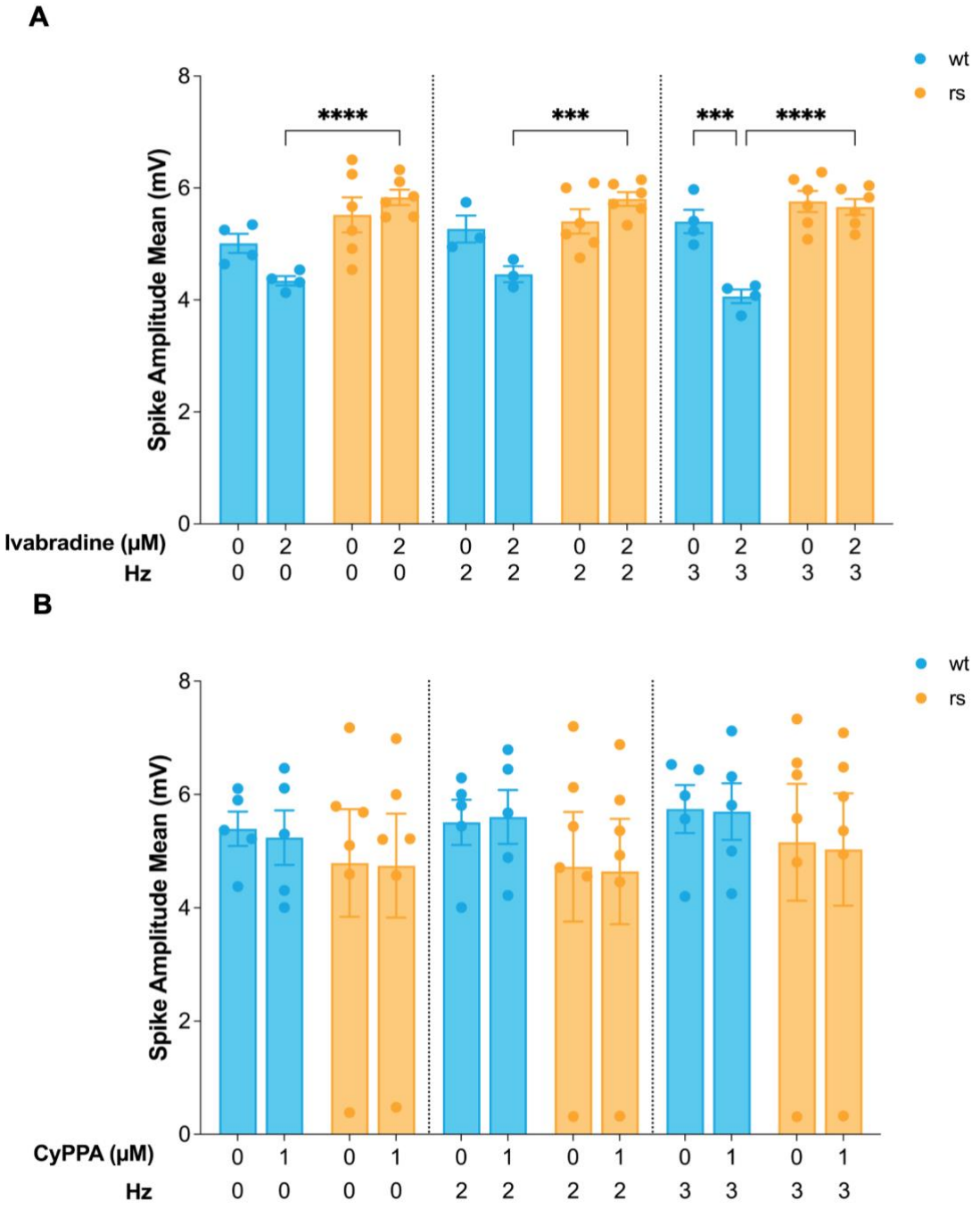

Figure 3.12 Spike amplitude in wild-type and rs13376333$^{+/-}$ hiPSC-aCMs treated with ivabradine and CyPPA.

Mean spike amplitude (mV) comparison between wild-type (wt, blue) and rs13376333$^{+/-}$ (rs, orange) hiPSC-aCMs. Each plot shows data from hiPSC-aCMs treated with (A) 2 μM ivabradine and (B) 1 μM CyPPA. Electrical stimulation conditions are indicated in each graph in Hz (0, 2, 3). Error bars reflect standard error of means (SEMs). Samples from at least 3 different differentiation batches of wild-type and rs13376333$^{+/-}$ hiPSC-aCMs were used. Significance level for the two-way ANOVA was determined as following: *p<0.5, **p<0.01, ***p<0.001, ****p<0.0001.

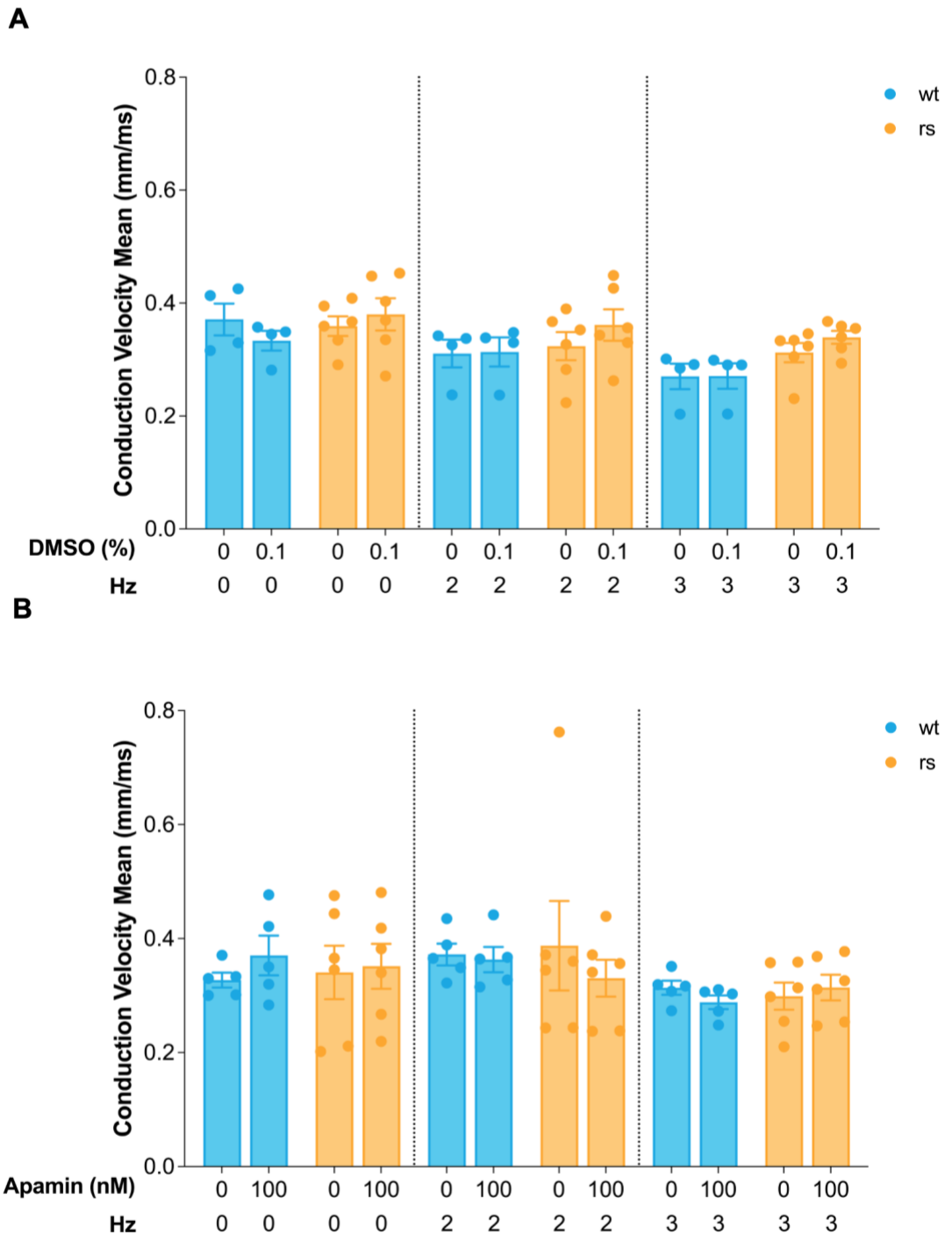

Figure 3.13 Conduction velocity in wild-type and rs13376333$^{+/-}$ hiPSC-aCMs treated with control DMSO solution and apamin.

Conduction velocity mean (mm/ms) comparison between wild-type (wt, blue) and rs13376333$^{+/-}$ (rs, orange) hiPSC-aCMs. Each plot shows data from hiPSC-aCMs treated with (A) DMSO 0.1% and (B)100 nM apamin. Electrical stimulation conditions are indicated in each graph in Hz (0, 2, 3). Error bars reflect standard error of means (SEMs). Samples from at least 3 different differentiation batches of wild-type and rs13376333$^{+/-}$ hiPSC-aCMs were used. Significance level for the two-way ANOVA was determined as following: *p<0.5, **p<0.01, ***p<0.001, ****p<0.0001.

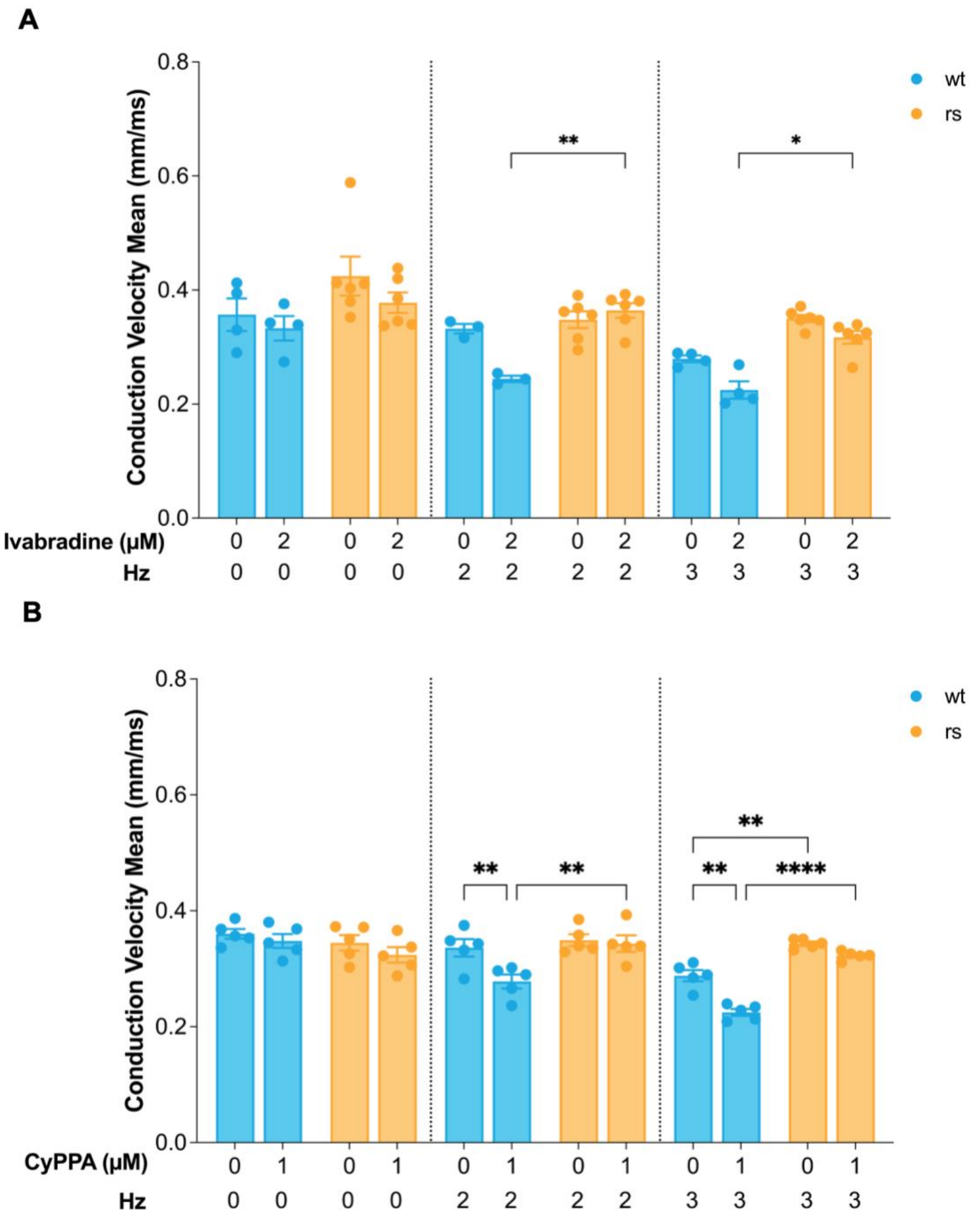

Figure 3.14 Conduction velocity in wild-type and rs13376333$^{+/-}$ hiPSC-aCM treated with ivabradine and CyPPA.

Conduction velocity mean (mm/ms) comparison between wild-type (wt, blue) and rs13376333$^{+/-}$ (rs, orange) hiPSC-aCMs. Each plot shows data from hiPSC-aCMs treated with (A) 2 μM ivabradine and (B)1 μM CyPPA. Electrical stimulation conditions are indicated in each graph in Hz (0, 2, 3). Error bars reflect standard error of means (SEMs). Samples from at least 3 different differentiation batches of wild-type and rs13376333$^{+/-}$ hiPSC-aCMs were used. Significance level for the two-way ANOVA was determined as following: *p<0.5, **p<0.01, ***p<0.001, ****p<0.0001.

3.3. Confocal Optical Mapping

The functional properties of isogenic WT control and rs13376333$^{+/-}$ hiPSC-aCMs were assessed using µOM using FluoVolt fluorescent dye for measurement of membrane voltage (V_m) as described in the Methods section 2.5.5.

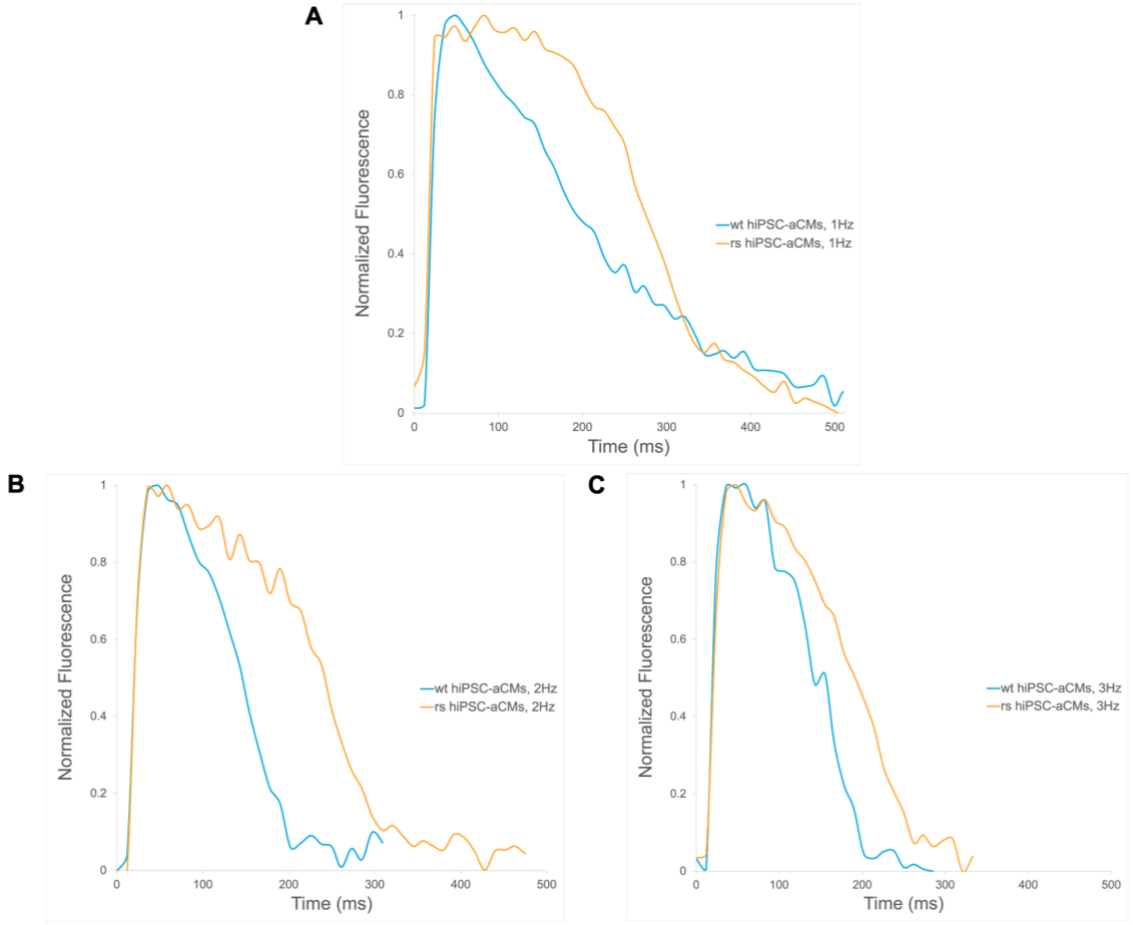

Figure 3.15 Wild-type and rs13376333$^{+/-}$ hiPSC-aCMs APD morphology in response to electrical field stimulation.

Representative traces of (A) APD morphology in wild-type (wt, blue) and rs13376333$^{+/-}$ (rs, orange) hiPSC-aCMs when paced at 1 Hz, (B) APD morphology in wt and rs hiPSC-aCMs when paced at 2 Hz, and (C) APD morphology in wt and rs hiPSC-aCMs when paced at 3 Hz. AP traces were recorded on µOM with FluoVolt.

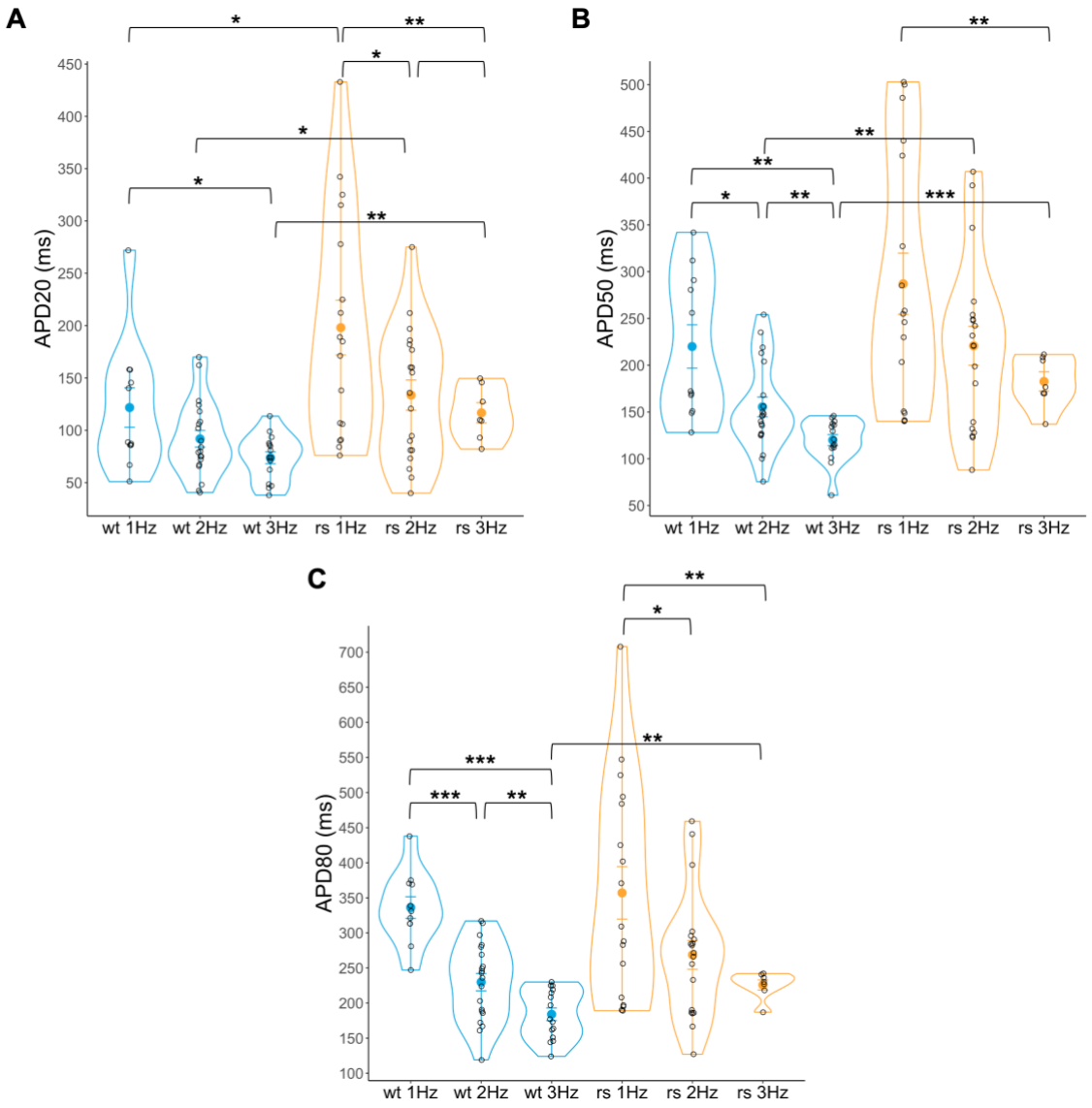

Figure 3.16 Comparison of APD_{20}, APD_{50}, and APD_{80} in wild-type and $rs13376333^{+/-}$ hiPSC-aCMs in response to electrical field stimulation in μOM.

Violin plots of (A) APD_{20}, (B) APD_{50}, and (C) APD_{80} in wild-type (wt, blue) and $rs13376333^{+/-}$ (rs, orange) hiPSC-aCMs in response to 1 Hz, 2 Hz, and 3 Hz electrical stimulation. Samples from at least 3 different differentiation batches of wild-type and $rs13376333^{+/-}$ hiPSC-aCMs were used. Significance level for two-sample t-test was determined as following: NS. = not significant, *p<0.5, **p<0.01, ***p<0.001. n=11, n=20, n=15 for wt hiPSC-aCMs stimulated at 1 Hz, 2 Hz, and 3 Hz, respectively; n=17, n=19, n=7 for rs hiPSC-aCMs stimulated at 1 Hz, 2 Hz, and 3 Hz, respectively.

3.3.1. $rs13376333^{+/-}$ hiPSC-aCMs Have Prolonged APD

AP durations at 20%, 50%, and 80% of repolarization (APD_{20}, APD_{50}, and APD_{80}, respectively) were recorded and analyzed in WT and $rs13376333^{+/-}$ hiPSC-aCMs to

determine if the variant increases AP duration (Figure 3.8). AP duration was analyzed at three different points: early repolarization (APD_{20}), mid-repolarization (APD_{50}), and late repolarization (APD_{80}). AP duration at early repolarization (APD_{20}) was significantly prolonged in the rs13376333$^{+/-}$ hiPSC-aCMs compared to the WT hiPSC-aCMs, respectively, at conditions with no electrical stimulation (200 ± 26 ms vs.124 ± 12 ms; $p<0.05$), and stimulation at 1 Hz (198 ± 26 ms vs. 122 ± 19 ms; $p<0.05$), 2 Hz (134 ± 15 ms vs. 92 ± 8 ms; $p<0.05$), and 3 Hz (117 ± 10 ms vs. 74 ± 6 ms; $p<0.01$). Furthermore, rs13376333$^{+/-}$ hiPSC-aCMs showed prolonged APD_{50} when the cells were not electrically stimulated (rs: 282 ± 28 ms; wt: 202 ± 16 ms; $p<0.05$), at 2 Hz (rs: 221 ± 21 ms; wt: 155 ± 11 ms; $p<0.01$), and 3 Hz (rs:183 ± 10 ms; wt:120 ± 6 ms; $p<0.001$). At 1 Hz, there was no difference in AP duration at 50% of repolarization in the variant-carrying (287 ± 33 ms) and wild-type cells (220 ± 23 ms). Interestingly, APD_{80} of rs13376333$^{+/-}$ hiPSC-aCMs was not significantly different from APD_{80} of the isogenic control with no electrical stimulation (336 ± 32 ms vs. 277 ± 17 ms), 1 Hz (357 ± 37 ms vs. 336 ± 16 ms), and 2 Hz (269 ± 21 ms vs. 230 ± 12 ms). However, APD_{80} was significantly prolonged in the variant-carrying cells (226 ± 7 ms vs. 184 ± 9 ms; $p<0.01$) when paced at 3 Hz. Compared to the wild-type hiPSC-aCMs AP morphology, APs recorded from the rs$^{+/-}$ hiPSC-aCMs appear to have a prolonged plateau phase reflected in significantly prolonged APD_{20} with electrical stimulation at 1 Hz, 2 Hz, and 3 Hz (Figure 3.12). Furthermore, rs13376333+/- hiPSC-aCMs had a significantly lower beating rate compared to WT hiPSC-aCMs prior to addition of drug treatments (wt: 68 ± 6 bpm; rs: 49 ± 4 bpm; $p<0.01$).

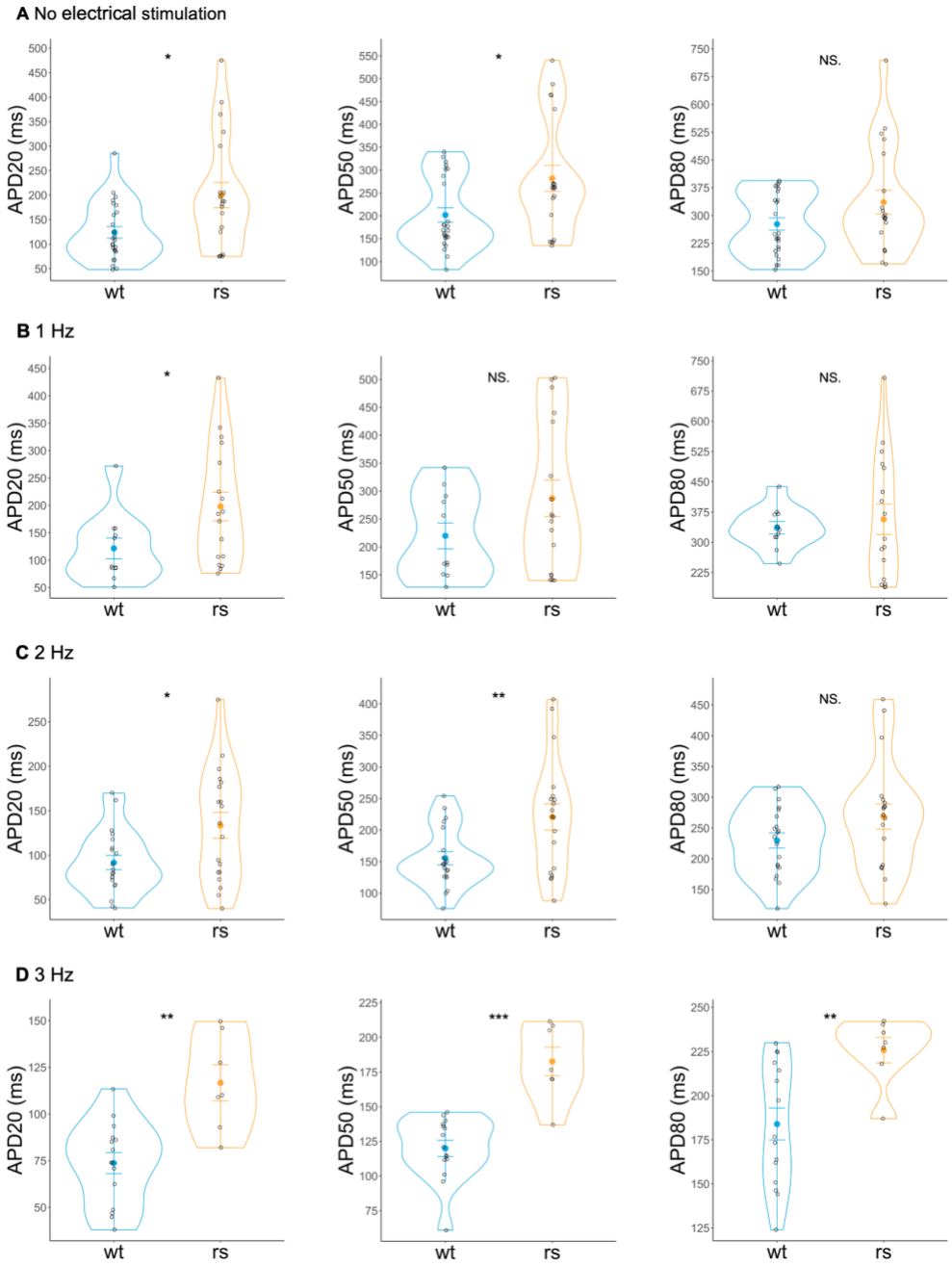

Figure 3.17 APD_{20}, APD_{50}, and APD_{80} in wild-type and rs13376333$^{+/-}$ hiPSC-aCMs. Action potential duration at 20%, 50%, and 80% repolarization (APD_{20}, APD_{50}, and APD_{80}, respectively) in wild-type (wt, blue) and rs13376333$^{+/-}$ (rs, orange) hiPSC-aCMs measured using µOM. (A) represents data collected without electrical stimulation, (B) through (D) show data collected with 1-3 Hz electrical stimulation. Each black circle represents an averaged value of an APD from a 10 sec recording from one region of interest. Colored circles and bars represent mean and standard error of mean (SEM), respectively. Samples from at least 3 different differentiation batches of wild-type and rs13376333$^{+/-}$ hiPSC-aCMs were used. Significance level for two-sample t-test was determined as following: NS. = not significant, *p<0.5, **p<0.01, ***p<0.001. n=25, n=11, n=20, n=15 for wt hiPSC-aCMs without pacing and stimulated at 1 Hz, 2 Hz, and 3 Hz, respectively; n=20, n=17, n=19, n=7 for rs hiPSC-aCMs without pacing and stimulated at 1 Hz, 2 Hz, and 3 Hz, respectively.

3.3.2. Apamin Increases APD_{80} in Wild-Type hiPSC-aCMs with No Effect on rs13376333$^{+/-}$ hiPSC-aCMs

Apamin is a known pore blocker of SK channels with SK2 and SK3 channels having a slightly higher sensitivity to the drug compared to SK1 channels.[65] The effect of apamin on APD in both wild-type and rs13376333$^{+/-}$ hiPSC-aCMs was investigated by comparing APD_{20}, APD_{50}, and APD_{80} before and after addition of 100 nM apamin (Figure 3.16 and 3.17). Treatment with 100 nM apamin significantly increased APD_{80} in WT hiPSC-aCMs when not electrically stimulated (before: 388 ± 27 ms; after: 494 ± 31 ms; $p<0.01$), and with electrical stimulation at 1 Hz (before: 373 ± 20 ms; after: 428 ± 20 ms; $p<0.01$) and 2 Hz (before: 273 ± 7 ms; after: 303 ± 11 ms; $p<0.01$). Apamin did not affect APD_{20} and APD_{50} in WT hiPSC-aCMs except when the cells were not electrically stimulated where addition of 100 nM apamin significantly increased APD_{50} (before: 243 ± 20 ms; after: 291 ± 20 ms; $p<0.05$). There was no significant effect of 100 nM apamin on APD_{80} in the rs13376333$^{+/-}$ hiPSC-aCMs with no electrical stimulation (before: 391 ± 38 ms; after: 412 ± 40 ms), and with electrical stimulation at 1 Hz (before: 396 ± 29 ms; after: 401 ± 37 ms) and at 2 Hz (before: 282 ± 18 ms; after: 292 ± 17 ms). Repolarization at 20% and 50% was not affected with addition of 100 nM apamin in the rs13376333$^{+/-}$ hiPSC-aCMs. AP morphology of both wild-type and rs$^{+/-}$ hiPSC-aCMs reflects prolongation of late repolarization (APD_{80}) but not early and mid-repolarization (APD_{20} and APD_{50}, respectively) at 1 Hz and 2 Hz of electrical stimulation (Figure 3.15).

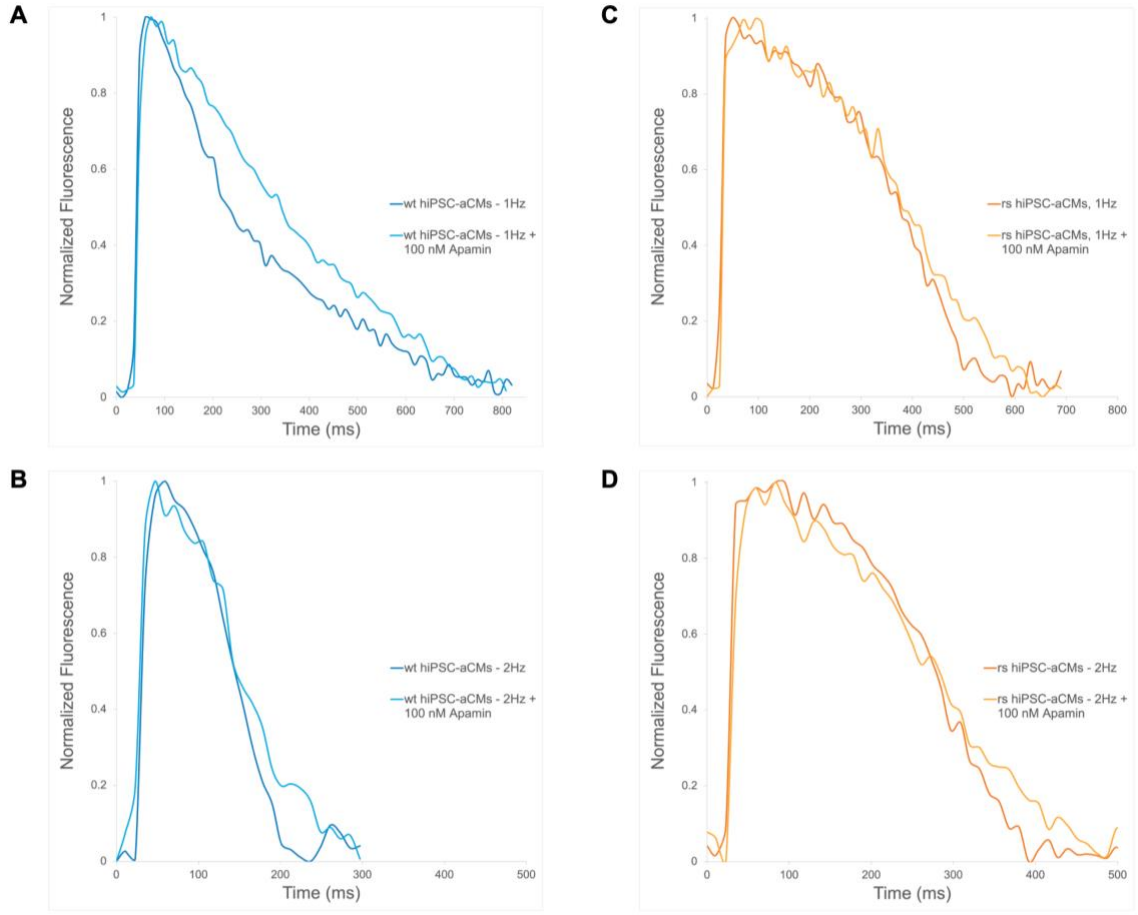

Figure 3.18 AP traces of wild-type and rs13376333$^{+/-}$ hiPSC-aCMs comparing the effect of 100 nM apamin.

Representative AP traces of (A) wild-type (wt) hiPSC-aCMs paced at 1 Hz with (light blue) and without (dark blue) 100 nM apamin, (B) wt hiPSC-aCMs paced at 2 Hz with (light blue) and without (dark blue) 100 nM apamin, (C) rs13376333$^{+/-}$ (rs) hiPSC-aCMs paced at 1 Hz with (light orange) and without (dark orange) 100 nM apamin, and (D) rs hiPSC-aCMs paced at 2 Hz with (light orange) and without (dark orange) 100 nM apamin. AP traces were recorded on µOM with FluoVolt.

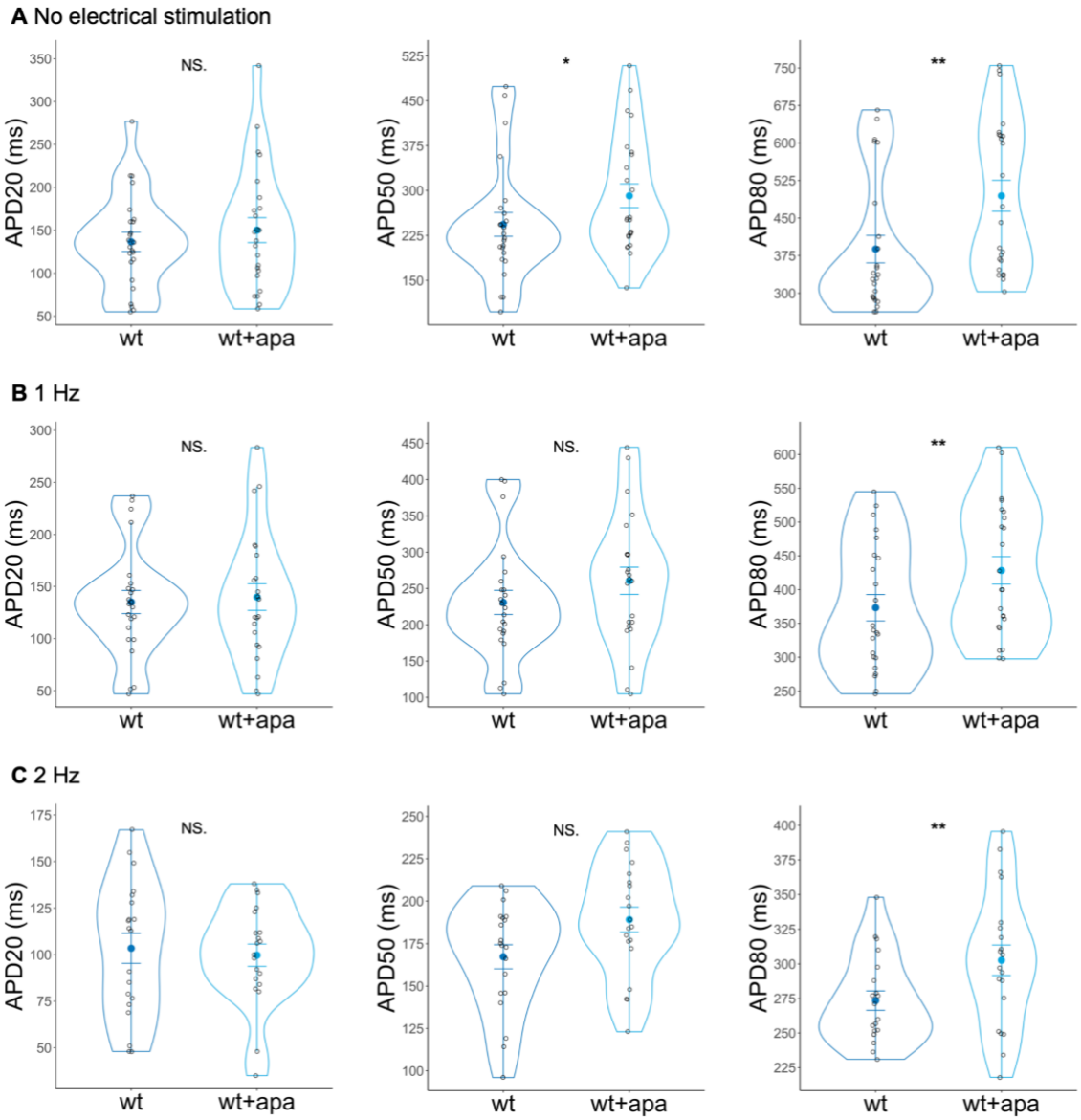

Figure 3.19 APD_{20}, APD_{50}, and APD_{80} in wild-type hiPSC-aCMs before and after 100 nM apamin treatment.

Action potential duration at 20%, 50%, and 80% repolarization (APD_{20}, APD_{50}, and APD_{80}, respectively) in wild-type (wt) hiPSC-aCMs before (dark blue) and after (light blue) treatment with 100 nm apamin (apa) measured using μOM. (A) represents data collected without electrical stimulation, (B) and (C) show data collected with 1 Hz and 2 Hz electrical stimulation. Each black circle represents an averaged value of an APD from a 10 sec recording from one region of interest. Colored circles and bars represent mean and standard error of mean (SEM), respectively. Samples from at least 3 different differentiation batches of wild-type hiPSC-aCMs were used. Significance level for two-sample t-test was determined as following: NS. = not significant, *p<0.5, **p<0.01, ***p<0.001. n=24, n=23, n=20 for wt hiPSC-aCMs without pacing and stimulated at 1 Hz and 2 Hz, respectively.

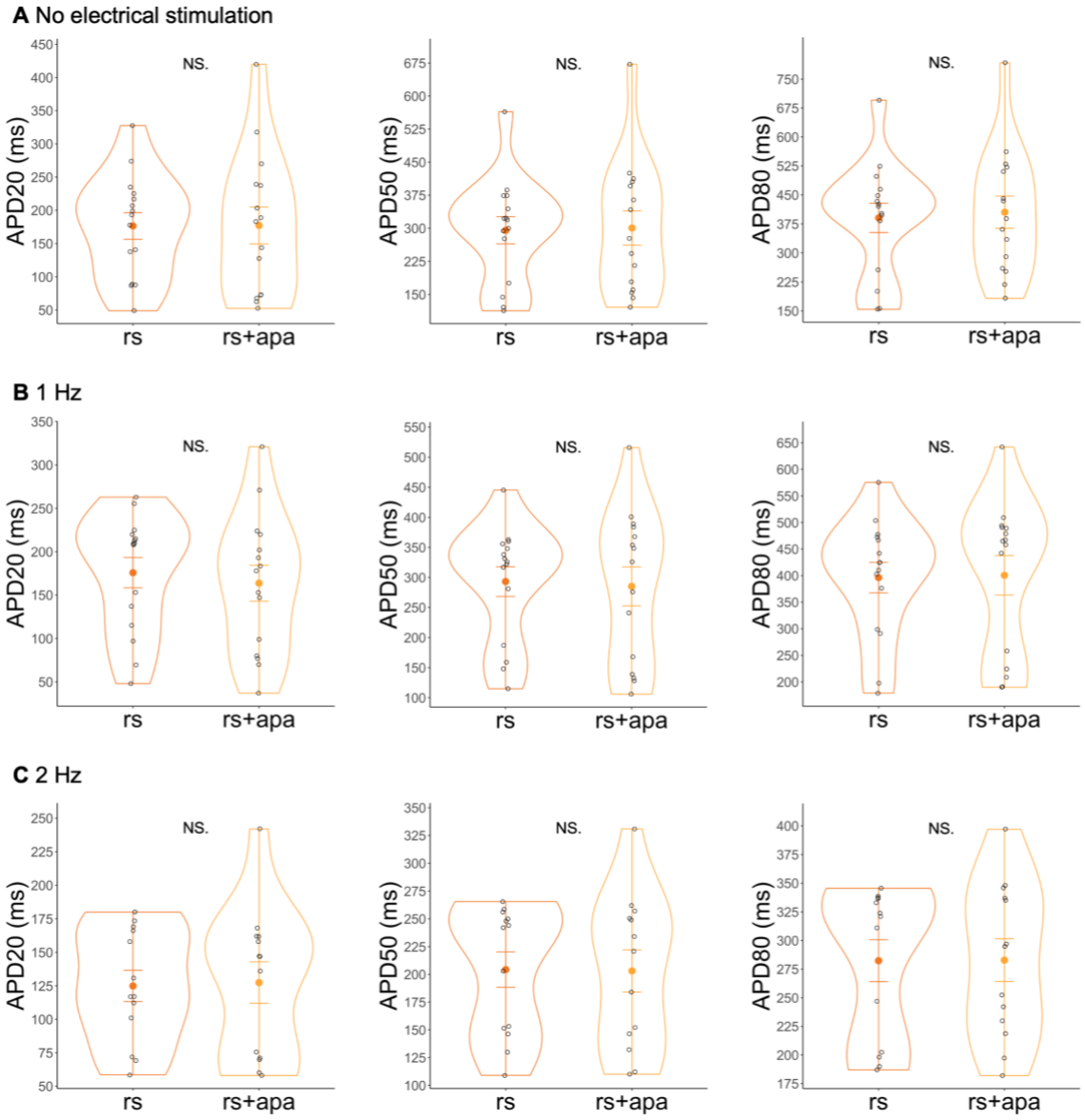

Figure 3.20 APD_{20}, APD_{50}, and APD_{80} in rs13376333$^{+/-}$ hiPSC-aCMs before and after 100 nM apamin treatment.

Action potential duration at 20%, 50%, and 80% repolarization (APD_{20}, APD_{50}, and APD_{80}, respectively) in rs13376333$^{+/-}$ (rs) hiPSC-aCMs before (dark orange) and after (light orange) treatment with 100 nm apamin (apa) measured using µOM. (A) represents data collected without electrical stimulation, (B) and (C) show data collected with 1 Hz and 2 Hz electrical stimulation. Each black circle represents an averaged value of an APD from a 10 sec recording from one region of interest. Colored circles and bars represent mean and standard error of mean (SEM), respectively. Samples from at least 3 different differentiation batches of wild-type hiPSC-aCMs were used. Significance level for two-sample t-test was determined as following: NS. = not significant, *p<0.5, **p<0.01, ***p<0.001. n=16, n=15, n=15 for rs hiPSC-aCMs without pacing and stimulated at 1 Hz and 2 Hz, respectively.

3.3.3. Ivabradine Increases APD_{80} in Wild-Type hiPSC-aCMs

An intrinsic beating rate higher than 60 bpm limits the ability of hiPSC-aCMs to entrain to electrical field stimulation of 1 Hz, 2 Hz, and 3 Hz. AP duration (APD_{20}, APD_{50}, APD_{80}) was analyzed before and after treatment with 4 μM ivabradine in wild-type and rs13376333$^{+/-}$ hiPSC-aCMs (Figure 3.19 and 3.20). Ivabradine prolonged APD_{80} in wild-type hiPSC-aCMs at conditions with no electrical stimulation (before: 277 ± 17 ms; after: 388 ± 27 ms; $p<0.001$), and at 1 Hz (before: 336 ± 16 ms; after: 373 ± 20 ms; $p<0.001$) and 2 Hz (before: 230 ± 12 ms; after: 273 ± 7 ms; $p<0.001$) of electrical stimulation. Addition of ivabradine did not significantly affect APD_{20}, APD_{50}, and APD_{80} in rs13376333$^{+/-}$ hiPSC-aCMs except increasing APD_{80} when paced at 2 Hz (before: 269 ± 21 ms; after: 282 ± 18 ms; $p<0.05$). AP morphology obtained with μOM show prolongation of APD_{80} without changes in APD_{20} and APD_{50} in both wild-type and variant-carrying hiPSC-aCMs (Figure 3.18), although only changes in APD_{80} of the wild-type samples showed to be significantly different with addition of 4 μM ivabradine.

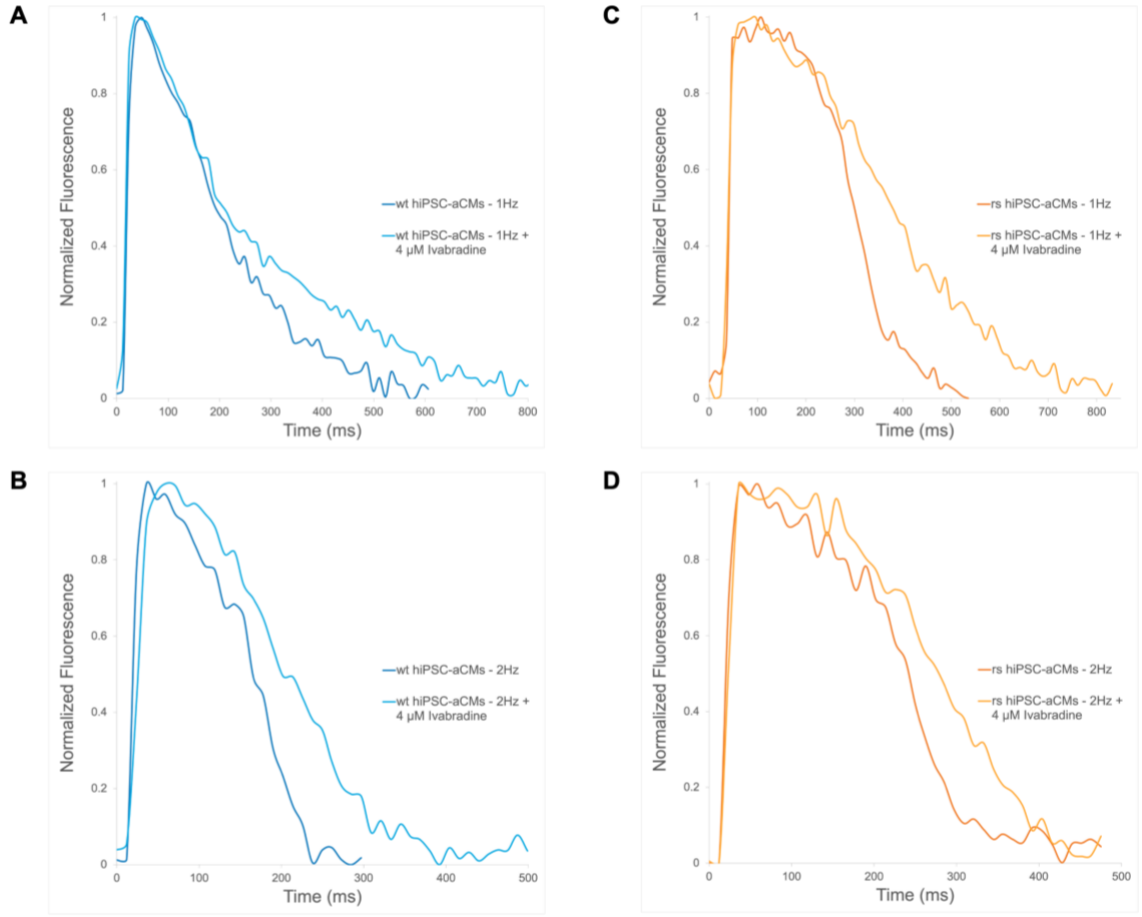

Figure 3.21 AP traces of wild-type and rs13376333$^{+/-}$ hiPSC-aCMs comparing the effect of 4 µM ivabradine.

Representative AP traces of (A) wild-type (wt) hiPSC-aCMs paced at 1 Hz with (light blue) and without (dark blue) 4 µM ivabradine, (B) wt hiPSC-aCMs paced at 2 Hz with (light blue) and without (dark blue) 4 µM ivabradine, (C) rs13376333$^{+/-}$ (rs) hiPSC-aCMs paced at 1 Hz with (light orange) and without (dark orange) 4 µM ivabradine, and (D) rs hiPSC-aCMs paced at 2 Hz with (light orange) and without (dark orange) 4 µM ivabradine. AP traces were recorded on µOM with FluoVolt.

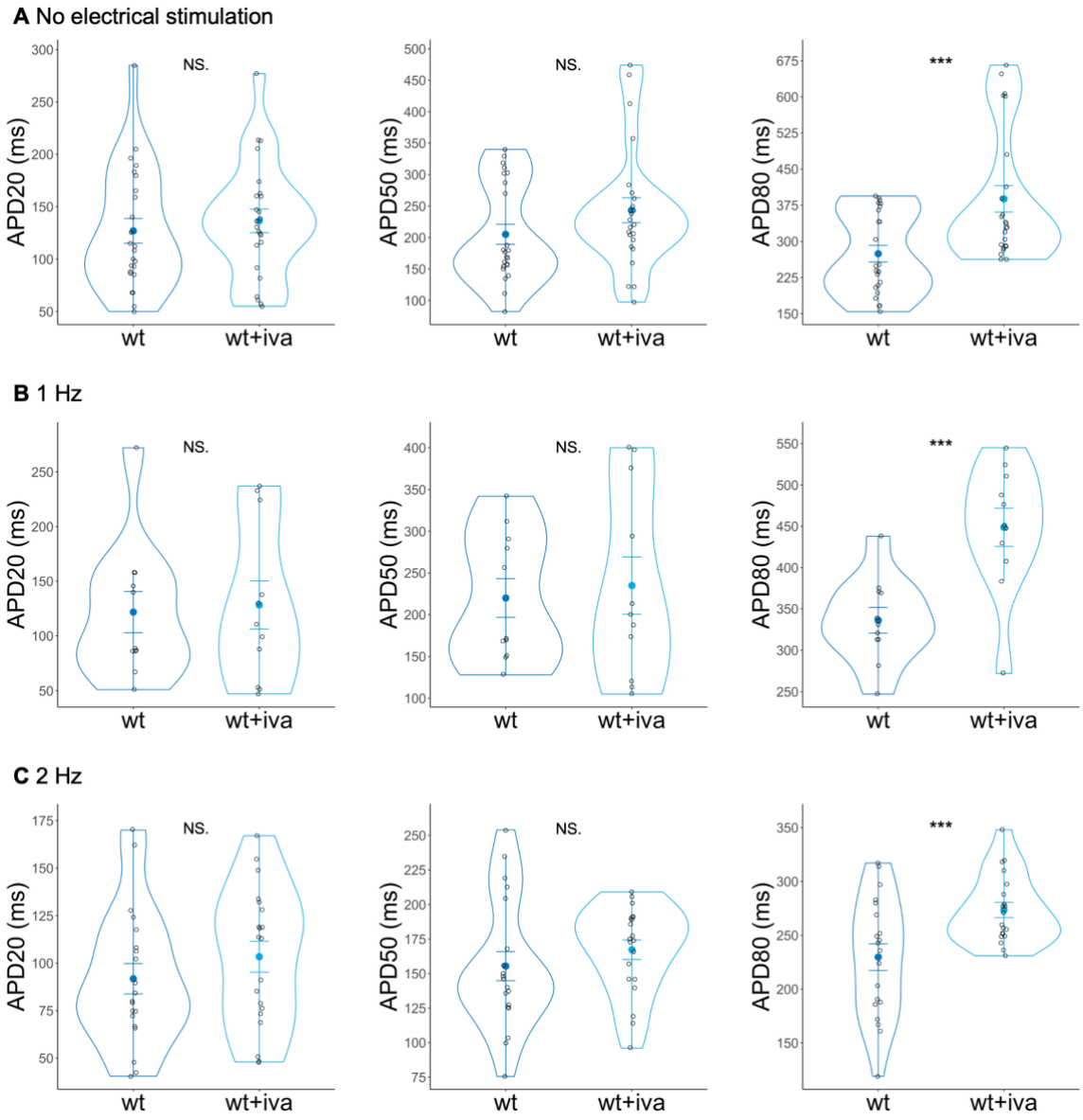

Figure 3.22 APD_{20}, APD_{50}, and APD_{80} in wild-type hiPSC-aCMs before and after 4 µM ivabradine treatment.

Action potential duration at 20%, 50%, and 80% repolarization (APD_{20}, APD_{50}, and APD_{80}, respectively) in wild-type (wt) hiPSC-aCMs before (dark blue) and after (light blue) treatment with 4 µM ivabradine (iva) measured using µOM. (A) represents data collected without electrical stimulation, (B) and (C) show data collected with 1 Hz and 2 Hz electrical stimulation. Each black circle represents the mean APD value from a 10 sec recording from one region of interest. Colored circles and bars represent mean and standard error of mean (SEM), respectively. Samples from at least 3 different differentiation batches of wild-type hiPSC-aCMs were used. Significance level for two-sample t-test was determined as following: NS. = not significant, *p<0.5, **p<0.01, ***p<0.001. n=24, n=23, n=20 for wt hiPSC-aCMs without pacing and stimulated at 1 Hz and 2 Hz, respectively.

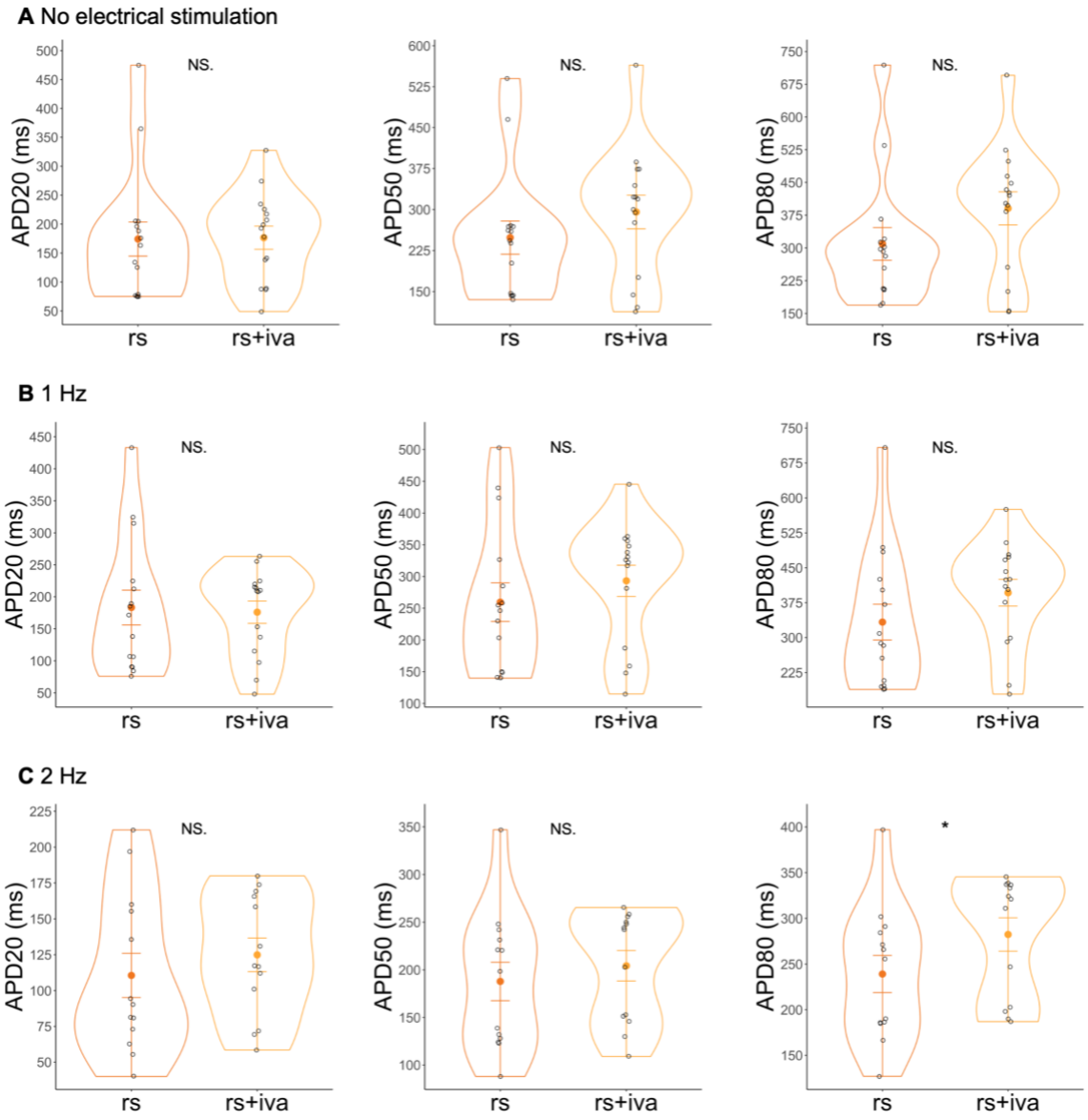

Figure 3.23 APD_{20}, APD_{50}, and APD_{80} in rs13376333$^{+/-}$ hiPSC-aCMs before and after 4 μM ivabradine treatment.

Action potential duration at 20%, 50%, and 80% repolarization (APD_{20}, APD_{50}, and APD_{80}, respectively) in rs13376333$^{+/-}$ (rs) hiPSC-aCMs before (dark orange) and after (light orange) treatment with 4 μM ivabradine (iva) measured using μOM. (A) represents data collected without electrical stimulation, (B) and (C) show data collected with 1 Hz and 2 Hz electrical stimulation. Each black circle represents an averaged value of an APD from a 10 sec recording from one region of interest. Colored circles and bars represent mean and standard error of mean (SEM), respectively. Samples from at least 3 different differentiation batches of wild-type hiPSC-aCMs were used. Significance level for two-sample t-test was determined as following: NS. = not significant, *p<0.5, **p<0.01, ***p<0.001. n=15, n=15, n=13 for rs hiPSC-aCMs without pacing and stimulated at 1 Hz and 2 Hz, respectively.

Chapter 4.

Discussion

This study aimed to provide insight into the effect of the GWAS-identified intronic rs13376333 variant in hiPSC-aCMs and possible underlying mechanisms in its contribution to the development of early-onset AF. Studies based on investigating AF linked to genetic variations can improve our knowledge of the pathophysiological mechanisms underlying AF and lead to improved treatment of the disease.

4.1. hiPSC Gene Editing Using CRISPR-Cas9

One of the initial aims of my project was to establish a genome-edited hiPSC line with the intronic rs13376333 variant, an SK3 knock-out hiPSC line, and isogenic control hiPSC lines using CRISPR-Cas9. In 2020, the Noble Prize in Chemistry was awarded to Emmanuelle Charpentier and Jennifer Doudna for the development of the CRISPR-Cas9 gene editing technology for precise gene editing. There are many applications of this gene editing technology where precise nucleotide changes are needed such as precision therapeutics and personalized medicine to treat and cure a variety of diseases. My results show a successful generation of the heterozygous rs13376333$^{+/-}$ hiPSC line and its respectful isogenic control hiPSC line which were used for MEA and µOM experiments. This confirms that the gene editing protocol and construct for the rs13376333 variant insertion were optimized and may be repeated in other hiPSC lines. Although the insertion of the intronic variant was successful, generation of the SK3 knock-out proved to be challenging. None of the SK3 knock-out transfected hiPSC clones showed homozygous insertion in the Sanger sequencing results. This reflects the need to optimize the gene editing construct and to increase the number of colonies picked for expansion and Sanger sequencing due to the low efficiency of HDR-based repairs in CRISPR-Cas9 gene editing. In case CRISPR-Cas9 technology proves to be suboptimal for an SK3 knock-out generation in this case, other gene editing techniques such as base and prime editing developed by the David Liu lab can be considered when attempting to insert a point mutation or a premature stop codon[96,97].

4.2. MEA – A High-Throughput Assay for Studying Inherited Heart Arrhythmias

The MEA instrument has multiple advantages including its high-throughput ability, field electrical stimulation allowing for continuous pacing of the hiPSC-aCMs, and ability to screen for drug treatment effects with a higher number of replicates at a given time. In my study, the MEA was used to fine-tune and optimize protocols for μOM including adjusting drug treatment concentrations and assessing the ability of hiPSC-aCMs to entrain to electrical stimulation from 1 Hz to 3 Hz. Another advantage of the MEA system is its ability to record and export a variety of endpoints. Four endpoints were chosen to be analyzed in the MEA experiments: field potential duration, beat period, spike amplitude, and conduction velocity.

Prior to the addition of drug treatments, the rs13376333$^{+/-}$ hiPSC-aCMs had a significantly higher spontaneous beating rate when compared to wild-type hiPSC-aCMs. In the MEA experiments, the FPD and beat period of the rs13376333$^{+/-}$ hiPSC-aCMs were significantly reduced reflecting the observed increased spontaneous beating rate. To account for differences in maturation and therefore spontaneous beating rate between the two groups, the cells were of the same age post-differentiation upon replating onto MEA plates. Although the spontaneous beating rate of the rs13376333$^{+/-}$ hiPSC-aCMs was considerably higher than that of the wild-type hiPSC-aCMs, both cell lines demonstrated a high beating rate compared to hiPSC-derived ventricular cardiomyocytes and the heart rate of a healthy adult (>100 bpm vs. 60-100 bpm). The beating rate of our hiPSC-aCMs resembled that of the fetal heart rate which falls between 110 and 160 bpm reflecting the lack of maturation of the cells. Based on the MEA measurements of conduction velocity, there was no significant difference between CV of the rs13376333 hiPSC-aCMs and the control hiPSC-aCMs. Interestingly, both measured at around or higher than 0.3 m/s demonstrating a feature of adult cardiomyocytes.[98]

Recently, SK channel inhibitors began to emerge as a potential novel pharmacological therapy for AF. Compared to the established antiarrhythmic therapies that can be classified as blockers of Na^+ channels, β-adrenergic receptors, K^+ channels, and Ca^{2+} channels, apamin inhibitors have the potential to selectively target SK channels which are predominantly expressed in the atria.[77,78] This can aid in reducing the harmful

side effects of the traditional treatments such as life-threatening ventricular arrhythmias. AP30663 is the first proposed SK channel inhibitor in development for conversion of AF into normal sinus rhythm.[99] Several studies using animal models report the antiarrhythmic effects of SK channel inhibitors with a dose-dependent prolongation of atrial ERP.[80,81,100–103] In my study, apamin was used to investigate the effect of blocking SK channels on the electrophysiological properties of the hiPSC-aCMs. Apamin did not result in a significant prolongation of FPD in wild-type and rs13376333$^{+/-}$ hiPSC-aCMs. The lack of an observed increase in the FPD of the wild-type cells in response to apamin was not expected since it is known to be an SK channel pore blocker. Additionally, I expected the rs13376333$^{+/-}$ hiPSC-aCMs to not have a significant response to 100 nM apamin which supports the hypothesis that the variant acts through a loss-of-function mechanism and increases AP duration. It is important to note that FPD reflects the time from the depolarization spike to the peak of the T-wave, which represents repolarization. Therefore, it is challenging to distinguish which phase of the action potential is prolonged in response to apamin using the MEA instrument. Interestingly, there was no significant differences in the FPD of wild-type and rs13376333$^{+/-}$ hiPSC-aCMs with the latter having higher variability within the FPD measurements. In rs13376333$^{+/-}$ hiPSC-aCMs, no effect of apamin was observed on all measured parameters: FPD, beat period, spike amplitude, and conduction velocity supporting the loss-of-function hypothesis.

Treatment with 1 μM CyPPA, a positive modulator of SK channels selective for SK2 and SK3, resulted in rather unexpected results in MEA experiments with wild-type and heterozygous variant hiPSC-aCMs. While addition of CyPPA did not result in any changes in spike amplitude in both WT and rs13376333$^{+/-}$ hiPSC-aCMs, conduction velocity of WT hiPSC-aCMs was significantly reduced with pacing at 2 Hz and 3 Hz. Since CyPPA is a positive modulator of SK2 and SK3 channels, these results were not expected. As there is a lack of studies investigating the effect of positive modulators of SK channels, more thorough experiments should be done on SK channel inhibitors and positive modulators to determine how these drug treatments affect the electrophysiology of the hiPSC-derived CMs.

Lastly, the effect of ivabradine on the above parameters was tested. Ivabradine is a proposed pharmacological treatment for AF which acts by suppressing pacemaker current, I_f, during the diastole to lower the heart rate and maintain normal sinus rhythm.[104] However, recent meta-analyses of clinical studies have shown that ivabradine

is associated with an increased incidence of AF, highlighting the need for more studies on its effect on cardiac electrophysiology.[105] In our MEA assay, addition of 2 μM ivabradine resulted in increased FPD and beat period in both wild-type and rs13376333$^{+/-}$ hiPSC-aCMs. The increase in beat period, and therefore a reduction in beating rate, is expected and is in agreement with other studies demonstrating the effect of ivabradine on heart rate. Preliminary pharmacological tests of the ivabradine effect on these parameters was important to consider before moving on to μOM experiments since changes in the above parameters can have a proarrhythmic effect.

4.3. Confocal Optical Mapping for Studying Action Potential Morphology and Duration

In μOM, AP durations at 20%, 50%, and 80% of repolarization (APD_{20}, APD_{50}, and APD_{80}, respectively) were recorded and analyzed on the hiPSC-aCMs to determine if the rs13376333 variant increases AP duration and therefore acts through a loss-of-function mechanism. A loss-of-function variant affecting an ion channel responsible for repolarizing outward K^+ current would delay repolarization and promote Ca^{2+} mediated afterdepolarization triggering AF.

Pre-treatment analysis of APD_{20}, APD_{50}, and APD_{80} showed prolonged plateau phase (APD_{20}) in rs13376333$^{+/-}$ hiPSC-aCMs when compared to their isogenic control. Mid-repolarization phase (APD_{50}) of the AP was also prolonged except when the variant-carrying hiPSC-aCMs were electrically stimulated at 1 Hz. However, APD_{80} was only prolonged in the rs13376333$^{+/-}$ hiPSC-aCMs with 3 Hz electrical stimulation. Based on the studies demonstrating SK channels being primarily active during the late repolarization (APD_{80}) phase of the AP[77–79,82], I expected this parameter to be increased in the rs13376333$^{+/-}$ hiPSC-aCMs. However, SK channel current increases when calcium is elevated since they are voltage-independent and calcium-activated ion channels. Therefore, given that SK channels primarily contribute to the early repolarization phase (APD_{20}) instead of the late repolarization phase (APD_{80}), and that the variant acts through a loss-of-function mechanism, the observed increase in APD_{20} can be expected. Generally, the heterozygous variant hiPSC-aCMs showed a higher variability reflected in increased SEM compared to the wild-type hiPSC-aCMs. A study looking at determining the role of SK channels in atrial arrhythmias using a canine model showed that SK channel blockade promotes arrhythmia which could be attributed to

increased APD heterogeneity.[106,107] Our results are supportive of this phenomenon, where APD heterogeneity might lead to increased susceptibility to arrhythmia demonstrated by the presence of EADs in rs13376333$^{+/-}$ hiPSC-aCM action potential traces compared to the control.

The other goal of this study was to investigate the effect of apamin on the electrophysiology of the rs13376333$^{+/-}$ and wild-type hiPSC-aCMs. All three SK channels (SK1-SK3) are sensitive to apamin with SK2 being the most sensitive (IC_{50} ~ 40 pM) followed by SK3 (IC_{50} ~ 1 nM) and SK1 (IC_{50} ~ 10 nM) channel which has the least sensitivity.[108,109] Therefore, treatment with apamin at 100 nM concentration was expected to significantly block all SK channels. Apamin significantly increased late repolarization (APD_{80}) in wild-type hiPSC-aCMs without a significant effect on APD_{20}, APD_{50}, and APD_{80} of the rs13376333$^{+/-}$ hiPSC-aCMs, which is consistent with the MEA results. This is supportive of the hypothesis that the rs13376333 variant acts through a loss-of-function mechanism and affects the function and expression or trafficking of SK3 channels. This might suggest that the heterozygous variant hiPSC-derived aCMs have a lower amount of functional SK channels or SK channels with decreased function compared to the wild-type hiPSC-aCMs. The importance of these results lies in the application of an SK channel inhibitor for the treatment of AF in patients with the rs13376333 variant. In these cases, it might not be as effective as it would be in patients without the variant and preliminary genetic screening might be needed. Notably, the rs13376333 variant appears to primarily affect the plateau phase as reflected in the prolongation of the AP duration at 20% repolarization. This contradicts the results of the effect of apamin on AP duration at different points of repolarization, where apamin prolonged APD_{80} and not APD_{20} in the control but not the rs13376333$^{+/-}$ hiPSC-aCMs. SK channels activate in a voltage-independent manner and are responsive to changes in cytosolic Ca^{2+}. Therefore, the effect of 100 nM apamin was expected to be the greatest in the control hiPSC-aCMs at higher electrical stimulation frequencies (i.e., 2 Hz) due to greater SK channel activation in response to an increase in Ca^{2+}.

One of the possible mechanisms of the variant affecting SK channels could be its effect on the transcription or translation of the *KCNN3* gene. Splice-altering intronic point mutations can be divided into different subtypes based on their effect on splicing: (1) point mutations creating a consensus splice donor or acceptor site, (2) point mutations creating an exonic splice enhancer, and (3) point mutations creating an acceptor site

resulting in the inclusion of a cryptic 3' terminal exon.[110] Some deep intronic variants are known to cause loss-of-function and result in disease phenotypes. For instance, a biallelic intronic variant c.5457+81T>A in the gene *TRIP11* which encodes for the Golgi microtubule-associated protein 210 causes the lethal chondrodysplasia achondrogenesis type 1A characterized by short trunk, narrow chest, and craniofacial malformations.[111] This variant was found to affect transcript splicing, reduce *TRIP11* mRNA and protein levels, and result in highly compacted Golgi apparatus in affected fibroblasts.[111] Another de novo intronic variant in the *ARCN1* gene which encodes the coatomer subunit delta protein, a component of the COPI coatomer complex involved in retrograde vesical trafficking from the Golgi complex to the endoplasmic reticulum, causes rhizomelic short stature with developmental delay.[112] This de novo variant was identified through whole-genome sequencing and resulted in a splicing defect of the *ARCN1* mRNA in the proband. Therefore, more in-depth studies on the effect of the variant on transcriptome and proteome are needed.

Although some studies suggest that ivabradine does not affect AP morphology but in fact acts to decrease heart rate by increasing the diastolic interval, our results are not in agreement with these studies and suggest that ivabradine significantly prolongs APD_{80} in hiPSC-aCMs.[113] In murine models, administration of ivabradine resulted in reduction of the heart rate and increase in its variability as seen in increased R-R interval duration and variability of the R-R intervals demonstrated by increased standard deviation.[95] Furthermore, ivabradine had an effect on the TP interval, the duration between the end of the T wave and the beginning of the following P wave, and therefore affected the diastolic interval.[95] This is important to consider when interpreting our data since apamin treatment was administered following addition of ivabradine and a full washout of ivabradine cannot be confirmed. A study investigating potentially effective drug treatments for short QT syndrome (SQTS) showed that ivabradine significantly increases late repolarization phase of the AP (APD_{90}) and having no effect on APD_{50} in patient-derived hiPSC-CMs.[114] Our µOM studies are in agreement with these results and show ivabradine significantly increasing APD_{80}. In our µOM experiments, ivabradine increased APD_{80} when WT hiPSC-aCMs were not electrically stimulated and when paced at 1 Hz and 2 Hz. Application of 4 µM ivabradine also increased APD_{80} in the variant-harboring hiPSC-aCMs when they were paced at 2 Hz. Both APD_{20} and APD_{50} were not affected by ivabradine treatment. The observed increase in the late

repolarization phase of the AP may be explained by ivabradine increasing the beating rate and the AP being prolonged due to AP restitution when the cells are electrically stimulated at a certain frequency.

4.4. Limitations

One of the limitations encountered with μOM experiments was a challenge to accomplish excitation-contraction uncoupling to reduce motion artifact while avoiding altering functional properties of hiPSC-derived aCMs. Motion artifact can greatly affect AP and CaT measurements in optical mapping experiments. Our lab has recently tested the use of 5 μM mavacamten to produce excitation-contraction uncoupling in hiPSC-derived ventricular CMs. Concentrations up to 20 μM of mavacamten did not affect excitation-contraction coupling and did not successfully remove motion artifact in the optical mapping experiments of hiPSC-aCMs. Alternatively, (-)-blebbistatin, a small molecule non-muscle myosin IIA inhibitor, has been used frequently in optical mapping studies. Para-amino-blebbistatin, a more stable and less phototoxic form of (-)-blebbistatin known to be degraded to an inactive product via cytotoxic intermediates by prolonged exposure to blue light (450-490 nm), was also tested.[115,116] However, one of the advantages of the described optical mapping experiments using co-labelling with FluoVolt and Calbryte 630 is to simultaneously measure APs and CaTs. The excitation wavelength for FluoVolt falls on the further end of the blue light spectrum (peak excitation at 490 nm), therefore inactivating both (-)-blebbistatin and para-amino-blebbistatin over time. Although blebbistatin is routinely used in optical mapping experiments, it remains unclear as to whether blebbistatin has an adverse effect on physiological properties on cardiac tissue with conflicting evidence in rabbit and rat models.[117–119] Electrophysiology of the hiPSC-aCMs can be affected with addition of a drug treatment for the purpose of facilitating excitation-contraction uncoupling and reducing motion artifact due to a limited knowledge in this area.

Furthermore, intrinsic beating rate of hiPSC-aCMs highly affects the ability of the cells to entrain to electrical stimulation (1 Hz, 2 Hz, and 3 Hz). Ivabradine, which is an *HCN* blocker, was used to slow down the spontaneous beating rate by blocking I_f current produced by pacemaker cells. Ivabradine decreased the spontaneous beating rate of the hiPSC-aCMs sufficiently to allow for more consistent entrainment to 1 Hz electrical

stimulation. However, more studies should be done to study the effect of ivabradine on electrophysiology of hiPSC-derived cardiomyocytes.

A lack of a microfluidic device to exchange imaging solution and drug treatment media was a limitation in our μOM experiments. It is unknown whether ivabradine is removed upon a washout and a media change to deliver the next drug treatment such as apamin, therefore the effect of ivabradine on the electrophysiology of the hiPSC-aCMs may overlap the effect of apamin.

Replating of matured hiPSC-aCMs proved to be challenging thereby limiting the ability to collect data on matured samples. The main and persistent issue was aggregation and clumping of the cells when replating onto CytoView MEA plates or coverslips for optical mapping experiments. Optimization of the dissociation and replating protocols should be considered to repeat these experiments on mature hiPSC-aCMs.

Lastly, one of the general limitations of the hiPSC model for studying inherited cardiac arrhythmias is its inability to recapitulate the complexity of the 3D structure of the atria and ventricles. The complexity of 3D structure compared to 2D structure lies in a lack of 3D cell-to-cell interaction between multiple cell types, and immature and fetal-like phenotype and gene expression profile. However, hiPSCs are more commonly used to investigate cellular and molecular mechanisms underlying excitability alterations in diseased hiPSC-CMs and 3D cultures are becoming a more common approach.

Chapter 5.

Future Directions

In addition to generating a heterozygous rs13376333$^{+/-}$ hiPSC line, it would be beneficial to generate a homozygous rs13376333$^{+/+}$ and SK3 knock-out hiPSC using CRISPR-Cas9 or other gene editing technologies such as base or prime editing. The choice of the gene editing method would depend on the complexity of the construct, the final goal of the edit (e.g., point mutation, deletion, insertion, etc.), and accessibility of the gene editing site. The experiments of this project can be repeated, and results validated using a homozygous variant hiPSC line. The results of this project can be further expanded by investigating the effect of the rs13376333 variant on the transcriptomic and proteomic profiles, as well as apamin-sensitive currents as can be studied using patch clamping.

To investigate how the variant affects mRNA and protein levels of the *KCNN3* gene, it would be useful to quantify the base level of *KCNN1-KCNN3* mRNA and protein expression in wild-type hiPSC-aCMs to improve our hiPSC-aCM model of atrial fibrillation. The research investigating mRNA and protein levels of SK1-SK3 channels in human hiPSC-derived cardiomyocytes and native tissues is limited. This is particularly important considering the controversy around whether SK channel blocking has a proarrhythmic or antiarrhythmic effect, and the variant being located in an intronic region of the *KCNN3* gene. The results of this project can lead to improving our knowledge of the genetic component of AF, improving screening approaches to identify the risk variants before the onset of AF, and developing precise treatments in patients with the rs13376333 variant. Studies using an hiPSC line with the SK3 knock-out would greatly facilitate our understanding of the role of SK3 ion channels in a normal physiological environment as well as extending the knowledge on the role of SK channels in inherited cardiac arrhythmias in hiPSC-derived CM model.

Patch clamp of the hiPSC-aCMs can be used to investigate apamin-sensitive currents in hiPSC-aCMs. Based on the results of my project, the rs13376333 variant prolongs AP duration, particularly at 20% repolarization. Therefore, these results can be

investigated further by assessing apamin-sensitive currents using patch clamping variant-harboring hiPSC-aCMs and their isogenic control cells.

Lastly, there is a trend towards generating and culturing 3D cardiac organoids (cardioids) and using 3D bioprinting to study a variety of diseases. The gene-edited hiPSC-aCMs can be used for both cardioids and 3D bioprinting and allow to generate lab-grown tissues carrying the variant of interest and their isogenic control.

5.1. High-Speed Optical Mapping

High-speed optical mapping (1000 fps) is a useful and high throughput tool to investigate Ca^{2+} transients and AP duration and morphology. While some setups only consist of a single-channel camera, it is possible to add a second-channel camera to be able to use different dyes for imaging both Ca^{2+} and AP parameters. Figures 5.1 and 5.2 show an example of the resolution and Ca^{2+} transients recorded on our HS-OM rig using Calbryte 520. Activation maps and conduction velocity maps, as well as Ca^{2+} transient and AP analysis can be done with the Workbench software. This tool can be particularly useful in assessing hiPSC-CMs for arrhythmias by looking for re-entry loops and evaluating the effect on drug treatments on Ca^{2+} transients, AP duration, and conduction velocity.

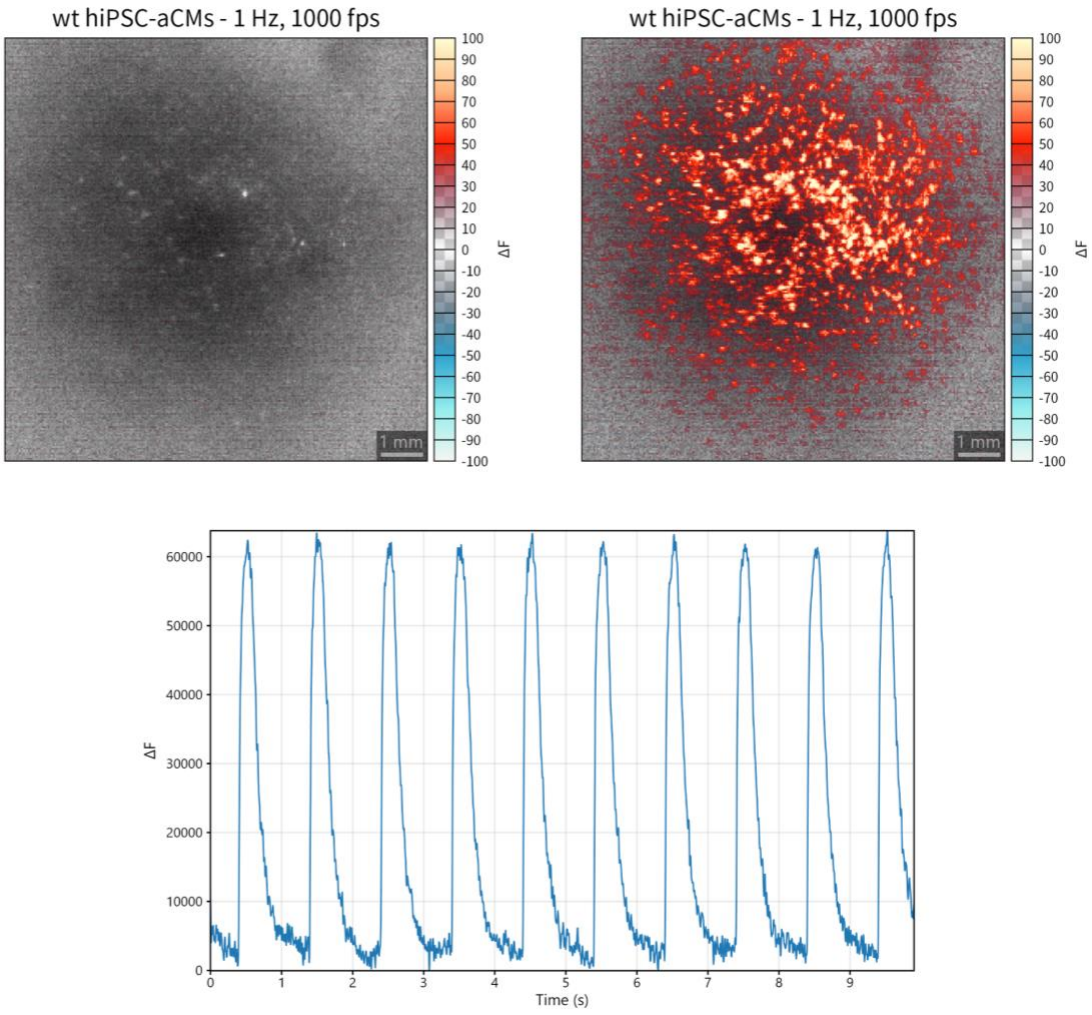

Figure 5.1 High-speed optical mapping of wild-type hiPSC-aCMs.
Representative calcium transients of wild-type (wt) hiPSC-aCMs stimulated and entrained to 1 Hz recorded with high-speed optical mapping. Top panel shows a snapshot preceding a calcium transient on the left, and peak calcium transient on the right. Bottom panel shows representative calcium transients traces during a 10 second recording.

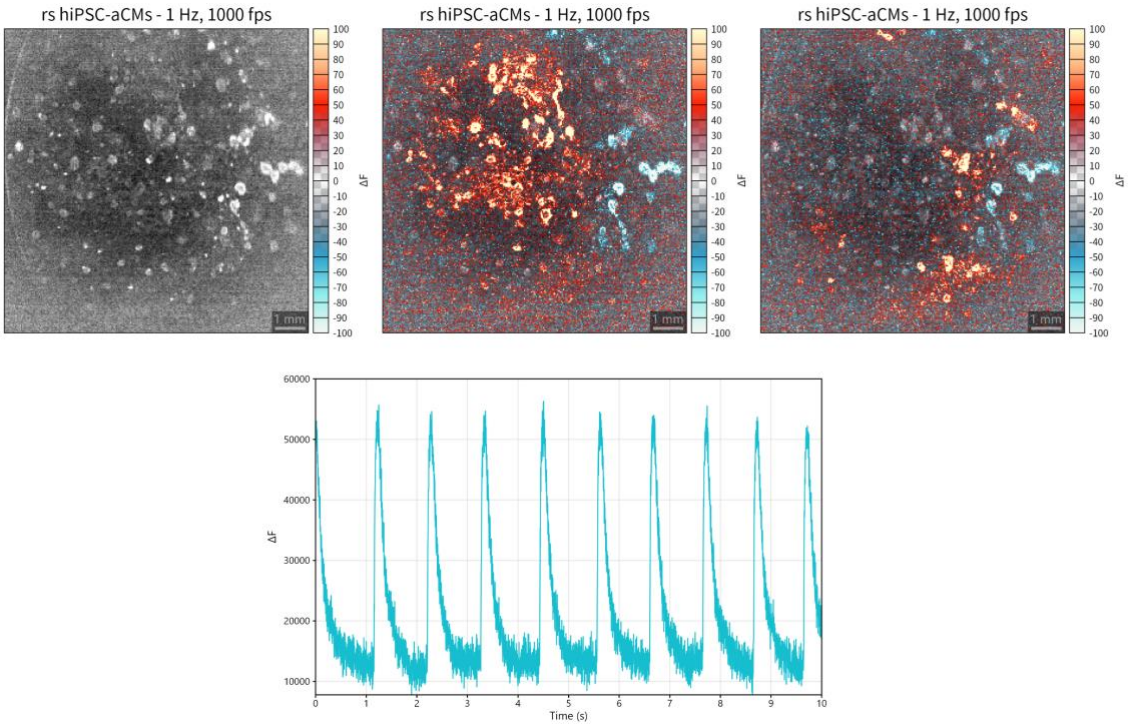

Figure 5.2 High-speed optical mapping of rs13376333$^{+/-}$ hiPSC-aCMs.
Representative calcium transients of rs13376333$^{+/-}$ (rs) hiPSC-aCMs stimulated and entrained to 1 Hz recorded with high-speed optical mapping. Top panel shows a snapshot preceding a calcium transient on the left, and peak calcium transient on the right. Bottom panel shows representative calcium transients traces during a 10 second recording.

Chapter 6.

Conclusion

In this study, I successfully gene edited an hiPSC line to contain the heterozygous rs13376333 variant for further experiments such as multielectrode, optical mapping, patch clamping, transcriptome, and proteome assays. In my study, I investigated the effect of the variant on multiple parameters using MEA and μOM. My results suggest that the rs13376333 variant acts through a loss-of-function mechanism and increases AP duration at 20% repolarization, increases variability within electrophysiological parameters of the hiPSC-aCMs, but did not affect spike amplitude and conduction velocity. Both increased AP duration and beat-to-beat variability have a potentially proarrhythmic effect. Overall, my study contributed to expanding the knowledge of the genetic basis of AF and using hiPSCs as a model to study inherited cardiac arrhythmias.

References

1. Chugh SS, Havmoeller R, Narayanan K, et al. Worldwide Epidemiology of Atrial Fibrillation: A Global Burden of Disease 2010 Study. *Circulation*. 2014;129(8):837-847. doi:10.1161/CIRCULATIONAHA.113.005119

2. Staerk L, Sherer JA, Ko D, Benjamin EJ, Helm RH. Atrial Fibrillation: Epidemiology, Pathophysiology, and Clinical Outcomes. *Circ Res*. 2017;120(9):1501-1517. doi:10.1161/CIRCRESAHA.117.309732

3. Kim EJ, Yin X, Fontes JD, et al. Atrial fibrillation without comorbidities: Prevalence, incidence and prognosis (from the Framingham Heart Study). *Am Heart J*. 2016;177:138-144. doi:10.1016/j.ahj.2016.03.023

4. Potpara TS, Lip GYH. Lone atrial fibrillation - an overview. *Int J Clin Pract*. 2014;68(4):418-433. doi:10.1111/ijcp.12281

5. Fuster V, Rydén LE, Cannom DS, et al. 2011 ACCF/AHA/HRS Focused Updates Incorporated Into the ACC/AHA/ESC 2006 Guidelines for the Management of Patients With Atrial Fibrillation. *Circulation*. 2011;123(10):e269-e367. doi:10.1161/CIR.0b013e318214876d

6. Arnar DO, Thorvaldsson S, Manolio TA, et al. Familial aggregation of atrial fibrillation in Iceland. *Eur Heart J*. 2006;27(6):708-712. doi:10.1093/eurheartj/ehi727

7. Schnabel RB, Yin X, Gona P, et al. 50 year trends in atrial fibrillation prevalence, incidence, risk factors, and mortality in the Framingham Heart Study: a cohort study. *Lancet Lond Engl*. 2015;386(9989):154-162. doi:10.1016/S0140-6736(14)61774-8

8. Humphries KH, Kerr CR, Connolly SJ, et al. New-Onset Atrial Fibrillation. *Circulation*. 2001;103(19):2365-2370. doi:10.1161/01.CIR.103.19.2365

9. Friberg J, Scharling H, Gadsbøll N, Truelsen T, Jensen GB, Copenhagen City Heart Study. Comparison of the impact of atrial fibrillation on the risk of stroke and cardiovascular death in women versus men (The Copenhagen City Heart Study). *Am J Cardiol*. 2004;94(7):889-894. doi:10.1016/j.amjcard.2004.06.023

10. Rodriguez CJ, Soliman EZ, Alonso A, et al. Atrial fibrillation incidence and risk factors in relation to race-ethnicity and the population attributable fraction of atrial fibrillation risk factors: the Multi-Ethnic Study of Atherosclerosis. *Ann Epidemiol*. 2015;25(2):71-76.e1. doi:10.1016/j.annepidem.2014.11.024

11. Marcus GM, Alonso A, Peralta CA, et al. European Ancestry as a Risk Factor for Atrial Fibrillation in African Americans. *Circulation*. 2010;122(20):2009-2015. doi:10.1161/CIRCULATIONAHA.110.958306

12. Benjamin EJ, Levy D, Vaziri SM, D'Agostino RB, Belanger AJ, Wolf PA. Independent Risk Factors for Atrial Fibrillation in a Population-Based Cohort: The Framingham Heart Study. *JAMA*. 1994;271(11):840-844. doi:10.1001/jama.1994.03510350050036

13. Lawler PR, Hiremath P, Cheng S. Cardiac Target Organ Damage in Hypertension: Insights from Epidemiology. *Curr Hypertens Rep*. 2014;16(7):446. doi:10.1007/s11906-014-0446-8

14. Dzeshka MS, Lip GYH, Snezhitskiy V, Shantsila E. Cardiac Fibrosis in Patients With Atrial Fibrillation: Mechanisms and Clinical Implications. *J Am Coll Cardiol*. 2015;66(8):943-959. doi:10.1016/j.jacc.2015.06.1313

15. Roselli C, Rienstra M, Ellinor PT. Genetics of Atrial Fibrillation in 2020: GWAS, Genome Sequencing, Polygenic Risk, and Beyond. *Circ Res*. 2020;127(1):21-33. doi:10.1161/CIRCRESAHA.120.316575

16. Ellinor PT, Lunetta KL, Glazer NL, et al. Common variants in KCNN3 are associated with lone atrial fibrillation. *Nat Genet*. 2010;42(3):240-244. doi:10.1038/ng.537

17. Yao JL, Zhou YF, Yang XJ, Qian XD, Jiang WP. KCNN3 SNP rs13376333 on Chromosome 1q21 Confers Increased Risk of Atrial Fibrillation. *Int Heart J*. 2015;56(5):511-515. doi:10.1536/ihj.15-133

18. Luo Z, Yan C, Zhang W, et al. Association between SNP rs13376333 and rs1131820 in the KCNN3 gene and atrial fibrillation in the Chinese Han population. *Clin Chem Lab Med CCLM*. 2014;52(12). doi:10.1515/cclm-2014-0491

19. Bauer CK, Schneeberger PE, Kortüm F, et al. Gain-of-Function Mutations in KCNN3 Encoding the Small-Conductance Ca2+-Activated K+ Channel SK3 Cause Zimmermann-Laband Syndrome. *Am J Hum Genet*. 2019;104(6):1139-1157. doi:10.1016/j.ajhg.2019.04.012

20. Gripp KW, Smithson SF, Scurr IJ, et al. Syndromic disorders caused by gain-of-function variants in KCNH1, KCNK4, and KCNN3—a subgroup of K+ channelopathies. *Eur J Hum Genet*. 2021;29(9):1384-1395. doi:10.1038/s41431-021-00818-9

21. Schwarz M, Ryba L, Křepelová A, et al. Zimmermann–Laband syndrome in monozygotic twins with a mild neurobehavioral phenotype lacking gingival overgrowth—A case report of a novel KCNN3 gene variant. *Am J Med Genet A*. 2022;188(4):1083-1087. doi:10.1002/ajmg.a.62616

22. Papasaikas P, Valcárcel J. The Spliceosome: The Ultimate RNA Chaperone and Sculptor. *Trends Biochem Sci*. 2016;41(1):33-45. doi:10.1016/j.tibs.2015.11.003

23. Carmel L, Chorev M. The Function of Introns. *Front Genet*. 2012;3. Accessed March 22, 2023. https://www.frontiersin.org/articles/10.3389/fgene.2012.00055

24. Popp MW, Maquat LE. Leveraging Rules of Nonsense-Mediated mRNA Decay for Genome Engineering and Personalized Medicine. *Cell*. 2016;165(6):1319-1322. doi:10.1016/j.cell.2016.05.053

25. Kelly S, Georgomanolis T, Zirkel A, et al. Splicing of many human genes involves sites embedded within introns. *Nucleic Acids Res*. 2015;43(9):4721-4732. doi:10.1093/nar/gkv386

26. Vaz-Drago R, Custódio N, Carmo-Fonseca M. Deep intronic mutations and human disease. *Hum Genet*. 2017;136(9):1093-1111. doi:10.1007/s00439-017-1809-4

27. Antonellis A, Dennis MY, Burzynski G, et al. A Rare Myelin Protein Zero (MPZ) Variant Alters Enhancer Activity In Vitro and In Vivo. *PLOS ONE*. 2010;5(12):e14346. doi:10.1371/journal.pone.0014346

28. Bovolenta M, Neri M, Martoni E, et al. Identification of a deep intronic mutation in the COL6A2 gene by a novel custom oligonucleotide CGH array designed to explore allelic and genetic heterogeneity in collagen VI-related myopathies. *BMC Med Genet*. 2010;11(1):1-12. doi:10.1186/1471-2350-11-44

29. Iwasaki Y ki, Nishida K, Kato T, Nattel S. Atrial Fibrillation Pathophysiology. *Circulation*. 2011;124(20):2264-2274. doi:10.1161/CIRCULATIONAHA.111.019893

30. Haïssaguerre M, Jaïs P, Shah DC, et al. Spontaneous Initiation of Atrial Fibrillation by Ectopic Beats Originating in the Pulmonary Veins. *N Engl J Med*. 1998;339(10):659-666. doi:10.1056/NEJM199809033391003

31. Cheniti G, Vlachos K, Pambrun T, et al. Atrial Fibrillation Mechanisms and Implications for Catheter Ablation. *Front Physiol*. 2018;9. Accessed October 25, 2022. https://www.frontiersin.org/articles/10.3389/fphys.2018.01458

32. Schotten U, Verheule S, Kirchhof P, Goette A. Pathophysiological Mechanisms of Atrial Fibrillation: A Translational Appraisal. *Physiol Rev*. 2011;91(1):265-325. doi:10.1152/physrev.00031.2009

33. Dobrev D, Voigt N, Wehrens XHT. The ryanodine receptor channel as a molecular motif in atrial fibrillation: pathophysiological and therapeutic implications. *Cardiovasc Res*. 2011;89(4):734-743. doi:10.1093/cvr/cvq324

34. Yeh YH, Wakili R, Qi XY, et al. Calcium-Handling Abnormalities Underlying Atrial Arrhythmogenesis and Contractile Dysfunction in Dogs With Congestive Heart Failure. *Circ Arrhythm Electrophysiol*. 2008;1(2):93-102. doi:10.1161/CIRCEP.107.754788

35. Pizzale S, Gollob MH, Gow R, Birnie DH. Sudden Death in a Young Man with Catecholaminergic Polymorphic Ventricular Tachycardia and Paroxysmal Atrial Fibrillation. *J Cardiovasc Electrophysiol*. 2008;19(12):1319-1321. doi:10.1111/j.1540-8167.2008.01211.x

36. Comtois P, Kneller J, Nattel S. Of circles and spirals: Bridging the gap between the leading circle and spiral wave concepts of cardiac reentry. *EP Eur*. 2005;7(s2):S10-S20. doi:10.1016/j.eupc.2005.05.011

37. Waks JW. Mechanisms of Atrial Fibrillation – Reentry, Rotors and Reality. Published online August 8, 2014. Accessed October 26, 2022. https://www.aerjournal.com/articles/mechanisms-atrial-fibrillation-reentry-rotors-and-reality

38. Moe GK, Abildskov JA. Atrial fibrillation as a self-sustaining arrhythmia independent of focal discharge. *Am Heart J*. 1959;58(1):59-70. doi:10.1016/0002-8703(59)90274-1

39. 2019 AHA/ACC/HRS Focused Update of the 2014 AHA/ACC/HRS Guideline for the Management of Patients With Atrial Fibrillation: A Report of the American College of Cardiology/American Heart Association Task Force on Clinical Practice Guidelines and the Heart Rhythm Society. *J Am Coll Cardiol*. 2019;74(1):104-132. doi:10.1016/j.jacc.2019.01.011

40. Morin DP, Bernard ML, Madias C, Rogers PA, Thihalolipavan S, Estes NAM. The State of the Art: Atrial Fibrillation Epidemiology, Prevention, and Treatment. *Mayo Clin Proc*. 2016;91(12):1778-1810. doi:10.1016/j.mayocp.2016.08.022

41. Van Gelder IC, Hagens VE, Bosker HA, et al. A Comparison of Rate Control and Rhythm Control in Patients with Recurrent Persistent Atrial Fibrillation. *N Engl J Med*. 2002;347(23):1834-1840. doi:10.1056/NEJMoa021375

42. Waldo AL. Rate Control versus Rhythm Control in Atrial Fibrillation: Lessons Learned from Clinical Trials of Atrial Fibrillation. *Prog Cardiovasc Dis*. 2015;58(2):168-176. doi:10.1016/j.pcad.2015.08.006

43. Calkins H, Kuck KH, Cappato R, et al. 2012 HRS/EHRA/ECAS expert consensus statement on catheter and surgical ablation of atrial fibrillation: recommendations for patient selection, procedural techniques, patient management and follow-up, definitions, endpoints, and research trial design: a report of the Heart Rhythm Society (HRS) Task Force on Catheter and Surgical Ablation of Atrial Fibrillation. Developed in partnership with the European Heart Rhythm Association (EHRA), a registered branch of the European Society of Cardiology (ESC) and the European Cardiac Arrhythmia Society (ECAS); and in collaboration with the American College of Cardiology (ACC), American Heart Association (AHA), the Asia Pacific Heart Rhythm Society (APHRS), and the Society of Thoracic Surgeons (STS). Endorsed by the governing bodies of the American College of Cardiology Foundation, the American Heart Association, the European Cardiac Arrhythmia Society, the European Heart Rhythm Association, the Society of Thoracic Surgeons, the Asia Pacific Heart Rhythm Society, and the Heart Rhythm Society. *Heart Rhythm*. 2012;9(4):632-696.e21. doi:10.1016/j.hrthm.2011.12.016

44. Andrade JG, Wells GA, Deyell MW, et al. Cryoablation or Drug Therapy for Initial Treatment of Atrial Fibrillation. *N Engl J Med*. 2021;384(4):305-315. doi:10.1056/NEJMoa2029980

45. Andrade JG, Deyell MW, Macle L, et al. Progression of Atrial Fibrillation after Cryoablation or Drug Therapy. *N Engl J Med*. 2023;388(2):105-116. doi:10.1056/NEJMoa2212540

46. Fozzard HA, Hanck DA. Structure and function of voltage-dependent sodium channels: comparison of brain II and cardiac isoforms. *Physiol Rev*. 1996;76(3):887-926. doi:10.1152/physrev.1996.76.3.887

47. Xu H, Guo W, Nerbonne JM. Four Kinetically Distinct Depolarization-activated K+ Currents in Adult Mouse Ventricular Myocytes. *J Gen Physiol*. 1999;113(5):661-678. doi:10.1085/jgp.113.5.661

48. Wang Z, Fermini B, Nattel S. Sustained depolarization-induced outward current in human atrial myocytes. Evidence for a novel delayed rectifier K+ current similar to Kv1.5 cloned channel currents. *Circ Res*. 1993;73(6):1061-1076. doi:10.1161/01.RES.73.6.1061

49. Firek L, Giles WR. Outward currents underlying repolarization in human atrial myocytes. *Cardiovasc Res*. 1995;30(1):31-38. doi:10.1016/S0008-6363(95)00014-3

50. Amos GJ, Wettwer E, Metzger F, Li Q, Himmel HM, Ravens U. Differences between outward currents of human atrial and subepicardial ventricular myocytes. *J Physiol*. 1996;491(1):31-50. doi:10.1113/jphysiol.1996.sp021194

51. Feng J, Xu D, Wang Z, Nattel S. Ultrarapid delayed rectifier current inactivation in human atrial myocytes: properties and consequences. *Am J Physiol*. 1998;275(5):H1717-1725. doi:10.1152/ajpheart.1998.275.5.H1717

52. Beeler GW, Reuter H. Membrane calcium current in ventricular myocardial fibres. *J Physiol*. 1970;207(1):191-209.

53. Gaborit N, Le Bouter S, Szuts V, et al. Regional and tissue specific transcript signatures of ion channel genes in the non-diseased human heart. *J Physiol*. 2007;582(Pt 2):675-693. doi:10.1113/jphysiol.2006.126714

54. Zhang Q, Timofeyev V, Qiu H, et al. Expression and roles of Cav1.3 (α1D) L-Type Ca2+ Channel in atrioventricular node automaticity. *J Mol Cell Cardiol*. 2011;50(1):194-202. doi:10.1016/j.yjmcc.2010.10.002

55. Zhang Z, Xu Y, Song H, et al. Functional Roles of Cav1.3 (α1D) Calcium Channel in Sinoatrial Nodes. *Circ Res*. 2002;90(9):981-987. doi:10.1161/01.RES.0000018003.14304.E2

56. Mangoni ME, Couette B, Bourinet E, et al. Functional role of L-type Cav1.3 Ca2+ channels in cardiac pacemaker activity. *Proc Natl Acad Sci*. 2003;100(9):5543-5548. doi:10.1073/pnas.0935295100

57. Marionneau C, Couette B, Liu J, et al. Specific pattern of ionic channel gene expression associated with pacemaker activity in the mouse heart. *J Physiol*. 2005;562(1):223-234. doi:10.1113/jphysiol.2004.074047

58. Mangoni ME, Couette B, Marger L, Bourinet E, Striessnig J, Nargeot J. Voltage-dependent calcium channels and cardiac pacemaker activity: From ionic currents to genes. *Prog Biophys Mol Biol*. 2006;90(1):38-63. doi:10.1016/j.pbiomolbio.2005.05.003

59. Christel CJ, Cardona N, Mesirca P, et al. Distinct localization and modulation of Cav1.2 and Cav1.3 L-type Ca2+ channels in mouse sinoatrial node. *J Physiol*. 2012;590(24):6327-6341. doi:10.1113/jphysiol.2012.239954

60. Calcium Cycling and Signaling in Cardiac Myocytes | Annual Review of Physiology. Accessed February 16, 2023. https://www-annualreviews-org.proxy.lib.sfu.ca/doi/10.1146/annurev.physiol.70.113006.100455

61. Dibb KM, Eisner DA, Trafford AW. Regulation of systolic [Ca2+]i and cellular Ca2+ flux balance in rat ventricular myocytes by SR Ca2+, L-type Ca2+ current and diastolic [Ca2+]i. *J Physiol*. 2007;585(2):579-592. doi:10.1113/jphysiol.2007.141473

62. Krapivinsky G, Gordon EA, Wickman K, Velimirović B, Krapivinsky L, Clapham DE. The G-protein-gated atrial K+ channel IKAch is a heteromultimer of two inwardly rectifying K+-channel proteins. *Nature*. 1995;374(6518):135-141. doi:10.1038/374135a0

63. Koumi S, Wasserstrom JA. Acetylcholine-sensitive muscarinic K+ channels in mammalian ventricular myocytes. *Am J Physiol-Heart Circ Physiol*. 1994;266(5):H1812-H1821. doi:10.1152/ajpheart.1994.266.5.H1812

64. Liang B, Nissen JD, Laursen M, et al. G-protein-coupled inward rectifier potassium current contributes to ventricular repolarization. *Cardiovasc Res*. 2014;101(1):175-184. doi:10.1093/cvr/cvt240

65. Köhler M, Hirschberg B, Bond CT, et al. Small-Conductance, Calcium-Activated Potassium Channels from Mammalian Brain. *Science*. 1996;273(5282):1709-1714. doi:10.1126/science.273.5282.1709

66. Kshatri AS, Gonzalez-Hernandez A, Giraldez T. Physiological Roles and Therapeutic Potential of Ca2+ Activated Potassium Channels in the Nervous System. *Front Mol Neurosci*. 2018;11. Accessed December 19, 2022. https://www.frontiersin.org/articles/10.3389/fnmol.2018.00258

67. Tuteja D, Rafizadeh S, Timofeyev V, et al. Cardiac Small Conductance Ca $^{2+}$ -Activated K $^{+}$ Channel Subunits Form Heteromultimers via the Coiled-Coil Domains in the C Termini of the Channels. *Circ Res*. 2010;107(7):851-859. doi:10.1161/CIRCRESAHA.109.215269

68. Xia XM, Fakler B, Rivard A, et al. Mechanism of calcium gating in small-conductance calcium-activated potassium channels. *Nature*. 1998;395(6701):503-507. doi:10.1038/26758

69. Bildl W, Strassmaier T, Thurm H, et al. Protein Kinase CK2 Is Coassembled with Small Conductance Ca2+-Activated K+ Channels and Regulates Channel Gating. *Neuron*. 2004;43(6):847-858. doi:10.1016/j.neuron.2004.08.033

70. Allen D, Fakler B, Maylie J, Adelman JP. Organization and Regulation of Small Conductance Ca2+-activated K+ Channel Multiprotein Complexes. *J Neurosci*. 2007;27(9):2369-2376. doi:10.1523/JNEUROSCI.3565-06.2007

71. Lu L, Zhang Q, Timofeyev V, et al. Molecular Coupling of a Ca $^{2+}$ -Activated K $^{+}$ Channel to L-Type Ca $^{2+}$ Channels via α-Actinin2. *Circ Res*. 2007;100(1):112-120. doi:10.1161/01.RES.0000253095.44186.72

72. Lu L, Timofeyev V, Li N, et al. α-Actinin2 cytoskeletal protein is required for the functional membrane localization of a Ca2+-activated K+ channel (SK2 channel). *Proc Natl Acad Sci*. 2009;106(43):18402-18407. doi:10.1073/pnas.0908207106

73. Rafizadeh S, Zhang Z, Woltz RL, et al. Functional interaction with filamin A and intracellular Ca2+ enhance the surface membrane expression of a small-conductance Ca2+-activated K+ (SK2) channel. *Proc Natl Acad Sci*. 2014;111(27):9989-9994. doi:10.1073/pnas.1323541111

74. Zhang Z, Ledford HA, Park S, et al. Distinct subcellular mechanisms for the enhancement of the surface membrane expression of SK2 channel by its interacting proteins, α-actinin2 and filamin A. *J Physiol*. 2017;595(7):2271-2284. doi:10.1113/JP272942

75. Zhang XD, Timofeyev V, Li N, et al. Critical roles of a small conductance Ca2+-activated K+ channel (SK3) in the repolarization process of atrial myocytes. *Cardiovasc Res*. 2014;101(2):317-325. doi:10.1093/cvr/cvt262

76. Bond CT, Sprengel R, Bissonnette JM, et al. Respiration and Parturition Affected by Conditional Overexpression of the Ca2+-Activated K+ Channel Subunit, SK3. *Science*. 2000;289(5486):1942-1946. doi:10.1126/science.289.5486.1942

77. Xu Y, Tuteja D, Zhang Z, et al. Molecular Identification and Functional Roles of a Ca2+-activated K+ Channel in Human and Mouse Hearts. *J Biol Chem*. 2003;278(49):49085-49094. doi:10.1074/jbc.M307508200

78. Tuteja D, Xu D, Timofeyev V, et al. Differential expression of small-conductance Ca^{2+}-activated K^{+} channels SK1, SK2, and SK3 in mouse atrial and ventricular myocytes. *Am J Physiol-Heart Circ Physiol*. 2005;289(6):H2714-H2723. doi:10.1152/ajpheart.00534.2005

79. Hancock JM, Weatherall KL, Choisy SC, James AF, Hancox JC, Marrion NV. Selective activation of heteromeric SK channels contributes to action potential repolarization in mouse atrial myocytes. *Heart Rhythm*. 2015;12(5):1003-1015. doi:10.1016/j.hrthm.2015.01.027

80. Qi XY, Diness JG, Brundel BJJM, et al. Role of Small-Conductance Calcium-Activated Potassium Channels in Atrial Electrophysiology and Fibrillation in the Dog. *Circulation*. 2014;129(4):430-440. doi:10.1161/CIRCULATIONAHA.113.003019

81. Diness JG, Skibsbye L, Simó-Vicens R, et al. Termination of Vernakalant-Resistant Atrial Fibrillation by Inhibition of Small-Conductance Ca^{2+}-Activated K^{+} Channels in Pigs. *Circ Arrhythm Electrophysiol*. 2017;10(10):e005125. doi:10.1161/CIRCEP.117.005125

82. Skibsbye L, Poulet C, Diness JG, et al. Small-conductance calcium-activated potassium (SK) channels contribute to action potential repolarization in human atria. *Cardiovasc Res*. 2014;103(1):156-167. doi:10.1093/cvr/cvu121

83. Yu T, Deng C, Wu R, et al. Decreased expression of small-conductance Ca2+-activated K+ channels SK1 and SK2 in human chronic atrial fibrillation. *Life Sci*. 2012;90(5-6):219-227. doi:10.1016/j.lfs.2011.11.008

84. Shamsaldeen YA, Culliford L, Clout M, et al. Role of SK channel activation in determining the action potential configuration in freshly isolated human atrial myocytes from the SKArF study. *Biochem Biophys Res Commun*. 2019;512(4):684-690. doi:10.1016/j.bbrc.2019.03.074

85. Heijman J, Zhou X, Morotti S, et al. Enhanced Ca $^{2+}$ -Dependent SK-Channel Gating and Membrane Trafficking in Human Atrial Fibrillation. *Circ Res*. Published online March 17, 2023:CIRCRESAHA.122.321858. doi:10.1161/CIRCRESAHA.122.321858

86. Darkow E, Nguyen TT, Stolina M, et al. Small Conductance Ca2 +-Activated K+ (SK) Channel mRNA Expression in Human Atrial and Ventricular Tissue: Comparison Between Donor, Atrial Fibrillation and Heart Failure Tissue. *Front Physiol*. 2021;12:650964. doi:10.3389/fphys.2021.650964

87. Bentzen BH, Bomholtz SH, Simó-Vicens R, et al. Mechanisms of Action of the KCa2-Negative Modulator AP30663, a Novel Compound in Development for Treatment of Atrial Fibrillation in Man. *Front Pharmacol*. 2020;11:610. doi:10.3389/fphar.2020.00610

88. Lian X, Zhang J, Azarin SM, et al. Directed cardiomyocyte differentiation from human pluripotent stem cells by modulating Wnt/β-catenin signaling under fully defined conditions. *Nat Protoc*. 2013;8(1):162-175. doi:10.1038/nprot.2012.150

89. Gunawan MG, Sangha SS, Shafaattalab S, et al. Drug screening platform using human induced pluripotent stem cell-derived atrial cardiomyocytes and optical mapping. *Stem Cells Transl Med*. 2021;10(1):68-82. doi:10.1002/sctm.19-0440

90. Zhang M, Pascal JM, Schumann M, Armen RS, Zhang JF. Identification of the functional binding pocket for compounds targeting small-conductance Ca2+-activated potassium channels. *Nat Commun*. 2012;3(1):1021. doi:10.1038/ncomms2017

91. Zhao Z, Lan H, El-Battrawy I, et al. Ion Channel Expression and Characterization in Human Induced Pluripotent Stem Cell-Derived Cardiomyocytes. *Stem Cells Int*. 2018;2018:e6067096. doi:10.1155/2018/6067096

92. Thollon C, Cambarrat C, Vian J, Prost JF, Peglion JL, Vilaine JP. Electrophysiological effects of S 16257, a novel sino-atrial node modulator, on rabbit and guinea-pig cardiac preparations: comparison with UL-FS 49. *Br J Pharmacol*. 1994;112(1):37-42. doi:10.1111/j.1476-5381.1994.tb13025.x

93. Thollon C, Bidouard JP, Cambarrat C, et al. Stereospecific in vitro and in vivo effects of the new sinus node inhibitor (+)-S 16257. *Eur J Pharmacol*. 1997;339(1):43-51. doi:10.1016/S0014-2999(97)01364-2

95. Stieber J, Wieland K, Stöckl G, Ludwig A, Hofmann F. Bradycardic and Proarrhythmic Properties of Sinus Node Inhibitors. *Mol Pharmacol*. 2006;69(4):1328-1337. doi:10.1124/mol.105.020701

96. Anzalone AV, Randolph PB, Davis JR, et al. Search-and-replace genome editing without double-strand breaks or donor DNA. *Nature*. 2019;576(7785):149-157. doi:10.1038/s41586-019-1711-4

97. Komor AC, Kim YB, Packer MS, Zuris JA, Liu DR. Programmable editing of a target base in genomic DNA without double-stranded DNA cleavage. *Nature*. 2016;533(7603):420-424. doi:10.1038/nature17946

98. Yang X, Pabon L, Murry CE. Engineering Adolescence. *Circ Res*. 2014;114(3):511-523. doi:10.1161/CIRCRESAHA.114.300558

99. Gal P, Klaassen ES, Bergmann KR, et al. First Clinical Study with AP30663 - a K_{Ca} 2 Channel Inhibitor in Development for Conversion of Atrial Fibrillation. *Clin Transl Sci*. 2020;13(6):1336-1344. doi:10.1111/cts.12835

100. Diness JG, Sørensen US, Nissen JD, et al. Inhibition of Small-Conductance Ca^{2+} -Activated K^{+} Channels Terminates and Protects Against Atrial Fibrillation. *Circ Arrhythm Electrophysiol*. 2010;3(4):380-390. doi:10.1161/CIRCEP.110.957407

101. Diness JG, Skibsbye L, Jespersen T, et al. Effects on Atrial Fibrillation in Aged Hypertensive Rats by Ca2+-Activated K+ Channel Inhibition. *Hypertension*. 2011;57(6):1129-1135. doi:10.1161/HYPERTENSIONAHA.111.170613

102. Skibsbye L, Diness JG, Sørensen US, Hansen RS, Grunnet M. The Duration of Pacing-induced Atrial Fibrillation Is Reduced in Vivo by Inhibition of Small Conductance Ca2+-activated K+ Channels: *J Cardiovasc Pharmacol*. 2011;57(6):672-681. doi:10.1097/FJC.0b013e318217943d

103. Haugaard MM, Hesselkilde EZ, Pehrson S, et al. Pharmacologic inhibition of small-conductance calcium-activated potassium (SK) channels by NS8593 reveals atrial antiarrhythmic potential in horses. *Heart Rhythm*. 2015;12(4):825-835. doi:10.1016/j.hrthm.2014.12.028

104. Soepriatna AH, Kim TY, Daley MC, Song E, Choi BR, Coulombe KLK. Human Atrial Cardiac Microtissues for Chamber-Specific Arrhythmic Risk Assessment. *Cell Mol Bioeng*. 2021;14(5):441-457. doi:10.1007/s12195-021-00703-x

105. Abdelnabi M. Ivabradine and AF: Coincidence, Correlation or a New Treatment? Published online January 8, 2020. Accessed February 8, 2023. https://www.aerjournal.com/articles/ivabradine-and-af-coincidence-correlation-or-new-treatment

106. Aslanidi OV, Boyett MR, Dobrzynski H, Li J, Zhang H. Mechanisms of Transition from Normal to Reentrant Electrical Activity in a Model of Rabbit Atrial Tissue: Interaction of Tissue Heterogeneity and Anisotropy. *Biophys J*. 2009;96(3):798-817. doi:10.1016/j.bpj.2008.09.057

107. Hsueh CH, Chang PC, Hsieh YC, Reher T, Chen PS, Lin SF. Proarrhythmic effect of blocking the small conductance calcium activated potassium channel in isolated canine left atrium. *Heart Rhythm*. 2013;10(6):891-898. doi:10.1016/j.hrthm.2013.01.033

108. Ishii TM, Maylie J, Adelman JP. Determinants of Apamin and d-Tubocurarine Block in SK Potassium Channels*. *J Biol Chem*. 1997;272(37):23195-23200. doi:10.1074/jbc.272.37.23195

109. Qi MM, Qian LL, Wang RX. Modulation of SK Channels: Insight Into Therapeutics of Atrial Fibrillation. *Heart Lung Circ*. 2021;30(8):1130-1139. doi:10.1016/j.hlc.2021.01.009

110. Waldrop MA, Moore SA, Mathews KD, et al. Intron mutations and early transcription termination in Duchenne and Becker muscular dystrophy. *Hum Mutat*. 2022;43(4):511-528. doi:10.1002/humu.24343

111. Upadhyai P, Radhakrishnan P, Guleria VS, et al. Biallelic deep intronic variant c.5457+81T>A in TRIP11 causes loss of function and results in achondrogenesis 1A. *Hum Mutat*. 2021;42(8):1005-1014. doi:10.1002/humu.24235

112. Tidwell T, Deshotel M, Palumbos J, Miller C, Bayrak-Toydemir P, Carey JC. Novel de novo ARCN1 intronic variant causes rhizomelic short stature with microretrognathia and developmental delay. *Mol Case Stud*. 2020;6(6):a005728. doi:10.1101/mcs.a005728

113. Haechl N, Ebner J, Hilber K, Todt H, Koenig X. Pharmacological Profile of the Bradycardic Agent Ivabradine on Human Cardiac Ion Channels | Cell Physiol Biochem. *Cell Physiol Biochem*. 2019;53(1):36-48.

114. Zhao Z, Li X, El-Battrawy I, et al. Drug Testing in Human-Induced Pluripotent Stem Cell–Derived Cardiomyocytes From a Patient With Short QT Syndrome Type 1. *Clin Pharmacol Ther*. 2019;106(3):642-651. doi:10.1002/cpt.1449

115. Kolega J. Phototoxicity and photoinactivation of blebbistatin in UV and visible light. *Biochem Biophys Res Commun*. 2004;320(3):1020-1025. doi:10.1016/j.bbrc.2004.06.045

116. Sakamoto T, Limouze J, Combs CA, Straight AF, Sellers JR. Blebbistatin, a Myosin II Inhibitor, Is Photoinactivated by Blue Light. *Biochemistry*. 2005;44(2):584-588. doi:10.1021/bi0483357

117. Fedorov VV, Lozinsky IT, Sosunov EA, et al. Application of blebbistatin as an excitation–contraction uncoupler for electrophysiologic study of rat and rabbit hearts. *Heart Rhythm*. 2007;4(5):619-626. doi:10.1016/j.hrthm.2006.12.047

118. Kanlop N, Sakai T. Optical mapping study of blebbistatin-induced chaotic electrical activities in isolated rat atrium preparations. *J Physiol Sci*. 2010;60(2):109-117. doi:10.1007/s12576-009-0074-2

119. Brack KE, Narang R, Winter J, Ng GA. The mechanical uncoupler blebbistatin is associated with significant electrophysiological effects in the isolated rabbit heart. *Exp Physiol*. 2013;98(5):1009-1027. doi:10.1113/expphysiol.2012.069369